ALMA MATER STUDIORUM · UNIVERSITÀ DI BOLOGNA

Dipartimento di Fisica e Astronomia "Augusto Righi"

Corso di Laurea Magistrale in Fisica del Sistema Terra

Hurricane induced changes in the ocean ecosystem with a coupled physical-biogeochemical model

Relatore:
Prof.ssa Nadia Pinardi

Presentata da:
Roberto Arcamone

Correlatore:
Dott. Momme Butenschön

Sessione V
Anno Accademico 2019-2020

Abstract

A thesis work is presented in which a coupled model of physics and biogeochemistry, BFM17-POM1D, is used in order to simulate the ocean dynamics in two areas of the Sargasso Sea and describe the impact of a hurricane on the marine ecosystem. The biogeochemical model tracks 17 state variables, divided into five living functional groups: phytoplankton, zooplankton, dissolved and particulate organic matter, and finally the nutrients. We focus our attention on the evolution of nutrients and oxygen in order to understand how variations in the physical forcing can change the concentrations in both time and depth. The model is spatially one dimensional (1D) and time dependent and the physical forcings are imposed in the whole water column except for the turbulent mixing coefficients that are calculated by a turbulence closure model. No lateral exchange of biochemical tracers is considered. So in order to understand the ocean ecosystem dynamics in two different locations in the North Atlantic subtropical gyre we used different temperature and salinity monthly mean profiles, different wind stress components and general circulation vertical velocity profiles. We tried also to understand the role of biochemical processes characterizing the marine ecosystem, nitrification and particulate remineralization rates, testing how the concentrations are changing for the case without and with the hurricane. Finally, the results are consistent with the expectations: after the passage of a hurricane nutrinets are upwelled and the subsurface chlorophyll maxima attains greater values as well as it is located closer to the surface layer.

Sommario

Viene presentato un lavoro di tesi in cui viene utilizzato un modello accoppiato di fisica e biogeochimica, BFM17-POM1D, per simulare la dinamica oceanica in due aree del Mar dei Sargassi e descrivere l'impatto di un uragano sull'ecosistema marino. Il modello biogeochimico traccia 17 variabili di stato, suddivise in cinque gruppi funzionali viventi: fitoplancton, zooplancton, materia organica disciolta e particolata e infine i nutrienti. Focalizziamo la nostra attenzione sull'evoluzione dei nutrienti e dell'ossigeno per comprendere come le variazioni della forzatura fisica possano modificare le concentrazioni sia nel tempo che in profondità. Il modello è spazialmente unidimensionale (1D) e dipendente dal tempo e le forzanti fisiche sono imposte nell'intera colonna d'acqua ad eccezione dei coefficienti di mixing turbolento che sono calcolati da un modello di chiusura della turbolenza. Non è considerato alcuno scambio laterale di traccianti biochimici. Quindi, al fine di comprendere le dinamiche dell'ecosistema oceanico in due diverse località nel gyre subtropicale del Nord Atlantico, abbiamo utilizzato diversi profili medi mensili di temperatura e salinità, diverse componenti di stress del vento e profili di velocità verticale di circolazione generale. Abbiamo anche cercato di capire il ruolo dei processi biochimici che caratterizzano l'ecosistema marino, i tassi di nitrificazione e remineralizzazione del particolato, testando come cambiano le concentrazioni per il caso senza e con l'uragano. Infine, i risultati sono coerenti con le aspettative: dopo il passaggio di un uragano le nutrienti si sono sollevati e il subsurface chlorophyll maxima raggiunge sia valori maggiori sia più vicini allo strato superficiale.

Contents

Chapter 1

Introduction

Hurricanes are something extremely fascinating and equally complex: their genesis, development, evolution and forecasting are still a controversial subject of study and research. Along with all this, another very interesting question is how they interact with the ocean, its physics and its biogeochemistry: the purpose of this thesis work is precisely to understand how a hurricane affects the ecosystem dynamics of a water column.
In order to understand the nature of these interactions, how they develop and evolve, modelling becomes then a fundamental help to describe the role of hurricanes in the ocean dynamics.
At the state of the art, the equations that govern the physics of the ocean are based on the laws of mechanics, while the biogeochemical equations are empirical. It can be said that the equations that govern ocean biology are not known with absolute certainty. However we need to advance in the understanding of the many processes that affect the marine ecosystem and, taking in consideration the uncertainties, we explore biogeochemical simulation solutions to evaluate sensitivities of the dynamics, to selected processes such as hurricanes.

1.1 Ocean Ecosystem dynamics

As over 70% of Earth's surface is covered in water, and 97% of that water is salt water, marine ecosystems are are the largest types of ecosystems on the planet. They are characterized by an enormous variety of species, both chemical and biological, which interact continuosly with each other.
Furthermore, the ocean continuously exchanges matter with the other compartments of the climate system, such as the lithosphere and the atmosphere, generating a recirculation of substances. Focusing on the ocean, the set of reactions and processes that take place between different chemical species, marine organisms, mainly microorganisms, and the geological processes that involve, for example, the Earth's mantle define the oceanic biogeochemical cycles.
So, biogeochemical cycling involves the various reservoirs that store elements, the fluxes between these reservoirs and the physical, chemical and biological parameters that regulate these fluxes. Additionally, the cycles of many elements, such as carbon, nitrogen and phosphorus, are coupled via numerous feedback mechanisms.
Later, for the purpose of this thesis, the main biogeochemical cycles of those chemical species that are closely correlated with the modeling study will be described.

1.1.1 Oxygen

The oxygen cycle involves biogeochemical transitions of oxygen atoms between different oxidation states in ions, oxides, and molecules through redox reaction within and between the spheres/reservoirs of the Earth [52].
Oxygen is added to the ocean thanks to exchanges and reactions that take place in the upper part of the water column, through the absorption of air and, up to the depths where the light arrives, or the so-called photic zone, through photosynthesis . On the other hand, at the surface, oxygen can be lost due to exchanges with the atmosphere, while, going deep, it is consumed by the respiration of animals and plants, including by the decomposition of organic matter by bacteria. The same resperation processes mentioned above require the oxidation of organic compounds which are formed only in the upper layers. Considering that the molecular diffusion rate of oxygen in water is too small to be effective in transporting dissolved matter over large distances, diffusion of oxygen to deeper areas occurs through the circulation of surface water (Fig.1.1).

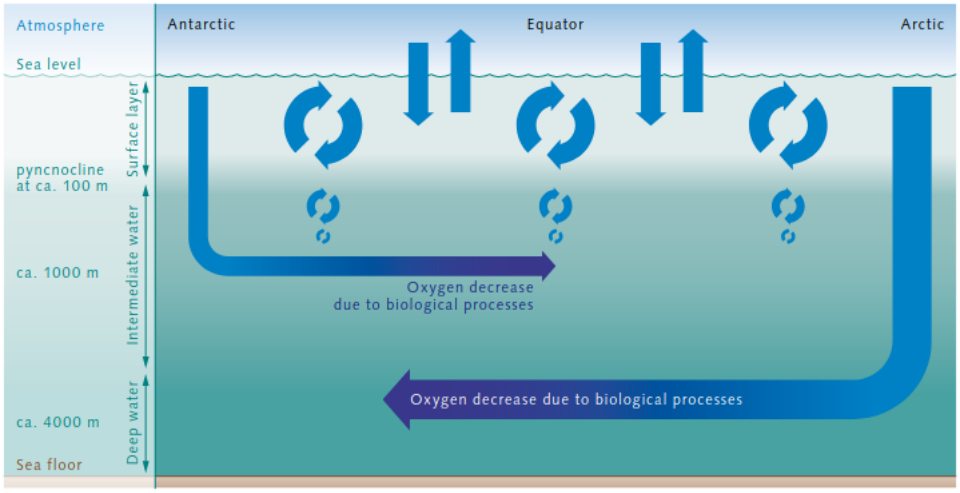

Figure 1.1: Oxygen from the atmosphere enters the near-surface waters of the ocean. This upper layer is well mixed, and is thus in chemical equilibrium with the atmosphere and rich in O2. It ends abruptly at the pyncnocline, which acts like a barrier. The oxygen-rich water in the surface zone does not mix readily with deeper water layers. Oxygen essentially only enters the deeper ocean by the motion of water currents, especially with the formation of deep and intermediate waters in the polar regions. In the inner ocean, marine organisms consume oxygen. This creates a very sensitive equilibrium. [56]

In order to determine the direction of exchange between the atmosphere and the ocean, the difference between the partial pressures of oxygen in the sea water and in the air is taken into account. Near the surface, local non-equilibrium concentrations can be found due to biological activity and upwelling but upon contact between surface and atmosphere, vertical mixing tends to eliminate these deficits and excesses [57]. In regions where there is extensive photosynthetic oxygen production, an excess of gas will tend to escape to the atmosphere while, in areas where upwelling leads to unsaturated oxygen rising to the surface, atmospheric oxygen will tend to be absorbed by the ocean [23] and, therefore, will result in a homogeneous surface layer, in thermodynamic equilibrium with the atmosphere. In the photic zone the oxygen content can significantly increase above that found on the surface and in many places it reaches values higher than 100% of the equilibrium-saturation concentrations (Fig. 1.2) due to the activity of plants and bacteria, the primary producers.

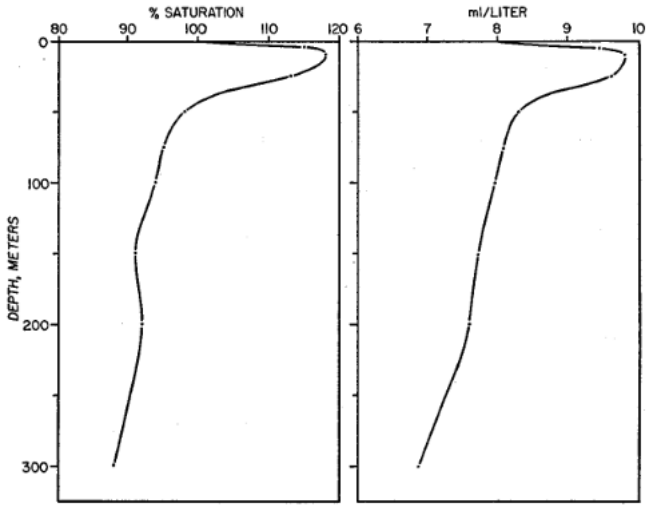

Figure 1.2: Vertical distribution of oxygen showing greater than 100% saturation. POLARBJORN Station 20, August 14, 1932, off the east coast of Greenland [36]

At depths down to the compensation depth photosynthetic production of oxygen exceeds its respiratory consumption, by definition, and at all greater depths the net change is a loss of oxygen, even though photosynthetic production continues [57]. The penetration of light is probably the most important factor in determining the compensation depth, but temperature, differences in the species of plankton, and nutrient supply are also important. In regions of intense photosynthetic activity the compensation depth will be nearer the surface because of decreased transparency corresponding to the large phytoplankton populations. At all depths of the ocean, oxygen is consumed by the respiration of plants and animals, including bacteria. Physiologically, the oxygen concentration change due to biological activity is accompanied by concurrent changes in the other elements which constitute living matter [55] and it is involved in the photosynthetic formation and respiratory decomposition of carbohydrate, as represented by the simple reversible equation:

$$CO_2 \;+\; H_2O \underset{\text{respiration}}{\overset{\text{photosynthesis}}{\rightleftharpoons}} CH_6O \;+\; O_2$$

Despite this, the processes of photosynthetic oxygen formation or consumption through breathing cannot be considered as something foreign and exclusive, but it must be taken into account that they are involved in many other processes carried out by different chemical species. It follows that, the previous equation should be

accompanied by a series of other equations of fixation and release by other elements (ie nitrogen and phosphorus) in order to be able to determine, with a more holistic view, the proportions and the amount of oxygen actually released and/or consumed.
After several studies on the relationship between different chemical species, also considering the physical effects of the ocean (i.e. the effect of salinity) [14] [66], it was possible to define a reference ratio, in atoms, between the main elements that affect ocean biochemistry, i.e. oxygen, carbon, nitrogen and phosphorus, which is O:C:N:P = 239:140:20:1. It is important to note that these ratios give an idea of the quantities of substances present in the ocean, but they must not be taken as something fixed and absolute: just think, there are strong deviations from these values in the near shore surface areas due to terrestrial drainage, river runoff and consequential variations in the composition of the plankton which also regulates the decomposition processes. On the other hand, these ratios are more reliable in the deepest parts of the ocean, where essentially complete oxidation occurs and only a small amount of organic compounds are present. Undoubtedly there are numerous other processes, biological and otherwise, that influence the biochemistry of oxygen and for this reason considering all these relationships gives a better description of the changes within the marine ecosystem rather than considering dissolved oxygen alone. Furthermore, although in the greater part of the global ocean oxygen does not represent a limiting factor for the growth of populations, it is closely related to the concentrations of other elements, as it has been noted from nitrogen and phosphorus, which can, instead, become limiting factors.
In conclusion, for a full understanding of the distribution of oxygen in the ocean, several factors must be taken into account: the processes of ventilation and air-sea exchange, the conditions of vertical mixing that determine the transport, production and consumption of oxygen from the marine biome and the biochemical and geochemical reactions that occur between different molecules, compounds and sediments.

1.1.2 Nitrogen

Nitrogen is present in the environment in different forms and plays a fundamental role in the biochemical processes of the marine ecosystem (i.e. primary production and decomposition).
First, it can enter the ocean in different ways, such as precipitation, runoff, and the exchange of molecular nitrogen (N_2) with the atmosphere. The latter, as it is, is hardly used by microorganisms and, for this reason, it undergoes various

biochemical processes that guarantee better accessibility and recirculation (Fig. 1.3).

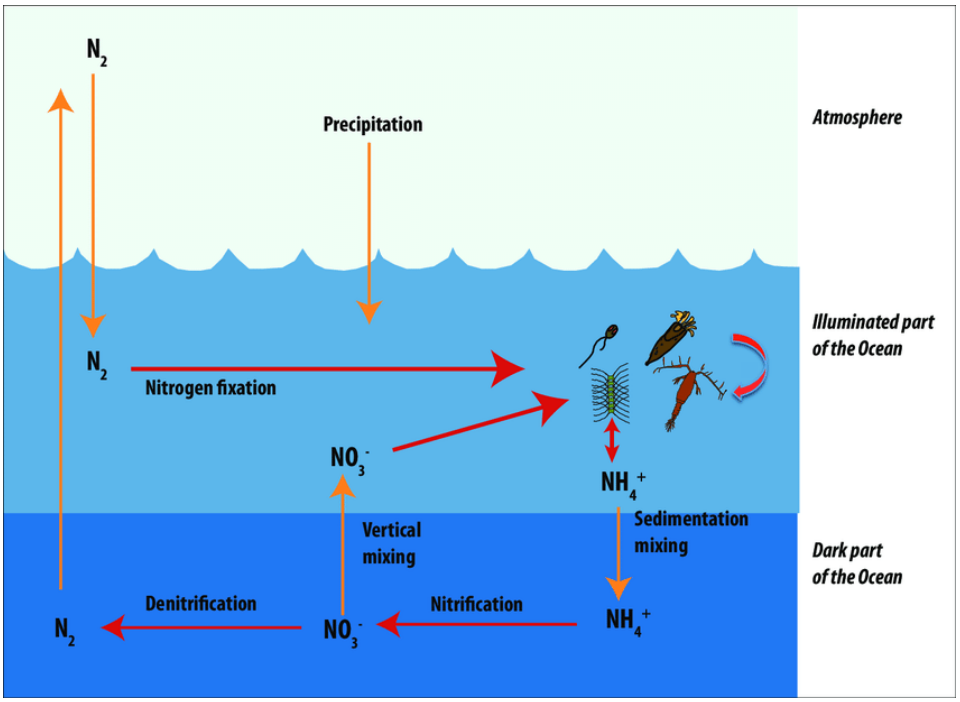

Figure 1.3: Schematic overview of the nitrogen cycle in the ocean [25]

Mainly, nitrogen in the ocean is found in the form of nitrate ion (NO_3^-), which is used, for example, by phytoplankton, although there are microorganisms capable to take up the nitrite ion (NO_2^-), ammonia (NH_4^+) and small molecules of amino acids and urea ($CO(NH_2)_2$).

So, the first step is the fixation of N_2: this process consists in the reduction of N_2 (that is, the acquisition of negative charges) to obtain ammonium ion. *Cyanobacteria* are considered to be the major N_2 -fixing microorganisms in the ocean [82] and part of the ammonium just produced is directly assimilated by the microorganisms themselves. Nitrogen sources are also removed from the euphotic zone by the downward movement of the organic matter: this can occur from sinking of phytoplankton, vertical mixing, or sinking of waste of vertical migrators. The sinking results in ammonia being introduced at lower depths below the euphotic

zone (i.e. sedimentation mixing). The factors that control the fixation rate of N_2 are different: temperature, light and environmental concentrations of O_2, NO_3^-, NH_4^+ and others. Nitrification, on the other hand, is a process that requires energy that comes from sunlight and, therefore, *Trichodesmium* perform this process optimally when they are in conditions of strong insolation and low levels of turbulence near the ocean surface [11].
The second step of the nitrogen cycle is represented by the nitrification. It is an oxidation process of nitrogen compounds divided into two phases: first there is the oxidation of ammonia into nitrite ions by means of ammonia-oxidizing bacteria (AOB) and ammonia-oxidizing archea (AOA) [28]; after which there is a further oxidation from nitrite ion to nitrates, carried out by nitrite-oxidizing bacteria (NOB) as shown by the following reactions:

$$2\mathrm{NH_4^+} \;+\; 3\mathrm{O_2} \longrightarrow 2\mathrm{NO_2^-} \;+\; 4\mathrm{H^+} \;+\; 2\mathrm{H_2O}$$

$$2\mathrm{NO_2^-} \;+\; \mathrm{O_2} \longrightarrow 2\mathrm{NO_3^-}$$

Generally, the first part of the process is carried out by microorganisms like *Nitrosomonas* and *Thaumarchaeota*, while the second phase is completed by *Nitrobacters* [28] [75]. Nitrate can be returned to the euphotic zone by vertical mixing and upwelling where it can be taken up by phytoplankton to continue the cycle.
Subsequently, the reverse process that leads to the formation of reduced nitrogen compounds occurs in almost completely anoxic environments: the denitrification. Denitrification is a process of reducing oxidized nitrogen ions (NO_3^- and NO_2^-) into gaseous nitrogen compounds (i.e. N_2 and N_2O), by means of different species of bacteria: those belonging to the genera *Pseudomonas* and *Bacillus* are the best known and most abundant [29]. These microorganisms use the different ionic compounds to perform a series of reactions in order to accept electrones extracted from the oxidation of organic substrates, so the complete process can be expressed as a net balanced redox reaction, where nitrate gets fully reduced to molecular nitrogen which can then return to the atmosphere and complete the cycle:

$$2\mathrm{NO_3^-} \;+\; 10\mathrm{e^-} \;+\; 12\mathrm{H^+} \longrightarrow \mathrm{N_2} \;+\; 6\mathrm{H_2O}$$

The main factor controlling denitrification is oxygen: since the energy required for the oxidation of organic matter is lower when you have NO_3^- as the final electron acceptor instead of oxygen, you can assert, as specified above, that this process is essentially limited to those oxygen deficient areas [26].
An essential aspect in the description of the marine nitrogen cycle concerns its

use for primary production. A part of the latter derives from the nitrogen recycled from the organic matter within the euphotic zone, while another fraction comes from the nitrogen produced in the aphotic zone of the water column. This "new" nitrogen, resulting from the nitrification processes described above, enters the photic zone thanks to vertical mixing and has a strong impact on the increase in phytoplankton production: it is possible to estimate that about one-third of the global pelagic primary production takes place in areas where new nitrogen is entering the euphotic zone; these coastal or upwelling areas represent only about 11% of the ocean surface; elsewhere, primary production depends predominantly on nitrogen that is recycled within the euphotic zone [41].

1.1.3 Phosphorus

Phosphorus (P) is an essential element and plays a crucial role in different structures and functional components of organisms: it is part of the molecules that carry chemical energy in living cells (*Adenosine triphosphate*, ATP), it forms the ester-phosphate backbone of DNA and RNA, and is an important constituent of various cellular components such as phosphoproteins and phospholipids.
Furthermore, phosphorus can impact on the primary production rate in the ocean, as well as on the distribution of species and the structure of the ecosystem. Recent studies have shown that orthophosphate, PO_4^{3-}, is a limiting nutrient in different areas of the ocean: in fact, it also plays a key role in the processes of photosynthesis and is closely linked to the sequestration of atmospheric CO_2 [31] [63]. Unlike nitrogen, phosphorus is not fixed directly by the atmosphere; it is mainly found in larger pools of water, soil and rocks. This makes the phosphorus cycle the slowest of the various cycles analyzed and, therefore, on geological time scales, P is often considered as the ultimate limiting macronutrient in marine ecosystem [68] [69].
The main source of phosphorus in the ocean is continental erosion, which transports P in dissolved and particulate form via riverine influx; however, atmospheric deposition by aerosols, mineral dust and volcanic ash is important for the most remote and offshore areas of the ocean (Fig. 1.4) [51].
Most of the riverine particulate phosphorus is retained by the continental shelf and therefore does not affect the pelagic processes of the open ocean [5] [60], while the dominant sink for oceanic P is deposition and burial in marine sediments (after transformation from dissolved to particulate forms) and a minor sink is rapresented by the uptake through seawater-oceanic crust interactions associated with hydrothermal activity on the ocean's floor. Furthermore, human activity represents an additional source of P, contained in fertilizers and which flows through

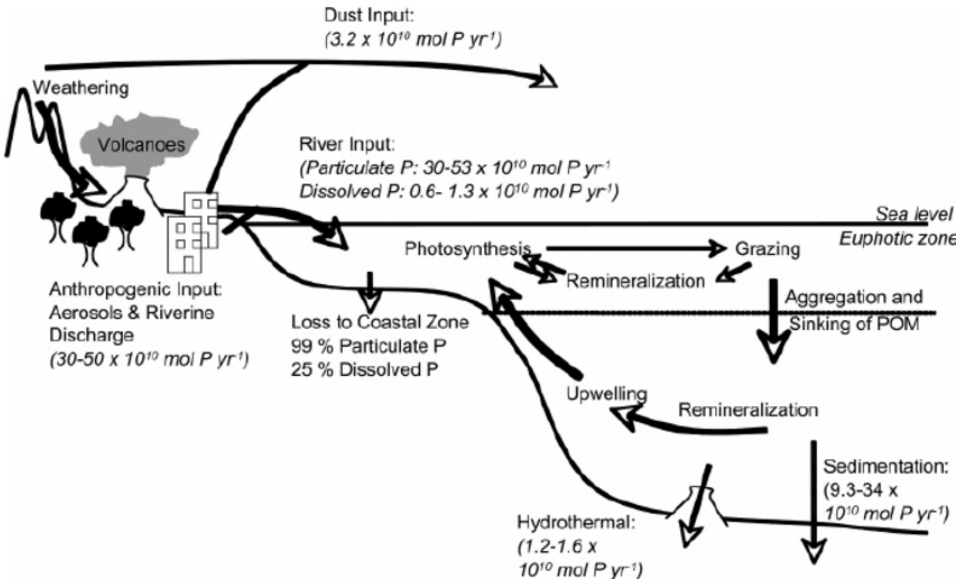

Figure 1.4: Schematic overview of the marine phosphorous cycle. Flux data are from Benitez-Nelson [4] and Follmi [24]

rivers and groundwater to the sea where a considerable amount of anthropogenic phosphorus is deposited and accumulated. [51].
Phosphorus has a strong impact on marine biota: in large regions of the ocean, mainly in the surface waters, the dissolved *P* is present as dissolved organic phosphourus (DOP) and oceanic productivity in these regions may be dependent on rigeneration of bioavailable *P* from the dissolved organic matter (DOM) [13].
Orthophosphate, PO_4^{3-}, which is a form of dissolved inorganic phosphorus (DIP), is assimilated by certain species of phytoplankton and it's converted into organic phosphorus compounds [51] [59]. The phytoplankton then releases dissolved cellular organic and inorganic phosphorus into the surrounding environment. Some of the organic *P* compounds can be hydrolyzed by enzymes that catalyze hydrolytic cleavage and subsequently assimilated [40], but the vast majority of phosphorus is remineralized within the water column and about 1% of the associated phosphorus transported to the deep sea by falling particles are removed from the ocean reservoir by burial in sediments [51]. A series of diagenetic processes act to enrich the phosphorus concentrations in the sediment interstitial water, resulting in an appreciable benthic backflow of phosphorus in the overlying bottom waters (e.g. microbial respiration of organic matter in sediments) which, due to the upwelling, may came back to the surface waters and, finally, complete the cycle.

1.1.4 Phytoplankton

The term phytoplankton refers to that part of the planktonic community that is photoautotrophic, so that needs sunlight to activate the cardinal process that allows it to obtain nourishment and energy: photosynthesis. For this reason, pythoplankton is generally located in the highest part of the water column (photic zone) and, moreover, it also plays a very important role in the so-called "biological carbon pump" (Fig. 1.5).
Briefly, the biological pump is part of the carbon cycle and consists of the simplest form of capture of atmospheric CO_2 by marine biota, the circulation of organic matter produced during photosynthesis and the recirculation of calcium carbonate ($CaCO_3$).

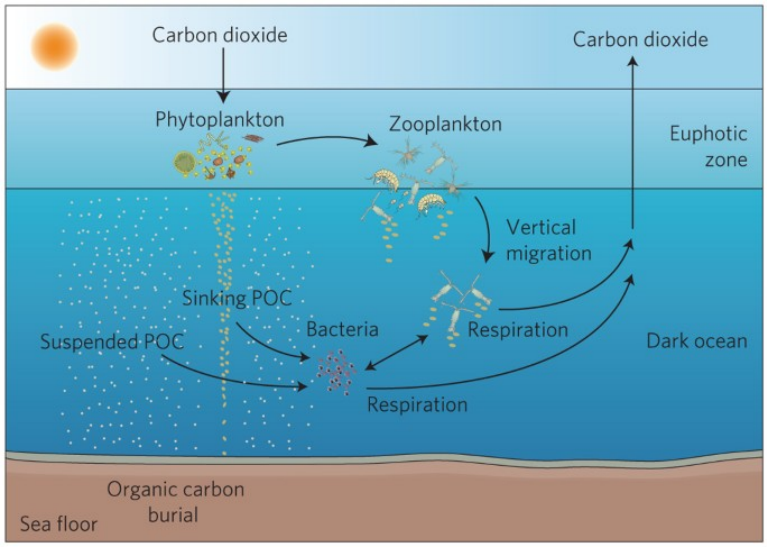

Figure 1.5: Schematic overview of the carbon biological pump [30]

In order to better understand the role and processes that have phytoplankton as protagonist, this section is divided into three subsections, in which, first of all, the biological characteristics of the main groups of phytoplankton will be briefly described, then we will move on to analyze more in detail the chlorophyll governing

photosynthesis process, and then finally focus on the factors of control and impact on the production.

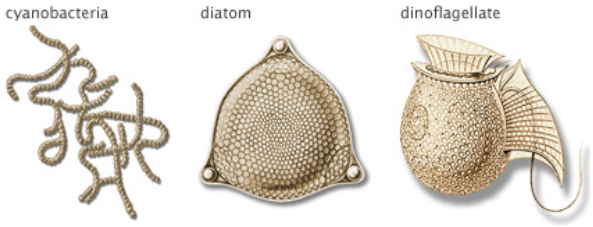

Figure 1.6: Some phytoplankton types. Left to right: cyanobacteria, diatom, dinoflagellate. Note that the drawings are not to scale (Collage adapted from drawings and micrographs by Sally Bensusen, NASA EOS Project Science Office `https://earthobservatory.nasa.gov/features/Phytoplankton`)

Taxonomic description of the major types of phytoplankton (Fig. 1.6)

1) *Diatoms*. Diatoms belong to a class of algae called the *Bacillariophyceae*. They are among the best studied of the planktonic algae and are often the dominant phytoplankton in temperate and high latitudes. Diatoms are unicellular, with cell size ranging from about 2 μm to over 2000 μm [27], and some species form larger chains or other forms of aggregates. Planktonic diatoms do not have any locomotor structures and are usually incapable of independent movement. Because it is essential for them to remain in lighted surface waters in order to carry out photosynthesis, these algae exhibit a variety of mechanisms which retard sinking. For example, these include their small size and general morphology, as the ratio of cell surface area to volume determines frictional drag in the water: so colony or chain formation also increases surface area and slows sinking [41].

2) *Dinoflagellates*. The second most abundant phytoplankton group belongs to the class of *Pyrrophyceae*, and commonly referred to as dinoflagellates. They are types of unicellular algae, which live mainly alone and are motile, in fact they have two flagella that allow them to move [41].
Furthermore, dinoflagellates can be classified according to the type of energy resource they need: there are autotrophic dinoflagellates, which photosynthesize to build organic materials, hetrotrophs, which do not have chloroplasts and therefore feed on smaller microorganisms (these re-enter, to be precise, in zooplankton) and

finally mixotrophic, which are capable of feeding in through both the previously described ways. One of the most important and macroscopically visible phenomena connected to dinoflagellates, are the red-tides (Fig. 1.7): in certain circumstances, the rate of reproduction of these microorganisms is enough to cause the waters to turn a dull and dark red, due to the reddish-brown pigments which they contain [41].

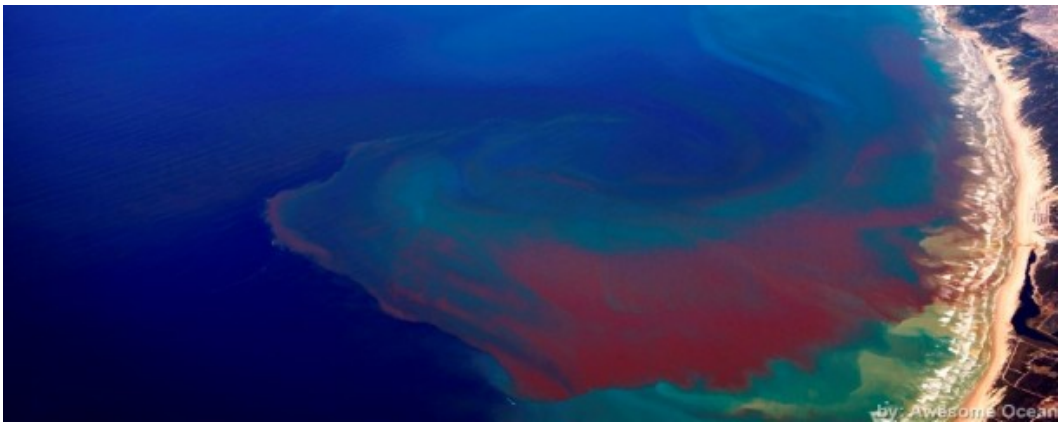

Figure 1.7: Harmful algae bloom off the coast of San Diego County, California. Photo by NOAA, Kai Schumann `https://estuaries.org/fighting-against-red-tide/`)

Despite the aesthetic beauty of this phenomenon, it does not go beyond having very serious repercussions on the ocean ecosystem. Dinoflagellates, are quite harmless; however, the problem arises as the concentration of the same can reach values of even 10^8 cells per liter [41]: this strong eutrophication will ensure that the useful nutrients will be rapidly consumed by the algae and, once this bloom decays, bacterial decomposition it will begin and consume an enormous amount of dissolved oxygen causing most of the marine and fish fauna to die.
These anoxic conditions are not exclusively a property of dinoflagellate blooms; such conditions can also occur following large blooms of other types of phytoplankton [41].

3) *Cyanobacteria*. Sometimes called also *Cyanophyceae*, but mainly known as "blue-green algae", cyanobacteria are a group of photosynthetic microorganisms, some of which are also nitrogen-fixing organisms, that live both as unicellular organisms and as filamentous or spherical colonies.
Thanks to the presence of specialized cells, the heterocysts, some cyanobacteria

are able to fix atmospheric nitrogen in anaerobic conditions: if they are present, therefore, these microorganisms are able to synthesize ammonia (NH_3), nitrites (NO_2^-) and nitrates (NO_3^-).
Another peculiar and fundamental characteristic of cyanobacteria is that they are the only bacteria to contain the chlorophyll-a pigment (in the next section there will be a more detailed description of the latter) which is a fundamental requirement for oxygenic photosynthesis to take place [77]:

$$6CO_2 \ + \ 6H_2O \xrightarrow{\text{photosynthesis (oxygenic)}} C_6H_{12}O_6 \ + \ 6O_2$$

This should not be confused with the erroneous idea that cyanobacteria are the only bacterioplankton species to photosynthesize; other bacteria carry out the same process but they use bacteriochlorophyll instead of chlorophyll-a and they also use CO_2 and hydrogen sulphide (instead of water) to synthesize sugars [7]. Finally, this process takes place in anaerobic conditions and that's why it's called anoxygenic photosynthesis:

$$6CO_2 \ + \ 12H_2S \xrightarrow{\text{photosynthesis (anoxigenic)}} C_6H_{12}O_6 \ + \ 6S \ + \ 6H_2O$$

In addition to chlorophyll-a, blue-green algae also contain the pigments phycoerythrin and phycocyanin, which give the bacteria their bluish tint (hence the name) which can be visible, as for dinoflagellates, with spectacular superficial blooms (Fig. 1.8).

Phytoplankton chlorophyll

Chlorophyll is the key pigment for oxygenated photosynthesis. It acts as a photoreceptor [44], that is, it uses solar energy which then leads to the formation of

Figure 1.8: Lake Erie experienced the worst blue-green algae bloom in decades, 2011 (Photo Credit: MERIS/NASA; processed by NOAA/NOS/NCCOS) [22]

sugars (i.e. glucose) and oxygen. Glucose can either be directly assimilated as an energy source for internal metabolisms and growth, or it can be polymerized into starch and be stored. On the other hand, oxygen, which is a waste product of this reaction, is excreted into the environment to be used by other organisms for aerobic respiration.

Although the main pigment is chlorophyll-a, it is important to specify that there are six different forms of chlorophyll (chl-a, b, c, d, e, f) plus accessory pigments, also known as carotenoids (e.g. carotenes, xanthophylls and so on). Carotenoids are defined as accessory pigments as they assist chlorophyll-a, transferring the energy stored by solar radiation, instead of directly taking part in the photosynthesis process [39]. All these photosynthetically active pigments absorb solar radiation in the visible band, more precisely in the range from 400 to 700 nm (photosynthetically active radiation, PAR), but with different absorption spectra [44] (Fig. 1.9).

As can be seen in the figure 1.9, chl-a has the maximum absorption peak in the red region of the electromagnetic spectrum (650-700 nm) and blue-violet (450 nm). Chl-b la is found mainly in terrestrial plants and green algae, chl-c and chl-d [43] are mainly present in red and dinoflagellated algae, while the rarer chl-e has been found in yellow-green algae. Finally, chl-f has been recently discovered in some

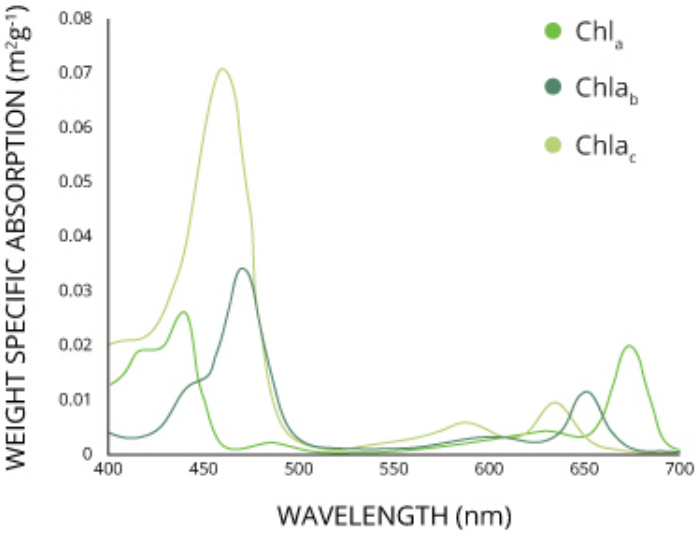

Figure 1.9: The different forms of chlorophyll absorb slightly different wavelengths for more efficient photosynthesis [22]

cyanobacteria from Australia [10], which best absorbs light at 706 nm.

Control factors on the production

Given the above, the availability of sunlight is certainly the first physical factor that controls the photosynthesis of phytoplankton. In the ocean, light can penetrate inside the water column only in the first 200m (photic zone) where the vast majority of algae and phytoplankton are concentrated. Temperature also affects the rate of photosynthesis in the ocean [67]: like any chemical reaction, photosynthesis is also speeded up by heat and therefore will lead to an increase in the reproduction rate of phytoplankton. However, when the temperature optimum is exceeded, the photosynthesis process stops. This happens because the excessive heat risks denature the enzymes used during these processes and, therefor, growth rate of microorganisms begins to decrease [22].
Another physical factor of enormous importance that controls the production of phytoplankton is represented by the set of physical forcings capable of mixing the water column, making nutrients rise from the depths to the euphotic zone, where they accumulate. This includes the fronts, characterized by large horizontal gradients of variables such as temperature, salinity and density, then there is the eddy-formation such as the large-scale gyres [41]. Focusing on the latter, in

the Northern Emisphere it is possible to observe anticyclonic gyres and cyclonic gyres where, rispectivly, the water flows in a clockwise and anticlockwise directions (Fig. 1.10).

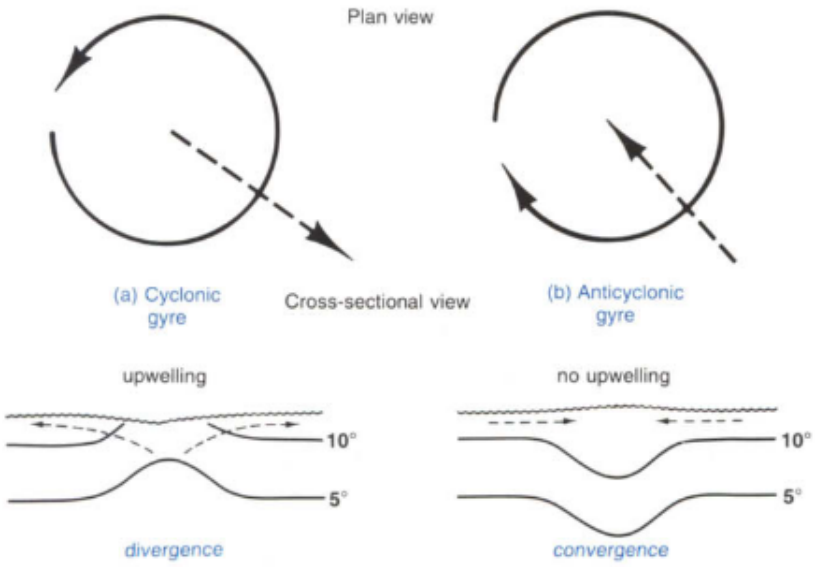

Figure 1.10: Plan and cross section viewa of a cyclonic and an anticyclonic gyre in the Norther Empisphere. [41]

In the figure 1.10 it is possible to see two dashed lines that indicate the direction of the water transfer, towards or from the center.
There are several implications related to these factors: in the northern hemisphere the anticyclonic gyres are convergent gyres in which it's possible to observe a deepening of the thermocline and a consequent non-rising of nutrients. In fact, precisely for this reason, the areas of the ocean characterized by large-scale convergence phenomena are considered real "deserts" of primary production (i.e. Sargasso Sea in the North Atlantic) [41].
The opposite case, however, for cyclonic gyres, which are divergent gyres where there is a rising thermocline and a consequent upwelling of nutrients from below that will lead, in these areas, to have very high values of primary production.
However, there is also a biological factor to mention: the influence of the nutrients that, priorly, are found in the ocean. As can be understood from what has been said so far, phytoplankton needs other nutrients, in addition to the sugars produced

by photosynthesis, to grow and reproduce: these chemical species are mainly nitrogen, phosphorus, iron and, in some cases, also silicon, calcium and other trace metals. The higher the concentration of these nutrients in the water, the higher the growth of phytoklankton [22].

Subsurface Chloropyll Maxima

The *Subsurface Chloropyll Maxima* (SCM) is the region of the ocean below the surface where the maximum concentration values of chlorophyll can be found inside the water column (Fig. 1.11) [1].

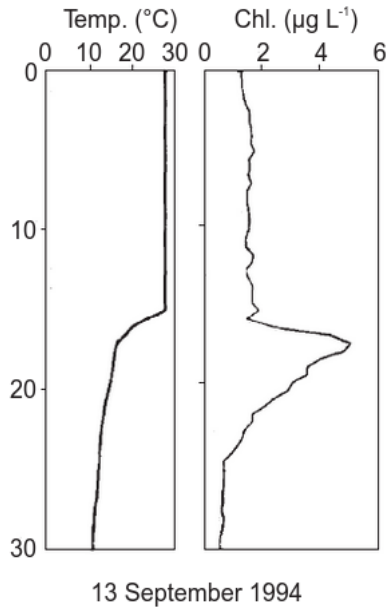

Figure 1.11: Example profile of subsurface chloropyll maxima [80]

It is not always possible to identify a region of SCM, but it is typical in areas of the global ocean where there is strong stratification, moreover it is not fixed even in terms of thickness, composition and, above all, depth [1] [17]. In general, an SCM is highlighted at the same depth as the nutricline, i.e. the region of the ocean where there is the greatest variation in nutrient concentration with depth [21].

There are many factors that influence the zone and composition of the SCM, both biotic and abiotic. First of all, of course, much depends on the attenuation level of the incident solar radiation [76], as the fitoplankton that composes it (e.g. cyanobacteria and dinoflagellates) needs light for its growth: this allows us to deduce that the depth reached by the SCM, generally, shouldn't be the dark zone of the water column. Indeed, it is within the photic zone where ther's a high concentration of nutrients and chlorophyll develops, mainly at the base of the same at the nutricline.
Finally, it is not possible to transcend the possibility, especially for some species of phytoplankton, to move along the water column to reach those areas with greater availability of nutrients and conditions suitable for carrying out their biological/physiological processes [18].

North Atlantic Subsurface Chloropyll Maxima

For the purposes of this thesis, the model will be tested in two different areas of the North Atlantic: one being the position where the maximum intensity of Hurricane Gonzalo was recorded, around 25.6°N and 68.7°W (Table 1.1), the second being the position where the BATS station is located, 31.4°N and 64.1°W (more details will be provided in Chapter 3), both, therefore, are located in the Sargasso Sea.
The Sargasso Sea is bounded on the west and northwest by the Gulf Stream and to the south by the North Atlantic equatorial current [64] (Fig. 1.12).
The region of interest is characterized by weak geostrophic circulation [61], with a net southward flow that will lead to a net downwelling rate of about 4 cm per day [45], and by hight eddy energetics: between 25°N and 32°N there is a real transition region between eutrophic waters that go north and are subject to winter mixing, with a consequential enrichment of surface nutrients [78] [79], and an oligotrophic subtropical convergence zone where rich waters of nutrients lie below the stratified euphotic zone [64].
The winter mixing of subtropical waters is caused by the passage of cold fronts on the Sargasso Sea which affect the thermal structure of the ocean, causing a convective mixing that leads to the erosion of the seasonal thermocline and a deepening of the mixing layer up to 150-300 m [79]. In summer, however, this region is dominated by high pressure systems that block the passage of the fronts, forming a warm mixed layer, which typically reaches 20 m (Fig. 1.13).

The seasonal pattern of the biogeochemistry of the Sargasso Sea and so primary

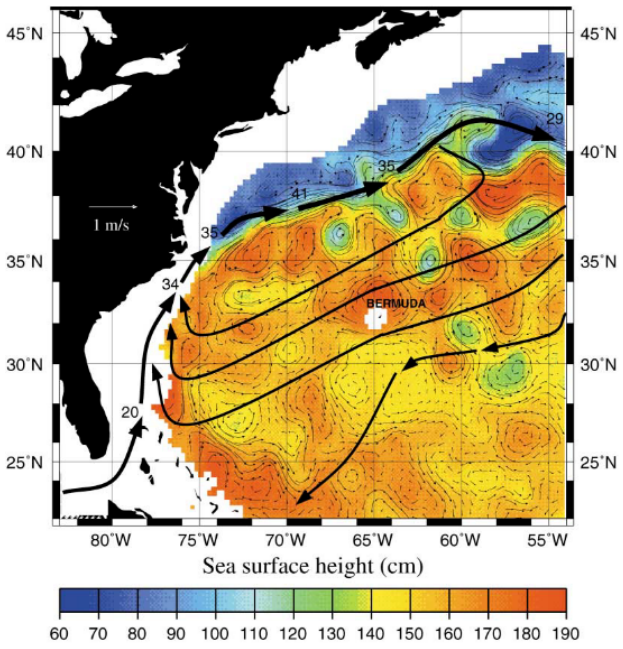

Figure 1.12: Satellite image of Sargasso Sea showing surface height (SSH) and geostrophic velocity, illustrating typical mesoscale variability. The mean direction of the currents, and the location of Bermuda are also shown. The long-term mean circulation of the warm waters of the subtropical gyre is shown as thick black arrows where the numbers indicate the transport. [64]

production are influenced by the deep winter mixing and by the strong summer thermal statification (Fig. 1.14 (a)).
This annual cycle is strictly connected to the physical forcing, as the vertical mixing induces a rise of nutrients from the deep waters and a consecutive pool of biomass in the euphotic zone during the winter [64]: generally, this flow towards the surface of nutrients leads to a short period of spring bloom (between January and March) and higher primary production rates linked to higher chlorophilic concentrations.

During the summer thermal stratification, it can be seen that the upper part of the water column is depleted of nutrients, leading to a reduction in primary production

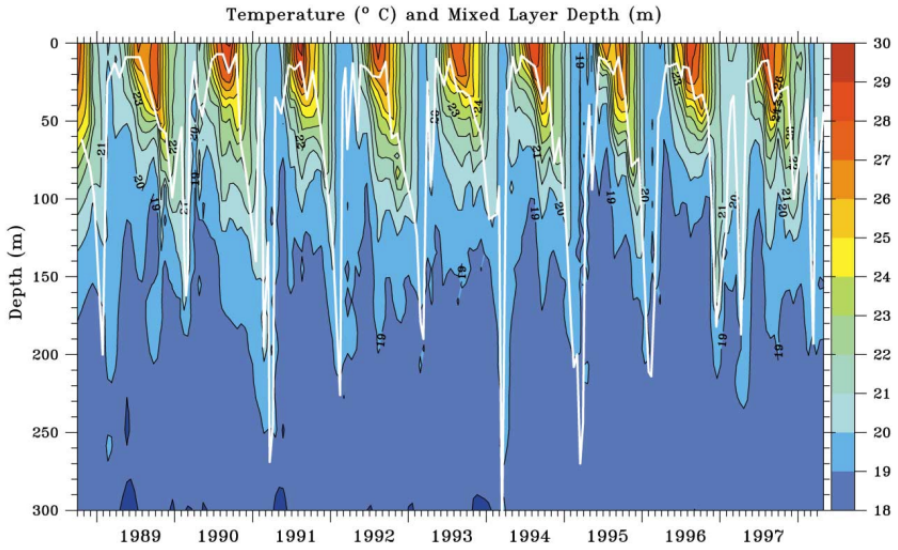

Figure 1.13: Time-series contour plot of temperature in Sargasso Sea (note that the solid white line indicates the mixed layer depth) [64]

rates and a deepening, near the nutricline, generating a localized SCM between 50 and 150 m (80 m for the 75% of the time series).
Focusing on BATS, the profiles of chlorophyll-a and b are shown (Fig. 1.14 (b)). The highest peaks of chlorophyll-a are located between 60 and 120 m associated with convective deep mixed layer. As far as chl-b is concerned, we see maximum values at depths almost coinciding with those of chlorophyll-a; despite this, however, it should be noted that there are differences that peak around 100 m, which suggest the presence of different species of phytoplankton [64].

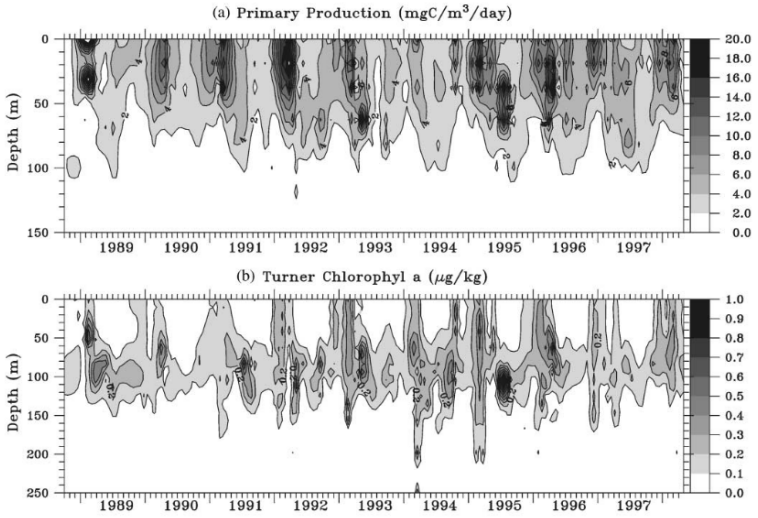

(a)

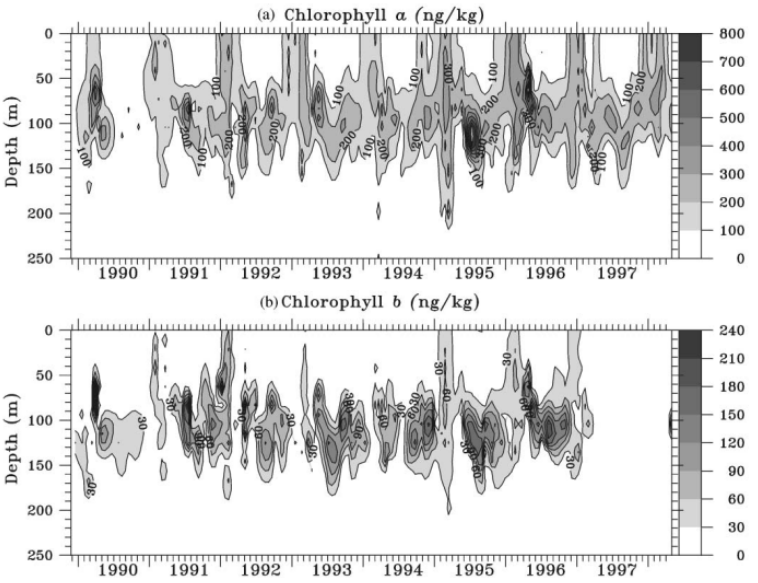

(b)

Figure 1.14: (a) Time-series contour plots of primary production and chl-a at Sargasso Sea ; (b) Time-series contour plots of chl-a and chl-b at BATS [64]

So, to conclude, for the purpose of this thesis it was fundamental to understand the

processes that characterize phytoplankton. They represent the primary producers of the ocean and are therefore the basis of the marine food web. It has been seen that there are numerous biological and physical processes that directly or indirectly affect their dynamics: they carry out photosynthesis with which they produce oxygen, sequester atmospheric CO_2, nourish themselves and become nourishment for the most advanced organisms of the trophic chain (eg zooplankton). Furthermore, it was explained that their vertical distribution depends mainly on their need for light and availability of nutrients but thay can also stay in the subsurface part of the water column, giving rise to the subsurface chloropyll maxima phenomena, or, if present in excessive quantities at the top layers (algal bloom and red tides), they can become a serious problem for the marine ecosystem due to oxygen depletion resulting from their decomposition.

1.2 Impact of a hurricane on the ocean

First of all, the near-surface wind from hurricanes is one of the driving factors for deep-water upwelling, which brings an abundance of nutrient enriched sediments to the surface [48]. Because of divergence generated by major storms, the water columns mixed layer deepens and brings cooler water to the surface, which can be evident within days following the passage of a hurricane [48] [54] [72], with surface chlorophyll and phytoplankton concentrations increased [37].
This phytoplankton bloom can have different impacts and implications on the marine ecosystem [49]. In fact, it undoubtedly represents an increase in nutrients and primary producers in the photic zone of the water column, but there are also negative feedbacks as a result of this, as these blooms block the incoming solar radiation [19], disturbing the deep photosynthetic processes, which they represent a source of essential nourishment for various benthic organisms, consequently altering the marine habitat.
As mentioned above, the surface temperature (hereinafter SST) is strongly influenced by the passage of a hurricane. There are two predominant features of the SST response: first, the maximum range of variation (ΔSST_{max}) is wide, ranging from -1 to $-6°C$, becoming increasingly noticeable as translation speed (U_H) and central pressure decrease, increasing the intensity of the hurricane itself [54]; secondly, the SST response is asymmetrical with respect to the hurricane trace, in fact for hurricanes that move fast ($U_H > 6\ ms^{-1}$) it's possible to measure that ΔSST_{max} is located in an area between 30 and 150 km to the right of the track, vice versa, for slower hurricanes, the ΔSST_{max} response is more extensive on the ocean surface [42]. Therefore, in order to identify a hurricane, what is sought is a decrease in ocean surface temperature, due to the rising water of cold and dense water, and a consequential increase in salinity [54] (Fig. 1.15 (a)).
Also, the Ekman pumping velocity increases significantly during the cyclone [12] suggesting strong upwelling and the strong cyclonic winds can also induce vertical mixing and thereby entrainment, as stated above, at the base of the mixed layer [65] with a consequential increase of the chlorophyll concentartion (Fig. 1.15 (b)).

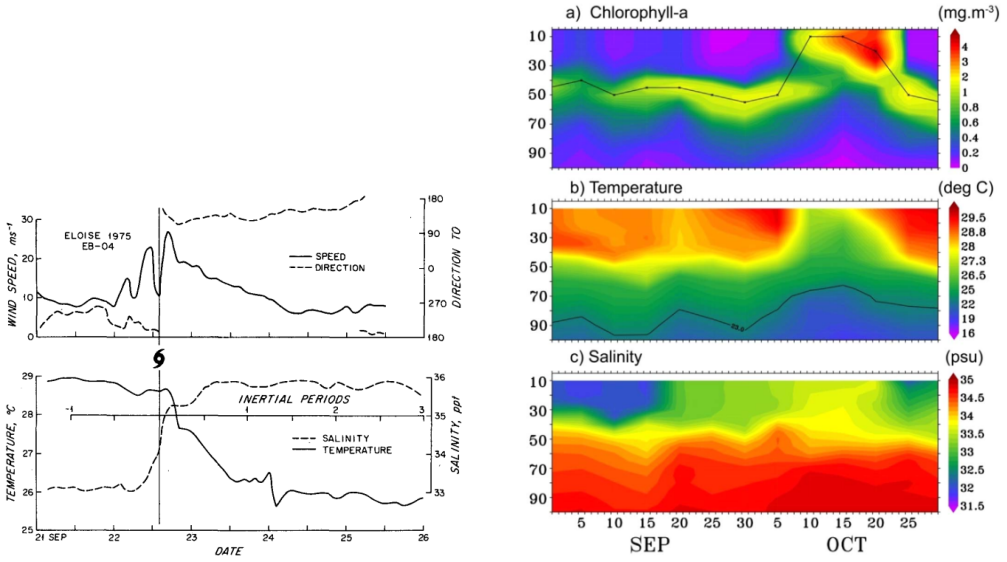

(a) (b)

Figure 1.15: (a) Air-sea measurement from EB-04 during the passage of Eloise (1975) [54] ; Depth-time sections of chl-a, temperature and salinity in the upper 100 m in the central BAY OF Bengala after the passage oh Hudhud hurricane (September 30,2014 - October 07, 2014) [12]

So, in conclusion, what one expects to find from the analysis carried out for this thesis is a situation comparable to that present in the literature (Fig.1.15 where it is possible to observe a rise in the subsurface chlorophyll maxima (*SCM*) after the passage of hurricane Gonzalo.

1.3 Hurricane Gonzalo

As described in NOAA report [9], the development of Gonzalo can be traced to a tropical wave that departed from the westcoast of Africa on the 4th of October. The wave was accompanied by a large area of cloudiness and thunderstorms while it moved westward across the tropical Atlantic during the next several days.
The "best track" chart of the tropical cyclone's path is given in Fig. 1.16.
Gonzalo rapidly intensified and became a major hurricane (category 3 or greater on the Saffir-Simpson Hurricane Wind Scale) at 1800 UTC 14 October when it was located about 145 nmi north of San Juan, Puerto Rico [9].

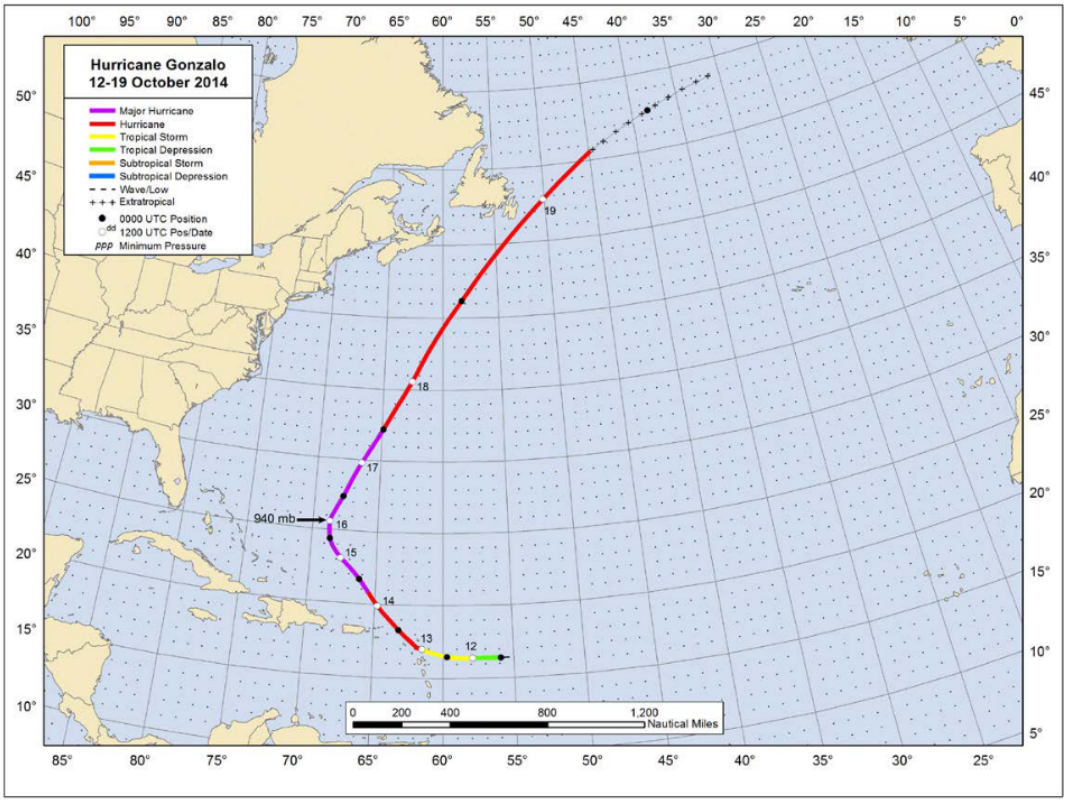

Figure 1.16: Best track positions for Hurricane Gonzalo, 12-19 October 2014. Track during the extratropical stage is based on analyses from the NOAA Ocean Prediction Cente [9]

Gonzalo became a category 4 hurricane 6 h later with an estimated intensity of 115 kt. Over the next 12 to 18 h an eyewall replacement occurred and Gonzalo weakened slightly. During this time, the hurricane began moving north-northwestward around the western portion of the ridge that was beginning to shift eastward. The hurricane intensified again early the next day while it turned northward, and Gonzalo reached its estimated peak intensity of 125 kt at 1200 UTC of the 16th October, when it was centered about 460 nmi south-southwest of Bermuda (Fig. 1.17). Late on the same day, the hurricane began to weaken. Increasing southwesterly shear and slightly cooler sea surface temperatures caused Gonzalo to weaken to a category 3 hurricane by 1200 UTC of the 17th October when it was centered about 180 nmi south-southwest of Bermuda. Gonzalo's maximum winds continued to decrease during the afternoon of the 17th while it moved north-northeastward toward Bermuda at about 15 kt. The hurricane made landfall on the southwestern coast of Bermuda with an estimated intensity of 95 kt (category 2 intensity) shortly after 0000 UTC of the 18th October.

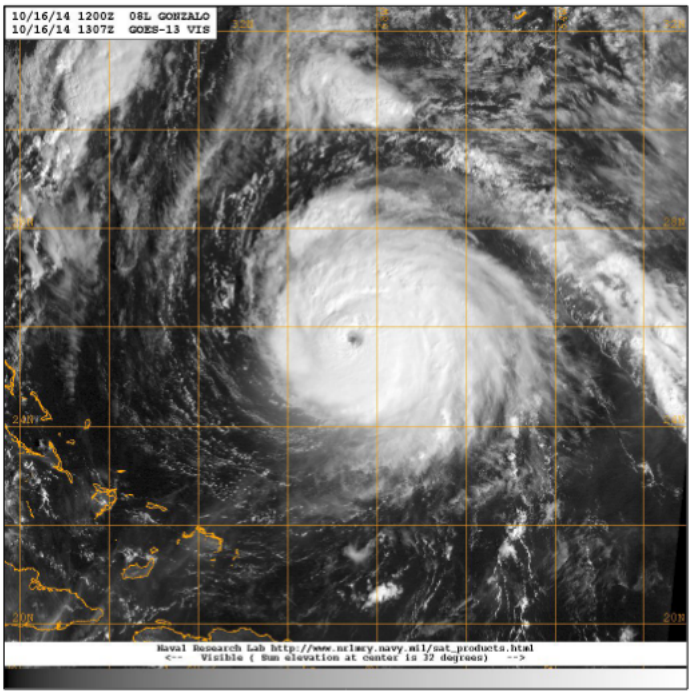

Figure 1.17: Visible satellite image of Hurricane Gonzalo at its estimated peak intensity of 125 kt (category four on the Saffir-Simpson Hurricane Wind Scale) at 1307 UTC 16 October [9]

After Gonzalo's passage over Bermuda, the hurricane continued to accelerate north-northeastward, and by 1800 UTC of the 18th, its forward speed exceeded 30 kt. Increasing southwesterly vertical wind shear and cool waters caused additional weakening as Gonzalo's cloud pattern became less symmetric.
Gonzalo became a 65-kt extratropical cyclone by 1800 UTC 19 October. The extratropical cyclone turned east-northeastward and weakened before it was absorbed by a cold front several hundred n mi south-southwest of Iceland by 1200 UTC 20 October. The front and remnants of Gonzalo brought strong winds and heavy rains to the United Kingdom and portions of northern Europe the next day.

1.3.1 Gonzalo Hurricane best track resume

Below is a table, also extracted from the NOAA report referring to Gonzalo, which shows dates, time and coordinates relating to the path of the hurricane in the period 12-19 October 2014 (Table 1.1) [9]:

Table 1.1: Best track for Gonzalo Hurricane, 12-19 October 2014, at 1200 UTC

Day	**Latitude (°N)**	**Longitude (°W)**
12	16.4	57.9
13	17.0	61.5
14	19.9	64.8
15	23.1	67.7
16	25.6	68.7
17	29.8	66.5
18	35.6	62.6
19	47.8	50.1

1.4 Thesis objectives and structure

For the purposes of this thesis a coupled model of physics and biogeochemistry was used to simulate the behavior of the ecosystem in two different locations of the North Atlantic subtropical gyre to finally describe how the impact of hurricane induced winds and vertical velocity affect the ecosystem behavior.
The simplifying assumption is that the ecosystem can be represented by a column of water without the interactions with the lateral neighbouring environment. Exchanges occur only in vertical, with the atmosphere and the deeper ocean.
Chapter 2 provides a description of the physical-biogeochemical coupled model used to simulate the behavior of the marine ecosystem within a water column, Chapter 3 describes the main datasets used for initialization, forcing and validation, while in Chapter 4 we describe the experiments performed.
Finally, Chapter 5 offers a summary of the work done and the conclusions we have reached.

Chapter 2

Numerical Model: BFM17-POM1D

For the purposes of this thesis a coupled model of the biogeochemical part and of the physical forcings has been used which is the BFM17-POM1D.
The one-dimensional version of the Princeton Ocean Model (POM-1D), calculates the vertical mean fields for velocity, temperature and salinity, together with the turbulent diffusion coefficients for momentum and tracers.
The BFM17 [62] is a reduced-order biogeochemical flux model that is complex and flexible enough to capture open-ocean ecosystem dynamics within the euphotic zone, but reduced enough to incorporate into numerical simulations without significant added computational cost. The reduced-order model follows a biological and chemical functional group approach and allows for the development of critical non-Redfield nutrient ratios [71].
Following, the characteristics and equations concerning both the physical and the biological models and how they are coupled will be shown.

2.1 The physical model: POM-1D

The *Priceton Ocean Model* (POM) is a three-dimensional, primitive equations, time-dependent, free surface numerical model for the ocean circulation [8]. POM-1D derives from POM, considering however only the variations over time within a water column.
The turbulent diffusion coefficient are always calculated with a second order closure scheme proposed by Mellor and Yamada [47] and are based on the structure of the vertical density profile and on the wind input, both prescribed [81]. The model, also, adopts the hydrostatic and the Boussinesq approximations.
The following subsections will describe the equations used for the physical forcings and the boundary conditions imposed for the functioning of the model.

2.1.1 POM-1D system of equations

The system of primitive equations that POM-1D solves is shown below [46] [62]:

$$\frac{\partial U}{\partial t} - fV = \frac{\partial}{\partial z}(K_M \frac{\partial U}{\partial z}) + F_x \tag{2.1}$$

$$\frac{\partial V}{\partial t} + fU = \frac{\partial}{\partial z}(K_M \frac{\partial V}{\partial z}) + F_y \tag{2.2}$$

$$\frac{\partial P}{\partial z} = -\rho g \tag{2.3}$$

$$\frac{\partial W}{\partial z} = 0 \tag{2.4}$$

$$\frac{\partial T}{\partial t} = \frac{\partial}{\partial z}(K_H \frac{\partial T}{\partial z}) + m_T \tag{2.5}$$

$$\frac{\partial S}{\partial t} = \frac{\partial}{\partial z}(K_H \frac{\partial S}{\partial z}) + m_S \tag{2.6}$$

In the equations 2.1 and 2.2, U and V (m/s) are the horizontal mean velocity components while $f = 2\Omega \sin\phi$ represents the Coriolis parameter where Ω is the angular velocity of the Earth and ϕ is the latitude.
Equation 2.4 states that W and U, V components are disconnected and that we can impose any field of W from external hypothesis.

T ($^{\circ}C$) and S (psu), in 2.5 and 2.6, indicate the mean temperature and salinity vertical fields, P (N/m^2) is the pressure and ρ (Kg/m^3) is the seawater density (2.3) [81].
K_M and K_H (m^2/s), 2.1, 2.2, 2.5, 2.6, are the turbulent diffusion coefficients for momentum and tracers respectively.
F_x and F_y (m^2/s) are the molecular viscosity terms in momentum equations; m_T and m_S are the molecular diffusivity terms in the temperature and salinity equations.
The molecular viscosity and diffusion terms in the equations 2.1, 2.2, 2.5, 2.6 have been written as follows:

$$F_x = \frac{\partial}{\partial z}(\chi \frac{\partial U}{\partial z}) \tag{2.7}$$

$$F_y = \frac{\partial}{\partial z}(\chi \frac{\partial V}{\partial z}) \tag{2.8}$$

$$m_T = \frac{\partial}{\partial z}(\chi \frac{\partial T}{\partial z}) \tag{2.9}$$

$$m_S = \frac{\partial}{\partial z}(\chi_S \frac{\partial S}{\partial z}) \tag{2.10}$$

Where χ and χ_S (m^2/s) are the background molecular diffusion coefficient.
The vertical viscosity K_M and diffusivity K_H are calculated using the closure hypothesis of Mellor and Yamada [47] as:

$$K_M = qlS_M \tag{2.11}$$

$$K_S = qlS_H \tag{2.12}$$

Where q is the turbulent kinetic energy, l is the turbulent lenght scale, S_M and S_H are stability functions written as:

$$S_H[1-(3A_2B_2+18A_1A_2)G_H] = A_1[1-6\frac{A_1}{A_2}] \tag{2.13}$$

$$S_M[1-9A_1A_2G_H] - S_H[(18A_1^2+9A_1A_2)G_H] = A_1[1-3C_1-6\frac{A_1}{A_2}] \tag{2.14}$$

The coefficients appearing in the above expressions are given as:

$$(A_1, B_1, A_2, B_2, C_1) = (0.92,16.6,0.74,10.1,0.08) \text{ [62]}$$

with

$$G_H = \frac{l^2 g}{q^2 \rho_0} \frac{\partial \rho}{\partial z} \tag{2.15}$$

Which can have a maximum value of 0.028 [46] and where ρ_0 = 1025 $kg\ m^{-3}$ is the reference seawater density and g=9.81 ms^{-2}.
The nonlinear equation of state that relates ρ to T and S is [46]:

$$\begin{aligned}\rho = 999.8 &+ (6.810^{-4} - 9.110^{-3}T + 1.010^{-4}T^2 - 1.110^{-6}T^3 + 6.510^{-}T^4)T \\ &+ (0.8 - 4.110^{-3}T + 7.610^{-5}T^2 - 8.310^{-7}T^3 + 5.410^{-9}T^4)S \\ &+ (-5.710^{-3} + 1.010^{-4}T - 1.610^{-6}T^2)S^1.5 + 4.810^{-4}S^2\end{aligned}$$

Finally, the governing equations solved to obtain the turbulence variables $\frac{q^2}{2}$ and l are:

$$\frac{\partial}{\partial t}(\frac{q^2}{2}) = \frac{\partial}{\partial z}[K_q \frac{\partial}{\partial t}(\frac{q^2}{2})] + K_M[(\frac{\partial U}{\partial z})^2 + (\frac{\partial V}{\partial z})^2] + \frac{g}{\rho_0} K_H \frac{\partial \rho}{\partial z} - \frac{q^3}{B_1 l} \tag{2.16}$$

$$\frac{\partial}{\partial t}(q^2 l) = \frac{\partial}{\partial z}[K_q \frac{\partial}{\partial t}(q^2 l)] + E_1 l K_M[(\frac{\partial U}{\partial z})^2 + (\frac{\partial V}{\partial z})^2] + E_1 l \frac{g}{\rho_0} K_H \frac{\partial \rho}{\partial z} - \frac{q^3}{B_1 l} \tilde{W} \tag{2.17}$$

Where $K_q = kK_H$ is the vertical diffusivity for turbulence variables, k = 0.4 is the von Karman constant, and

$$\tilde{W} = 1 + \frac{E_2 l^2}{k^2}(\frac{1}{|z|} + \frac{1}{|z - H|})^2 \tag{2.18}$$

with (E_1, E_2) = (1.8, 1.33).

In both equations 2.16 and 2.17, the time rate of change of the turbolance quantities is equal to the diffusion of turbolance (the first term on the right-hand side of both equations), the shear and buoyancy turbolence production (second and third terms) and the dissipation (the fourth term) [62].

2.1.2 POM-1D vertical boundary conditions

In the following section will be present the boundary conditions applied to physical forcings in POM-1D [62]:

At the surface (z=0)

$$K_M \frac{\partial \mathbf{U}}{\partial z} = \tau_{\mathbf{w}} \tag{2.19}$$

$$q^2 = B_1^{\frac{2}{3}} \frac{\tau_{\mathbf{w}}}{C_d} \tag{2.20}$$

$$q^2 l = 0 \tag{2.21}$$

At the bottom (z=$-H$)

$$K_M \frac{\partial \mathbf{U}}{\partial z} = \tau_{\mathbf{b}} \tag{2.22}$$

$$q^2 = B_1^{\frac{2}{3}} \frac{\tau_{\mathbf{w}}}{C_b} \tag{2.23}$$

$$q^2 l = 0 \tag{2.24}$$

with the surface wind stress be:

$$\tau_{\mathbf{w}} = (\tau_w^{(x)}, \tau_w^{(y)}) = C_d \mid \mathbf{u_w} \mid \mathbf{u_w} \tag{2.25}$$

where $\mathbf{u_w}$ is the surface wind vector.
C_d is the Drag Coefficient defined as:

$$C_d = [\frac{k}{\ln \frac{z}{z_0}}]^2 \tag{2.26}$$

2.2 The biogeochemical model: BFM17

The *Biogeochemical Flux Model* (BFM) descends from *European Regional Seas Ecosystem Model* (ERSEM) [2] [3] with which it shares characteristics and original formulation. In turn, the BFM17 is a model that was born starting from the full 56-state-variables BFM56 [71].
Like its predecessor, BFM17 follows an approach of both chemical and biological functional groups [71], in which matter is expressed as units of carbon, nitrogen and phosphorus. As can be deduced from its name, BFM17 tracks 17 state variables divided into phytoplankton, zooplankton, dissolved organic matter (DOC), particulate organic matter (POC) and nutrients [62] (Fig. 2.1). The reduction of equations that the model solves, compared to the BFM56, has the purpose of reducing the difficulty of calculation, focusing on an open ocean with a superior thermocline and characterized by non-limiting conditions of neither iron nor silicates. To achieve this, certain processes, such as benthic ones, are not considered, while others are parameterized, i.e. bacterial loop.

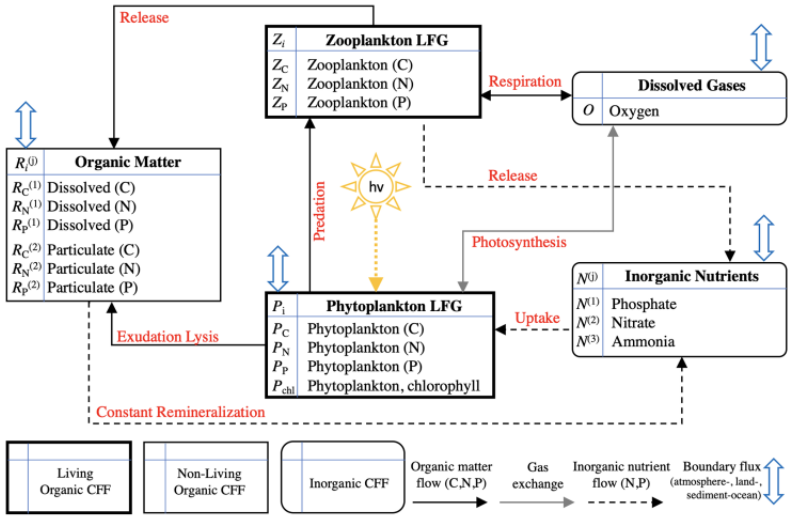

Figure 2.1: Schematic of the 17-state-equation BFM17 model. The dissolved organic matter, particulate organic matter, and living organic matter CFFs are each comprised of three chemical constituents (i.e., carbon, nitrogen, and phosphorus). The living organic CFF is further subdivided into phytoplankton and zooplankton living functional groups (LFGs). [62]

As can be seen from the figure 2.1, Chemical Functional Families (CFF) are divided into living, non-living and inorganic components , while living organic CFFs are used to define the Living Funcitional Groups (LFG) which represent the biomass-based functional prototype of the real organism (Fig. 2.2) [71]. Both CFFs and LFGs are theorethical constructs which allow to relate measurable proprieties of marine biogeochemistry to the state variables used in a deterministic model.

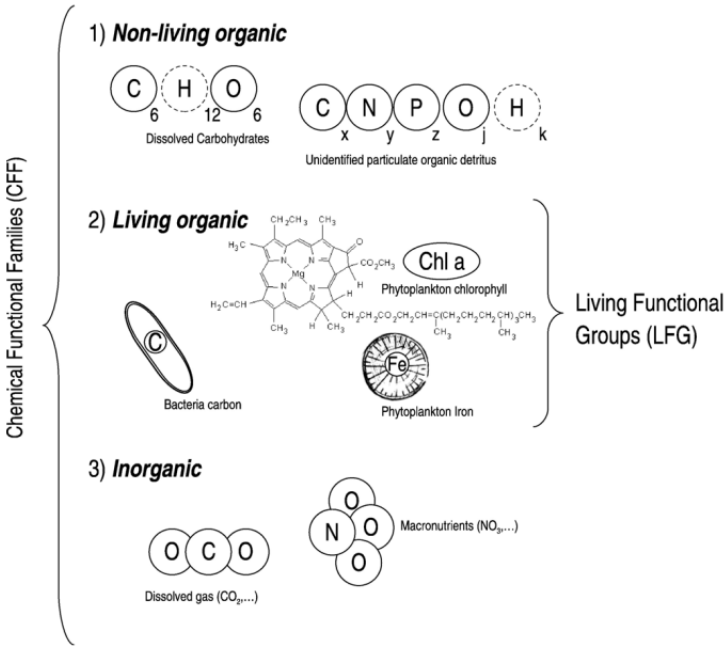

Figure 2.2: Scheme of the various types of Chemical Functional Families (CFF) expressed in terms of basic biogeochemical elements. Living organic CFFs are the basis for the modelling of Living Functional Groups (LFGs).[71]

In BFM17 there are two LFGs (Fig. 2.3), phytoplankton and zooplankton which, compared to the more complex BFM56, represent respectively only the families of flagellates and microzooplankton [62]. The model is used to track chlorophyll, dissolved oxygen, phosphate, nitrate, and ammonium, since their distributions and availability can greatly enhance or hinder important biological and chemical processes: particular interest is focused on dissolved oxygen as, historically, it has always been the most complex to predict with a biogeochemical model. Furthermore, it is also possible to determine the concentrations of dissolved and particu-

late organic matter in order to be able to observe the recycling of nutrients and the export of CO_2 by means of particulate deposition. Finally, as mentioned above, the remineralization processes of the nutrients are obtained by parameterizing the bacterial closure terms.

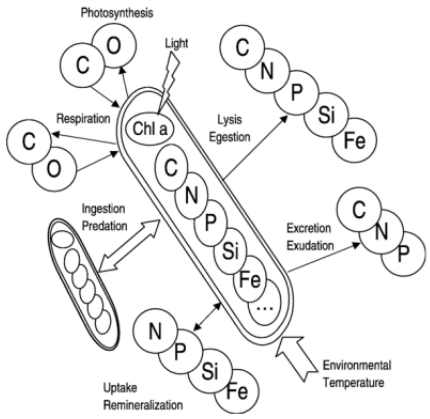

Figure 2.3: Scheme of the standard organism, which is the prototype of any Living Functional Group (LFG), and the physiological/trophic relationships among the Chemical Functional Families and major environmental forcings. [71]

With this kind of approach, all the nutrient:carbon ratios in chemical organic and living functional groups are allowed to vary within their given ranges and each component has a distinct biological time rate of change. This kind of parameterizations are meant to mimic the adaptation of organisms to the diverse availability of nutrients and light observed in the world ocean, and also allow to recycle organic matter along the water column depending on the actual nutrient content [2] [53] [70].
In order to have a clear reading and understanding of the equations that solve the biochemical part of the model, below are the 17 state variables of the BFM17 and the biological/physiological processes that affect them (Fig. 2.4).

Symbol	CFF	Units	Description
P_C	LO	mg C m^{-3}	Phytoplankton carbon
P_N	LO	mmol N m^{-3}	Phytoplankton nitrogen
P_P	LO	mmol P m^{-3}	Phytoplankton phosphorus
P_{chl}	LO	mg Chl *a* m^{-3}	Phytoplankton chlorophyll
Z_C	LO	mg C m^{-3}	Zooplankton carbon
Z_N	LO	mmol N m^{-3}	Zooplankton nitrogen
Z_P	LO	mmol P m^{-3}	Zooplankton phosphorus
$R_C^{(1)}$	NO	mg C m^{-3}	Dissolved organic carbon
$R_N^{(1)}$	NO	mmol N m^{-3}	Dissolved organic nitrogen
$R_P^{(1)}$	NO	mmol P m^{-3}	Dissolved organic phosphorus
$R_C^{(2)}$	NO	mg C m^{-3}	Particulate organic carbon
$R_N^{(2)}$	NO	mmol N m^{-3}	Particulate organic nitrogen
$R_P^{(2)}$	NO	mmol P m^{-3}	Particulate organic phosphorus
O	IO	mmol O_2 m^{-3}	Dissolved oxygen
$N^{(1)}$	IO	mmol P m^{-3}	Phosphate
$N^{(2)}$	IO	mmol N m^{-3}	Nitrate
$N^{(3)}$	IO	mmol N m^{-3}	Ammonium

(a)

Abbreviation	Process
gpp	Gross primary production
rsp	Respiration
prd	Predation
rel	Biological release: egestion, excretion, mortality
exu	Exudation
upt	Uptake
lys	Lysis
syn	Biochemical synthesis
loss	Biochemical loss
nit	Nitrification

(b)

Figure 2.4: (a) Notation used for the 17 state variables in the BFM17 model, as well as the chemical functional family (CFF), units, description,and rate equation reference for each state variable. CFFs are divided into living organic (LO), non-living organic (NO), and inorganic (IO) families [62]; (b) List of all the abbreviations used to indicate the physiological and ecological processes in BFM17 [62]

To use the same notation style used for BFM56 [50],[71],[81], the biological rate of change of a generical state variable C is written as:

$$\left.\frac{\partial C}{\partial t}\right|_{bio} = \sum_{i=1}^{n}\sum_{j=1}^{m}\left.\frac{\partial C}{\partial t}\right|_{V_i}^{e_j} \tag{2.27}$$

where V_i indicates the state variable involved in the considered process (Fig. 2.4 (a)) and e_j rapresents itself the process which is determining the variation (Fig. 2.4 (b)). So, the following subsections will describe, as was previously done with POM-1D, the equations and the boundary conditions regarding the time variation of the 17 state variables of BFM17 due to biological processes.

2.2.1 BFM17 system of equations

Phytoplankoton equations

The phytoplankton LFG in BFM17 is part of the living organic CFF and is composed of separate state variables for the constituents carbon, nitrogen, phosphorous, and chlorophyll, denoted P_C, P_N, P_P and P_{chl} (Fig. 2.4 (a)) [62]:

$$\left.\frac{\partial P_C}{\partial t}\right|_{bio} = \left.\frac{\partial P_C}{\partial t}\right|_{CO_2}^{gpp} - \left.\frac{\partial P_C}{\partial t}\right|_{CO_2}^{rsp} - \left.\frac{\partial P_C}{\partial t}\right|_{R_C^{(1)}}^{lys} - \left.\frac{\partial P_C}{\partial t}\right|_{R_C^{(2)}}^{lys} - \left.\frac{\partial P_C}{\partial t}\right|_{R_C^{(1)}}^{exu} - \left.\frac{\partial P_C}{\partial t}\right|_{Z_C}^{prd} \tag{2.28}$$

$$\left.\frac{\partial P_N}{\partial t}\right|_{bio} = max[0, \left.\frac{\partial P_N}{\partial t}\right|_{N^{(2)}}^{upt} + \left.\frac{\partial P_N}{\partial t}\right|_{N^{(3)}}^{upt}] - \left.\frac{\partial P_N}{\partial t}\right|_{R_N^{(1)}}^{lys} - \left.\frac{\partial P_N}{\partial t}\right|_{R_N^{(2)}}^{lys} - \left.\frac{\partial P_N}{\partial t}\right|_{Z_N}^{prd} \tag{2.29}$$

$$\left.\frac{\partial P_P}{\partial t}\right|_{bio} = max[0, \left.\frac{\partial P_P}{\partial t}\right|_{N^{(1)}}^{upt}] - \left.\frac{\partial P_P}{\partial t}\right|_{R_P^{(1)}}^{lys} - \left.\frac{\partial P_P}{\partial t}\right|_{R_P^{(2)}}^{lys} - \left.\frac{\partial P_P}{\partial t}\right|_{Z_P}^{prd} \tag{2.30}$$

$$\left.\frac{\partial P_{chl}}{\partial t}\right|_{bio} = \left.\frac{\partial P_{chl}}{\partial t}\right|^{syn} - \left.\frac{\partial P_{chl}}{\partial t}\right|^{loss} \tag{2.31}$$

Zooplankton equations

The zooplankton LFG in BFM17 is part of the living organic CFF and is composed of separate state variables for the constituents carbon, nitrogen and phosphorous, denoted Z_C, Z_N, Z_P (Fig. 2.4 (a)) [62]:

$$\left.\frac{\partial Z_C}{\partial t}\right|_{bio} = \left.\frac{\partial Z_C}{\partial t}\right|_{P_C}^{prd} - \left.\frac{\partial Z_C}{\partial t}\right|_{CO_2}^{rsp} - \left.\frac{\partial Z_C}{\partial t}\right|_{R_C^{(1)}}^{rel} - \left.\frac{\partial Z_C}{\partial t}\right|_{R_C^{(2)}}^{rel} \tag{2.32}$$

$$\left.\frac{\partial Z_N}{\partial t}\right|_{bio} = \left.\frac{\partial Z_N}{\partial t}\right|_{P_N}^{prd} - \left.\frac{\partial Z_N}{\partial t}\right|_{R_N^{(1)}}^{rel} - \left.\frac{\partial Z_N}{\partial t}\right|_{R_N^{(2)}}^{rel} - \left.\frac{\partial Z_N}{\partial t}\right|_{N^{(3)}}^{rel} \tag{2.33}$$

$$\left.\frac{\partial Z_P}{\partial t}\right|_{bio} = \left.\frac{\partial Z_P}{\partial t}\right|_{P_P}^{prd} - \left.\frac{\partial Z_P}{\partial t}\right|_{R_P^{(1)}}^{rel} - \left.\frac{\partial Z_P}{\partial t}\right|_{R_P^{(2)}}^{rel} - \left.\frac{\partial Z_P}{\partial t}\right|_{N^{(1)}}^{rel} \tag{2.34}$$

Dissolved organic matter equations

The governing equation for the dissolved organic carbon ($R_C^{(1)}$), nitrogen ($R_N(1)$) and phosphorus ($R_P^{(1)}$) (Fig. 2.4 (a)) [62]:

$$\left.\frac{\partial R_C^{(1)}}{\partial t}\right|_{bio} = \left.\frac{\partial P_C}{\partial t}\right|_{R_C^{(1)}}^{lys} + \left.\frac{\partial P_C}{\partial t}\right|_{R_C^{(1)}}^{exu} + \left.\frac{\partial Z_C}{\partial t}\right|_{R_C^{(1)}}^{rel} - \alpha_{R_C(1)}^{(sink_C)} R_C^{(1)} \tag{2.35}$$

$$\left.\frac{\partial R_N^{(1)}}{\partial t}\right|_{bio} = \left.\frac{\partial P_N}{\partial t}\right|_{R_N^{(1)}}^{lys} + \left.\frac{\partial Z_N}{\partial t}\right|_{R_N^{(1)}}^{rel} - min[0, \left.\frac{\partial P_N}{\partial t}\right|_{N^{(2)}}^{upt} + \left.\frac{\partial P_N}{\partial t}\right|_{N^{(3)}}^{upt}] - \zeta_{N^{(3)}} R_N^{(1)} \tag{2.36}$$

$$\left.\frac{\partial R_P^{(1)}}{\partial t}\right|_{bio} = \left.\frac{\partial P_P}{\partial t}\right|_{R_P^{(1)}}^{lys} + \left.\frac{\partial Z_P}{\partial t}\right|_{R_P^{(1)}}^{rel} - min[0, \left.\frac{\partial P_P}{\partial t}\right|_{N^{(1)}}^{upt}] - \zeta_{N^{(1)}} R_P^{(1)} \tag{2.37}$$

Particulate organic matter equations

The governing equation for the particulate organic carbon ($R_C^{(2)}$), nitrogen ($R_N(2)$) and phosphorus ($R_P^{(2)}$) (Fig. 2.4 (a)) [62]:

$$\left.\frac{\partial R_C^{(2)}}{\partial t}\right|_{bio} = \left.\frac{\partial P_C}{\partial t}\right|_{R_C^{(2)}}^{lys} + \left.\frac{\partial Z_C}{\partial t}\right|_{R_C^{(2)}}^{rel} - \alpha_{R_C(2)}^{(sink_C)} R_C(2) \tag{2.38}$$

$$\left.\frac{\partial R_N^{(2)}}{\partial t}\right|_{bio} = \left.\frac{\partial P_N}{\partial t}\right|_{R_N^{(2)}}^{lys} + \left.\frac{\partial Z_N}{\partial t}\right|_{R_N^{(2)}}^{rel} - \xi_{N^{(3)}} R_N^{(2)} \tag{2.39}$$

$$\left.\frac{\partial R_P^{(2)}}{\partial t}\right|_{bio} = \left.\frac{\partial P_P}{\partial t}\right|_{R_P^{(2)}}^{lys} + \left.\frac{\partial Z_P}{\partial t}\right|_{R_P^{(2)}}^{rel} - \xi_{N^{(1)}} R_P^{(2)} \tag{2.40}$$

Dissolved gas and nutrient equations

The only dissolved gas resolved by BFM17 is oxygen, O (carbon dioxide is treated as an infinite source/sink), and the the dissolved nutrients in the model are phosphate, $N^{(1)}$), nitrate $N^{(2)}$ and ammonium, $N^{(3)}$ 2.4 (a)) [62].

The governing equations for each of these of these variables are:

$$\left.\frac{\partial O}{\partial t}\right|_{bio} = \Omega_C^{(O)}\left[\left.\frac{\partial P_C}{\partial t}\right|_{CO_2}^{gpp} - \left.\frac{\partial P_C}{\partial t}\right|_{CO_2}^{rsp} - \left.\frac{\partial Z_C}{\partial t}\right|_{CO_2}^{rsp} - \alpha_{R_C(1)}^{(sink_C)} R_C^{(1)} - \alpha_{R_C(2)}^{(sink_C)} R_C^{(2)}\right] - \Omega_N^{(O)} \left.\frac{\partial N^{(3)}}{\partial t}\right|_{N^{(2)}}^{nit} \tag{2.41}$$

$$\left.\frac{\partial N^{(1)}}{\partial t}\right|_{bio} = -\left.\frac{\partial P_P}{\partial t}\right|_{N^{(1)}}^{upt} + \zeta_{N^{(1)}} R_P^{(1)} + \xi_{N^{(1)}} R_P^{(2)} + \left.\frac{\partial Z_P}{\partial t}\right|_{N^{(1)}}^{rel} \tag{2.42}$$

$$\left.\frac{\partial N^{(2)}}{\partial t}\right|_{bio} = -\left.\frac{\partial P_N}{\partial t}\right|_{N^{(2)}}^{upt} + \left.\frac{\partial N^{(2)}}{\partial t}\right|_{N^{(3)}}^{nit} \tag{2.43}$$

$$\left.\frac{\partial N^{(3)}}{\partial t}\right|_{bio} = -\left.\frac{\partial P_N}{\partial t}\right|_{N^{(3)}}^{upt} + \zeta_{N^{(3)}} R_N^{(1)} + \xi_{N^{(3)}} R_N^{(2)} + \left.\frac{\partial Z_N}{\partial t}\right|_{N^{(3)}}^{rel} - \left.\frac{\partial N^{(3)}}{\partial t}\right|_{N^{(2)}}^{nit} \tag{2.44}$$

For a complete and detailed description of the variables and coefficients present in the 17 equations above, we recommend reading the article presented by Smith et al. [62].

Below, however, only some of the parameters of the BFM that have been modified for the purposes of this thesis will be shown.

The parameters that have been observed and possibly modified, as will be seen in Chapter 4, are those concerning the main nutrients and particulate matter. In this case, it will be possible to observe the sensitivity of the model to the variation of the relaxation constants for oxygen, nitrate and phosphate and variations of the nitrification and particulate remineralization rates.

Starting from the relaxation constants, they appear within the equation of the bottom boundary condition of the aforementioned nutrients (Eq. 2.54), and their intial values will be shown in the table 2.1.

Secondly, we tried to modify those parameters that play a pivotal role in the nitrification process and therefore in the concentrations of nitrate and ammonium. In the equations 2.43 and 2.44, the nitrification process is parametrized as:

$$\left.\frac{\partial N^{(2)}}{\partial t}\right|_{N^{(3)}}^{nit} = \left.\frac{\partial N^{(3)}}{\partial t}\right|_{N^{(2)}}^{nit} = \Lambda_{N^{(3)}}^{(nit)} f_N^{(T)} f_Z^{(O)} N^{(3)} \tag{2.45}$$

where $\Lambda_{N^{(3)}}^{(nit)}$ is the specific nitrification rate, while the non-dimensional regulation factor for temperature, $f_j^{(T)}$, is given by:

$$f_j^{(T)} = Q_{10,j}^{(T-T^*)/T^*}, j = P, Z \tag{2.46}$$

where T^* is a base temperature and $Q_{10,j}$ is a coefficient that may differ for phytoplakton and zooplankton LFGs. The model, additionally, employs a temperature-dependent nitrification parameter:

$$f_N^{(T)} = Q_{10,N}^{(T-T^*)/T^*} \tag{2.47}$$

Finally, the remineralization processes of the particulate organic matter, due to bacteria activity, are parametrized with three specific remineralization rates: $\alpha_{R_C(2)}^{(sink_C)}$, $\xi_{N^{(1)}}$ and $\xi_{N^{(3)}}$ (rispectively for particulate organic carbon, phosphorus and nitrogen, from equation 2.38 to 2.40).
Below, a summary table is provided which shows the values, units and descriptions of the parameters presented with the equation of the BFM17 (Tab. 2.1).

Table 2.1: Notation initial values of nutrients and particulate matter parameters. Note that those that have been modified during the experimental simulations are highlighted in red.

Symbol	Value	Units	Description
λ_O	0.06	md^{-1}	Relaxation constant for oxygen at bottom
$\lambda_{N^{(1)}}$	0.06	md^{-1}	Relaxation constant for phosphate at bottom
$\lambda_{N^{(2)}}$	0.06	md^{-1}	Relaxation constant for nitrate at bottom
$\alpha_{R_C(2)}^{(sink_C)}$	0.1	d^{-1}	Specific remineralization rate of particulate carbon
$\xi_{N^{(1)}}$	0.1	d^{-1}	Specific remineralization rate of particulate phosphorus
$\xi_{N^{(3)}}$	0.1	d^{-1}	Specific remineralization rate of particulate nitrogen
$\Lambda_{N^{(3)}}^{(nit)}$	0.01	d^{-1}	Specific nitrification rate at 10°C
$\Omega_C^{(O)}$	12.0	$mmolO_2mgC^{-1}$	Stoichiometric coefficient for oxygen reaction
$\Omega_N^{(O)}$	12.0	$mmolO_2mmolN^{-1}$	Stoichiometric coefficient for nitrification reaction

In conclusion, the boundary conditions of the 17 state variables of BFM17 will be shown in the next subsection, as they take into account the overall coupling equation between the physical and biogeochemical parts.

2.3 The coupled model: BFM17-POM1D

2.3.1 The total BFM17-POM1D equation

The coupled BFM17-POM1D model is a time-depth model that integrates in time the generic equation for all biological state variables [62]. This total time dipendent rate of change for a generic LFG or CFF (A_j) can be written as follow:

$$\frac{\partial A_j}{\partial t} = \left.\frac{\partial A_j}{\partial t}\right|_{bio} + \left.\frac{\partial A_j}{\partial t}\right|_{phys} \tag{2.48}$$

where the first term of the equation right hand side indicates the rate of change dependent on the biogeochemical processes (handled by BFM), while the second term indicates the rate of change dependent on the physical processes (handled by the BFM-POM1D coupling) [81].
So, the total coupled equation is a typical "advection, diffusion, reaction" equation [33] written as:

$$\frac{\partial A_j}{\partial t} = \left.\frac{\partial A_j}{\partial t}\right|_{bio} - [W + W_E + \nu^{(set)}]\frac{\partial A_j}{\partial z} + \frac{\partial}{\partial z}(K_H \frac{\partial A_j}{\partial z}) \tag{2.49}$$

the first term on thr right hand is a source/sink term due to biological and chemical reactions (eqs. from 2.28 to 2.44), W and W_E are the vertical velocities due to large scale circulation and mesoscale eddies, $\nu^{(set)}$ is the sinking velocity and K_H is the vertical eddy diffusivity [62].

2.3.2 The BFM17-POM1D flow-chart

The time evolution of physical variables (U, V, T, S, ρ, q^2/l and l) is managed by the POM1D component of the modeling system, in order to compute the turbulent diffusivity term K_H appearing in the equation 2.49, and transferred to BFM [63]. For the purposes of this thesis, the model was run in a diagnostic mode, which means that vertical temperature and salinity profiles are prescribes and imposed from given climatological monthly profiles obtained from different data sources [6] [50] [62].
The flow of information that occurs between the components of the system model is schematized in Fig. 2.5

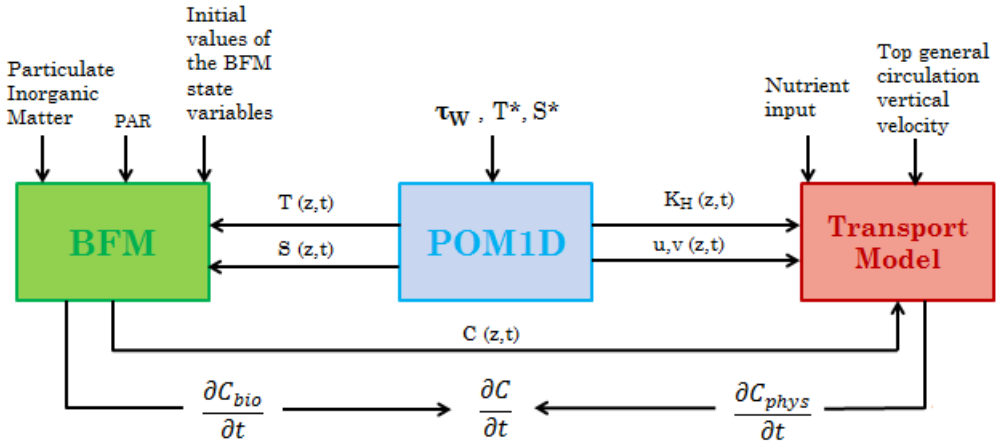

Figure 2.5: Scheme of the information flow between the ocean model and the biogeochemical state variables. Note that in this picture C rapresents the A_j variable in 2.49.

The initial conditions that the diagnostic BFM17-POM1D requires are the temperature and salinity climatologies (T^* and S^* in the figure), the wind stress (τ_w), the general circulation vertical velocity, the fraction of sunlight between 400 and 700 nm (PAR) and, finally, the initial vertical profiles of nutrients and the values of each biochemical state variable of the BFM17, included particulate inorganic matter.

2.3.3 BFM17 vertical boundary conditions

Now that the total coupled equation has been written (2.49), it's possible to finally define the boundary conditions for the 17 state variables of BFM17 (eqs. from 2.28 to 2.44).

For every variable A_j, except the oxygen, the surface boundary condition ($z = 0$)is:

$$K_H \frac{\partial A_j}{\partial z} = 0 \tag{2.50}$$

while for the oxygen, O, the boundary condition is:

$$K_H \frac{\partial O}{\partial z} = \Phi_0 \tag{2.51}$$

where Φ_0 is the air-sea interface flux of oxygen computed by Wanninkhof [73] [74].
At the bottom vertical open boundary, supposed to be at ($z = -150m$), we imposed different conditions depending on the biochemical tracer.
So, for phytoplankton, zooplankton, dissolved and particulate organic matte, it is:

$$K_H \frac{\partial A_j}{\partial z} = 0 \tag{2.52}$$

Integrating equation 2.49 over the water cokumn depth (H), neglecting the bio-geochemical contributions and and using the equation 2.52, yelds:

$$\frac{\partial}{\partial z} \int_{-H}^{0} A_j dz = \left[W + W_E + \nu^{(set)} \right] A_j \Big|_{z=-H} \tag{2.53}$$

with $|W + W_E| < |\nu^{(set)}|$ resulting in a negative rate of change in the integrated scalar A_j [62].
For oxygen, phosphate and nitrate, the bottom boundary condition is:

$$K_H \left. \frac{\partial A_j}{\partial z} \right|_{z=-H} = \lambda_j (A_j \big|_{z=-H} - A_j^*) \tag{2.54}$$

where λ_j is the relaxation velocity, and A_j^* is the observed-at-bottom boundary climatologies field data [62].
Finally, since observations of ammonium concentration in the observed area are not availeble, it was chosen to assume that nitrogen dissufive flux, from depth to the equophotic zone, occours mostly in form of nitrate flux [62]. So, to conclude, the bottomom boundary condition for ammonium is:

$$K_H \left. \frac{\partial N^{(3)}}{\partial z} \right|_{z=-H} = 0 \tag{2.55}$$

Chapter 3

Initialization, forcing and control simulation experiment

In this chapter we will provide a description of the characteristics of the data used and finally the control simulation experiment, obtained by carrying out a simulation experiment of the model in the BATS coordinate point, will be shown.

3.1 Observation and model datasets

3.1.1 CMEMS

Copernicus is the European Union's Earth observation program, looking at our planet and its environment: it offers information services that draw from satellite Earth Observation and in-situ (non-space) data [15]. Copernicus is subdivided into six thematic streams of services: *Copernicus Atmosphere Monitoring Service* (CAMS), *Copernicus Land Monitoring Service* (CLMS), *Copernicus Marine Environment Monitoring Service* (CMEMS), *Copernicus Climate Change Service* (C3S), *Copernicus service for Security applications* and *Copernicus Emergency Management Service* (Copernicus EMS).
For the purposes of this thesis we have focused on the use of CMEMS.
CMEMS is the marine component of the Copernicus: it provides free, regular and systematic authoritative information on the state of the ocean. This data covers analysis of the current situation, forecasts of the situation a few days in advance and the provision of retrospective data records (re-analysis). CMEMS calculates and provides products describing currents, temperature, wind, salinity, sea level, sea ice and biogeochemistry [16], to support several marine applications such as marine resources and sefety, coastal environment, weather and seasonal ocean forcasting.
The CMEMS data were used in several experiments by setting the initial conditions of the temperature and salinity model. Specifically, the file from which the initial profiles of T and S were extracted is *GLOBAL-REANALYSIS-PHY-001-031* (Tab. 3.1).
As specified above, only the temperature and salinity values were taken from here: the first 150 m of the water column (depth range on which we focused for the simulations), then averaged monthly, for the year 2014 (Gonzalo passed in October 2014), from a square around the coordinates of Gonzalo maximum intensity point (25.6°N, -68.7°W).

3.1.2 ECMWF

European Centre for Medium-Range Weather Forecasts (ECMWF) has three main missions: produce numerical weather forecasts and monitor the Earth system, carry out scientific and technical research to improve forecast skill and, finally, maintain an archive of meteorological data [20].

Table 3.1: General informations GLOBAL-REANALYSIS-PHY-001-031: summary of the main features of the global reanalysis product

Product	**Values**
Total geographical coverage	[-180,180]°E ; [-89,90]°N
Variables	T, S, u_{10}, v_{10}, SSH, mixed layer depth
Availeble time series	From January 1993 and regularly uodated
Reanalysis model	NEMO
Temporal resolution	3D daily avarage fields
Horizontal resolution	0.25°
Geographical area considered	[-69,-67]°W ; [24,26]°N
Number of vertical levels	75

The ECMWF data used are hourly analysis data of the horizontal wind components, taken directly from *Meteorological Archival and Retrieval System* (MARS) (Table 3.2).

Table 3.2: General informations of ECMWF data from MARS: summary of the main features of the analysis product

Product	**Values**
Variables	u_{10}, v_{10}
Period of the time series	from 01/01/2014 to 31/12/14
Temporal resolution	6 h
Horizontal resolution	0.1°
Geographical area considered	[-70,-55]°W ; [20,35]°N

The horizontal wind components (u_{10} and v_{10}) were first averaged daily and then monthly to be, finally, used to compute the wind stress components (τ_x and τ_y) needed to define the initial conditions of the wind input for the model.

3.1.3 GOFS16

The *Global Ocean Forcasting System* (GOFS16) is an operational ocean analysis and forcast system that runs daily at the *Euro-Mediterranean Centre on Climate Change* (CMCC) [35], since 2017. GOFS16 produces 7-day forcasts of the state of the global ocean and sea ice: three-dimensional ocean temperatures, salinities and currents, as well as sea ice thickness, concentration and drift. The system is based on a global eddying ocean [34], combined with a state-of-the-art data assimilation system, OceanVar, capable of assimilating all high resolution space-borne and conventional observing networks, including hydrographic profiles and several satellite data. The CMCC data (Tab. 3.3) have been used to simulate the hurricane impact on the ocean ecosystem. In order to achieve this goal, we tried to insert a vertical velocity profile given from another hurricane which passed in the same area some years after Gonzalo's passage, hurricane José.

Table 3.3: General informations of CMCC data from GFOS16: summary of the main features of the product

Product	**Values**
Variables	W
Period of the time series	from 2017 to 2019
Temporal resolutions	daily, monthly mean, 3 years monthly mean
Horizontal resolution	1/16° at the equator increasing polarward
Reanalysis model	NEMOv3.4-LIM2
Number of vertical levels	98

Finally, a fundamental consideration must be made: in the process of preparation of the data (for T, S, τ_x and τ_y), averages were performed to which, then, the temporal interpolation scheme of the Killworth forcing was applied [38].
This is of primary importance because, especially when considering monthly mean data as forcing for a whole month, there are several potential errors in the estimation of forcing flows: for example, as regards the temperature, there is an obvious trend to remove phenomena of extreme heating or cooling of the surface; while as far as wind stress is concerned, there are brutal changes that can generate unwanted inertial oscillations [38].
In order to avoid this type of system perturbation error, the Killworth algorithm has been applied, considering all the months of 30 days, as wastily requested by the BFM17-POM1D.

3.2 Control simulation experiment: BFM17-BATS

To obtain a validation field capable of correctly calibrating the subsequent experiments, the first objective was to recreate the conditions proposed by Smith et al. [62], who tested the BFM17-POM1D model using data fields taken in two sites of the Sargasso Sea, BATS and BTM, both subject to the action of the North Atlantic subtropical gyre.
The *Bermuda Atlantic Time-series Study* (BATS) and the *Bermuda Testbed Mooring* (BTM) are both part of the *US Joint Global Ocean Flux Study* program (JGOFS), which collect data,rispectivly, since 1988 and 1994.

The region encompassing BATS and BTM is an open-ocean oligotrophic regime, phosphate limited, with a non-Redfield ratio of the chemical compounds [62] [64]. It has been used also in this thesis as target field of the simulations and also to define the initial and boundary conditions for BFM17-POM1D.
As specified in Chapter 2, the physical model uses prescribed temperature and salinity, as well as wind stress components, to calculate the density profile and turbulent variables of viscosity and diffusivity. In this simulation, the general circulation vertical velocity, W, and the mesoscale eddy velocity, W_E, have been adapted and imposed, assuming that they are zero at the surface, and then reach their maximum at the base of the Ekman layer (which acts as boundary bottom for this job) [6] [62].
The general large-scale upwelling or downwelling circulation is due to Ekman pumping as showed below:

$$W = \hat{\mathbf{k}} \cdot \nabla \times (\frac{\tau_{\mathbf{w}}}{\rho f}) \tag{3.1}$$

where $\hat{\mathbf{k}}$ denotes the unit vector in the vertical direction and $\nabla \times \tau_{\mathbf{w}}$ is the wind stress curl, which was taken from the Scatterometer Climatology of Ocean Winds database [58].
The mesoscale eddy volocity, W_E is an additional positive upwellling vertical velocity introduced to take into account the mesoscale eddies [32] that, tipically, influence the BATS/BTM region which can provide am episodic upwelling of nutrients to the upper water column [62]. As W, also W_E is zero at the surface and has a maximum magnitude at the Ekman depth.

Next, will be shown the profiles of the physical forcings that during the different simulations of this thesis have been modified, as initial conditions, to test the goodness and sensitivity with which the model shows the variations of the marine ecosystem (Fig. 3.1).

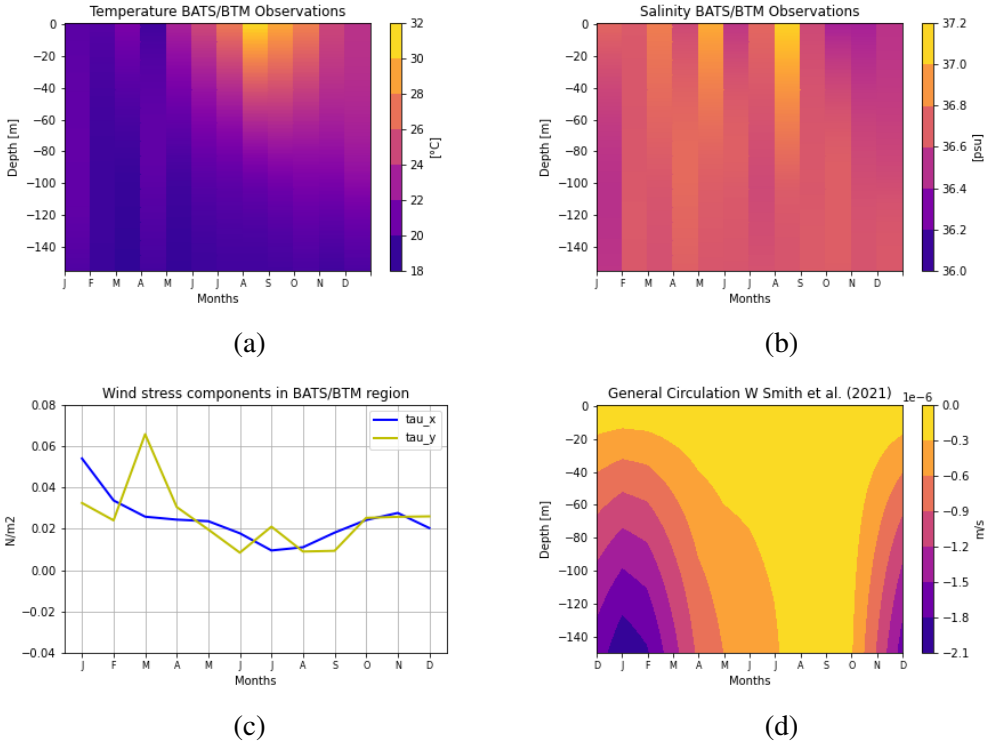

Figure 3.1: (a) Temperature profile at BATS/BTM region ; (b) Salinity profile at BATS/BTM region; (c) Wind stress components at BATS/BTM region; (d) General circulation vertical velocity at BATS/BTM region

The control experiment (hereinafter *BFM17-BATS*) uses the BATS/BTM biogeochemical data as initial condition, surface and bottom boundary conditions, trying to reproduce the interior water column field of figure 3.1. Note that BFM17-POM1D considers each month as 30 days, so in one year there are 360 days and in five years there are 1800 days. Here (Fig. 3.2), the nutrient profiles will be shown only in the last year of the simulation, where it is assumed that the dynamics of the model have reached a stable situation.

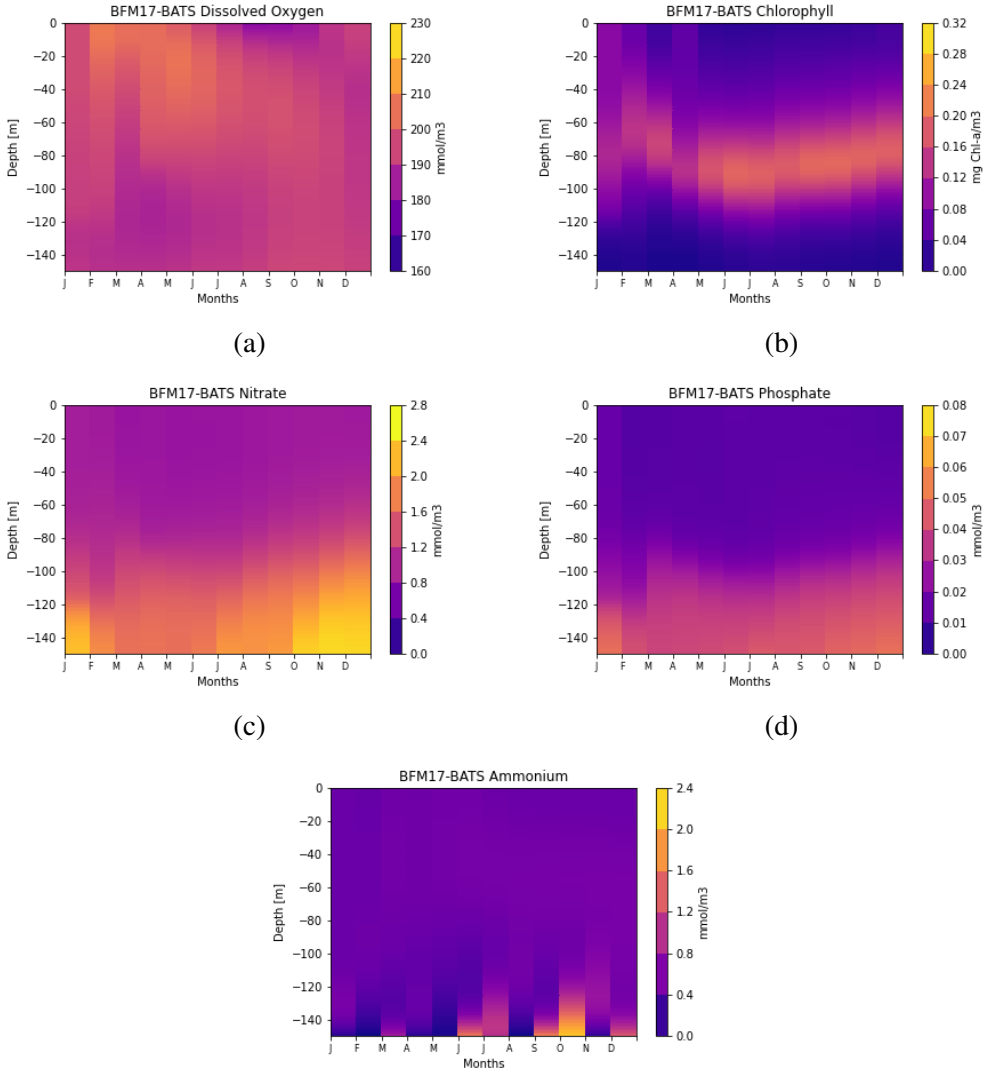

Figure 3.2: BFM17-POM1D concentration results for the simulation BFM17-BATS: (a) Dissolved Oxygen, (b) Chlorophyll, (c) Nitrate, (d) Phosphate and (e) Ammonium

Chapter 4

Numerical experiments with coupled physical-biogeochemical model

This chapter will be divided into three sections showing the three major parts of the work done. First of all, BFM17 will be implemented in a different position, the maximum intensity Gonzalo hurricane position (hereinafter G.P.), described oreviously and compared to the BATS/BTM control experiment. Secondly, model parameter sensitivity experiments will be carried out at G.P. and lastly the hirricane conditions will be imposed and the biogeochemical changes discussed.

4.1 Comparison of BFM17-POM1D between BATS and G.P.

The G.P. point is located at southwest of the location of the BATS station (Fig. 4.1). The experiments performed are summarized in the Table 4.1.

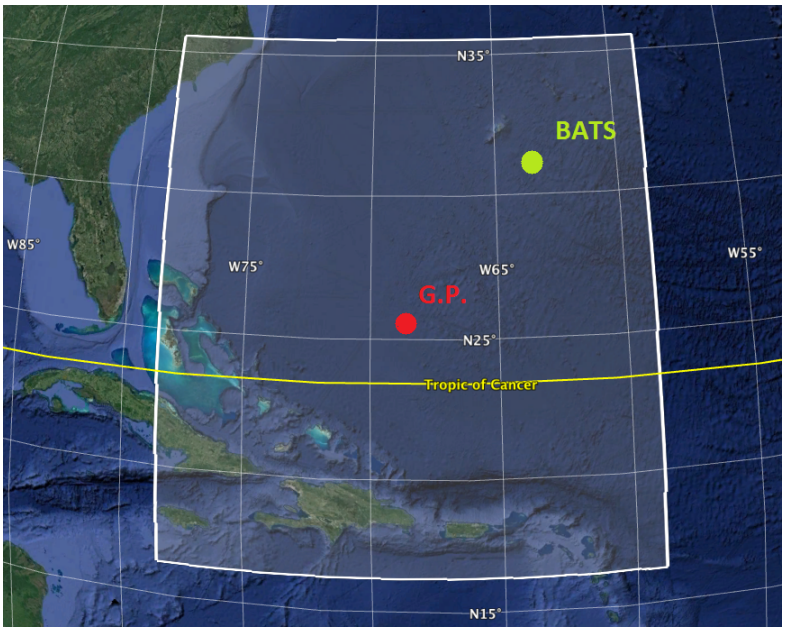

Figure 4.1: Location of the BATS station (green dot) and G.P. (red dot) whitin the considered domain

Table 4.1: Experiments changing the location of the model from Bermuda (BATS) to southwestern position (G.P.)

Name	**Specified T and S profiles**	**Wind stress components**	**W analytical profile from 20 yrs data**
BFM17-BATS	BATS/BTM Obs.	BATS/BTM Obs.	BATS/BTM Obs.
BFM17-BS0	CMEMS Reanalysis	BATS/BTM Obs.	BATS/BTM Obs.
BFM17-BS01	BATS/BTM Obs.	ECMWF Analysis at BATS	BATS/BTM Obs.
BFM17-BS1	CMEMS Reanalysis	ECMWF Analysis at G.P.	BATS/BTM Obs.

While the experiment BFM17-BATS was already shown in Chapter 3, here we are going to present the model inputs that have been changed in these experiments, as reported in Table 4.1.

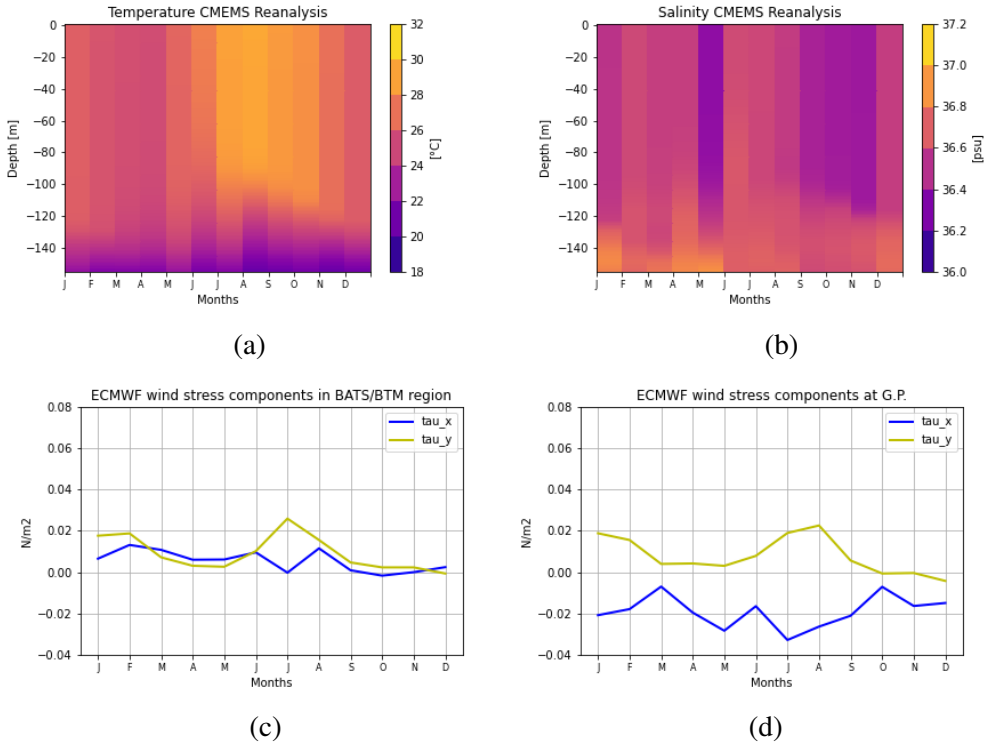

Figure 4.2: (a) Temperature profile from CMEMS Reanalysis ; (b) Salinity profile from CMEMS Reanalysis; (c) Wind stress components at BATS/BTM region from ECMWF data; (d) Wind stress components at G.P. from ECMWF data

As can be seen by comparing the figures 3.1 and 4.2, there are many differences between the inputs used in these experiments; and this is also reflected in some results of the various simulations (Fig. 4.3-4.5).
So, from the comparison of the three sequences of results can be deduced that the change in position in which the simulation is performed affects the dynamics of the ocean nutrients, especially on the basis of which forcing we are going to vary.

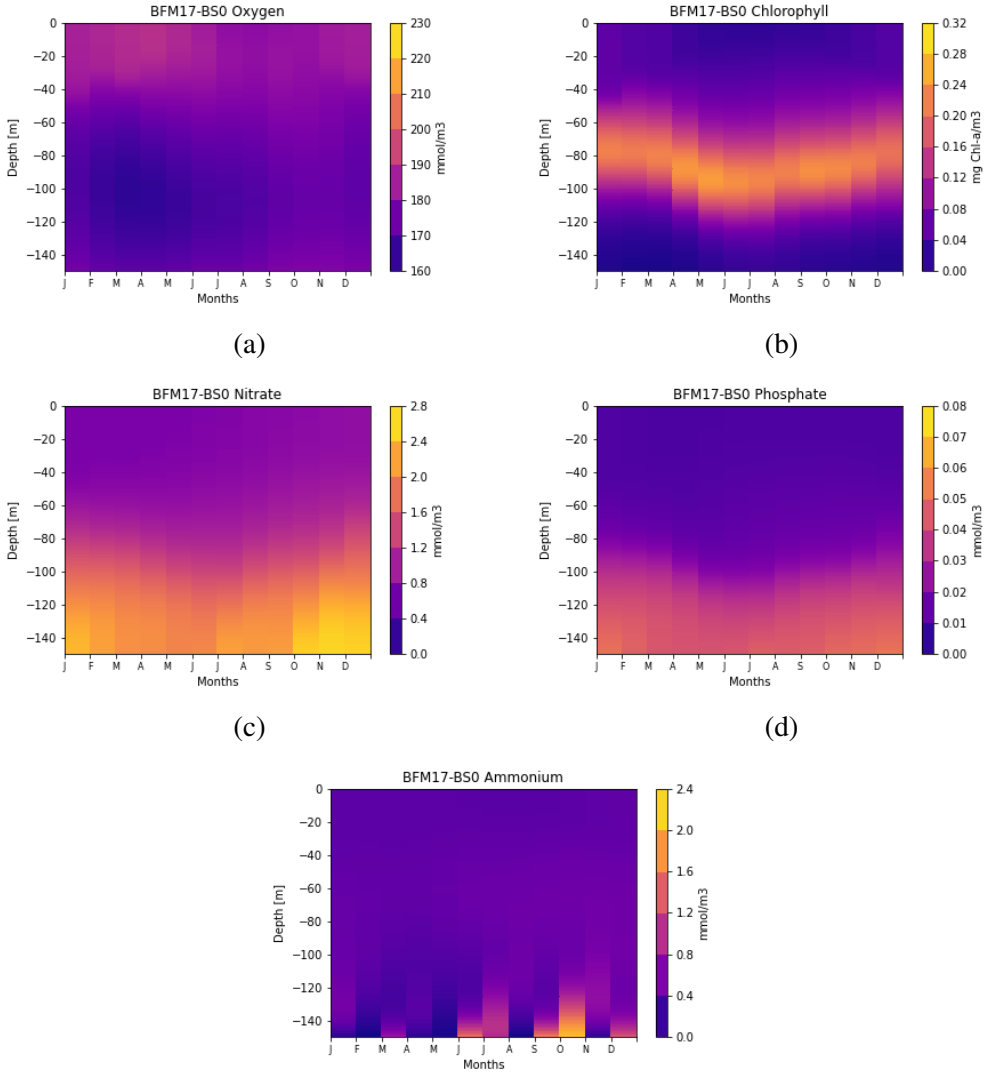

Figure 4.3: BFM17-POM1D concentration results for the last year of simulation BFM17-BS0: (a) Dissolved Oxygen, (b) Chlorophyll, (c) Nitrate, (d) Phosphate and (e) Ammonium

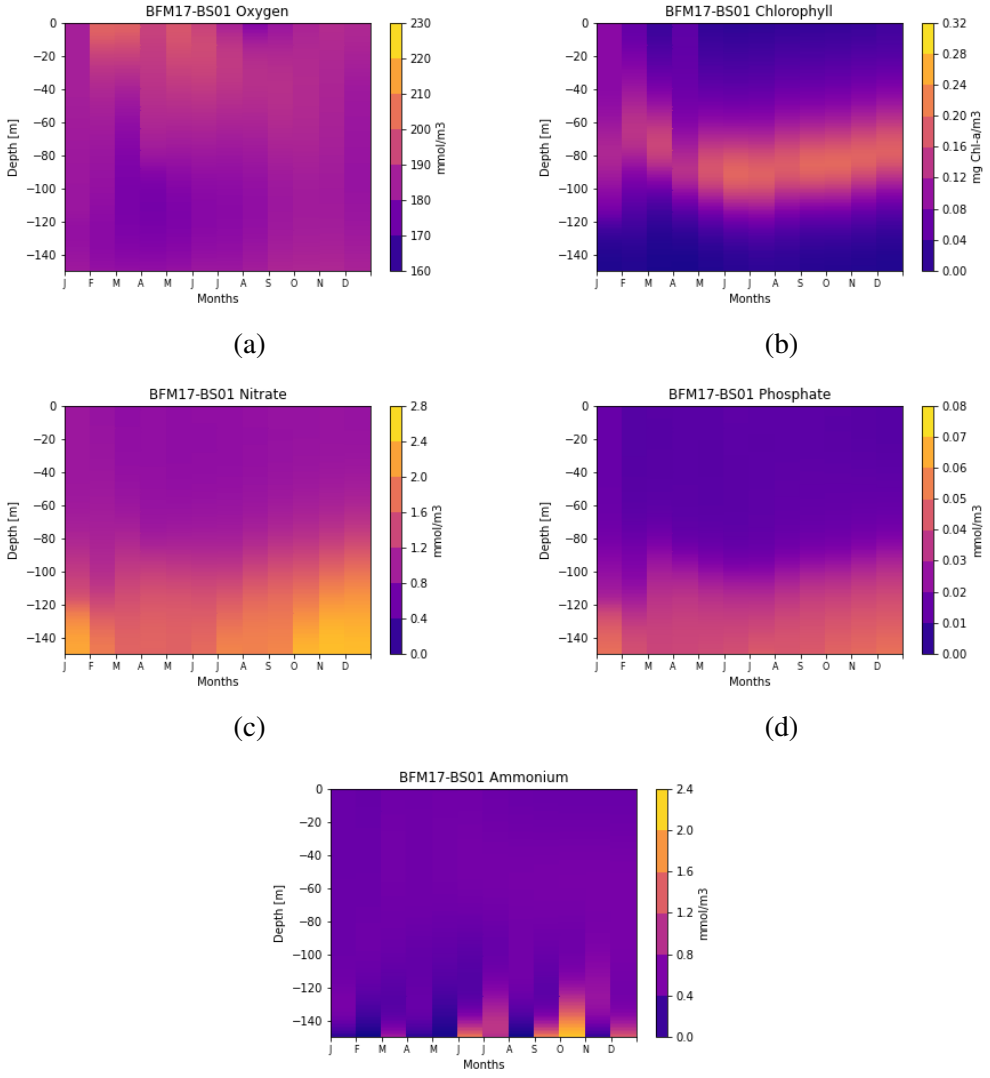

Figure 4.4: BFM17-POM1D concentration results for the last year of simulation BFM17-BS01: (a) Dissolved Oxygen, (b) Chlorophyll, (c) Nitrate, (d) Phosphate and (e) Ammonium

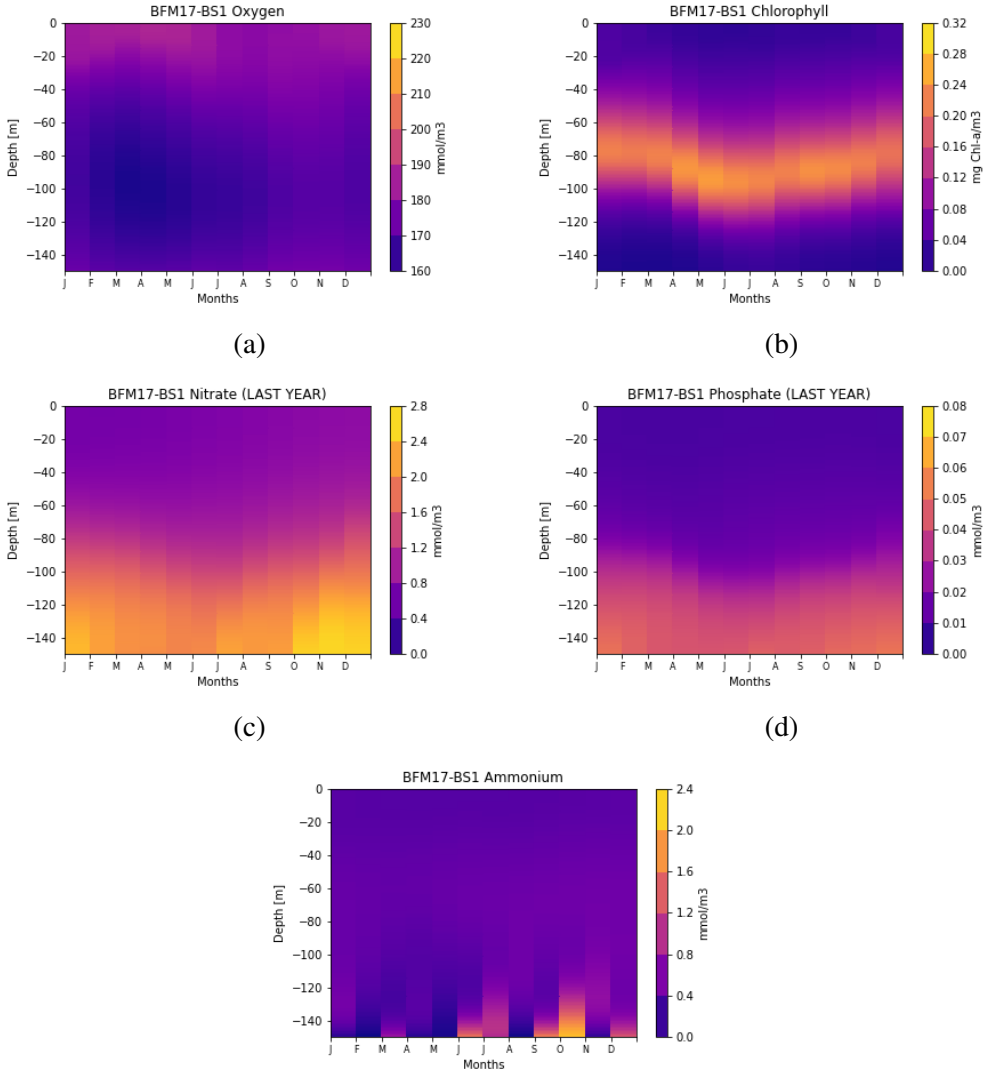

(a) (b) (c) (d) (e)

Figure 4.5: BFM17-POM1D concentration results for the last year of simulation BFM17-BS03: (a) Dissolved Oxygen, (b) Chlorophyll, (c) Nitrate, (d) Phosphate and (e) Ammonium

Comparing the observations resulting from these first three experiments, we see a

great similarity in the results between BFM17-BS0 and BFM17-BS1 compared to BFM17-BS01 which, however, presents profiles with ranges of values much more similar to those of our validation field, BFM17-BATS. Looking, for example, at oxygen and comparing the various profiles ((a) in figures 4.3-4.5), it can be seen that the change in temperature and salinity has a much greater influence than the wind: this may be attributed to the fact that the exchange of oxygen between ocean and atmosphere is parameterized within the flow defined by Wanninkhof [73] [74]. In fact, in the Wanninkhof parametrization the oxygen flux is defined as:

$$\Phi_0 = k(C_W - C_a) \tag{4.1}$$

where C_W and C_a are, respectively, the concentration in the bulk liquid and at the top of the liquid boundary layer adjacent to the atmosphere [74]. k, the gas transfer velocity, is directly proportional to the square of the 10 m wind components and inversely proportional to the square root of the Schmidt number which is a polynomial function that depends on the temperature, defined as:

$$Sc = A - BT + CT^2 - DT^4 \tag{4.2}$$

where $A = 1953.4$, $B = 128$, $C = 3.99$ $D = 0.05$ [73]. So, as it is possible to deduce by comparing the temperature profiles in figures 3.1 and 4.2 , in which it can be seen that for almost the whole year, in the case of CMEMS reanalyses, there are values of T greater than the BATS profile, that brings consequentially to lower values of oxygen, which leads to the conclusion that a variation of temperature affects more than the modification of the wind stress components.

4.2 Sensitivity experiments at G.P.

In this section, we want to show the results obtained by modifying some parameters that regulate certain biochemical processes (in red in Table 2.1), focusing only on the Gonzalo area and using a new vertical velocity profile.

The carried out experiments with each characteristic rates are summarized in the Table 4.2.

Table 4.2: Sensitivity experiments at Southwestern G.P.

Name	**T and S profiles**	**Wind stress components**	**W profile**	**Notes**
BFM17-BS03	*CMEMS Reanalysis*	*ECMWF Analysis at G.P.*	GOFS16	-
BFM17-BS03.01	*CMEMS Reanalysis*	*ECMWF Analysis at G.P.*	GOFS16	$Wx0.1$
BFM17-BS03.02	*CMEMS Reanalysis*	*ECMWF Analysis at G.P.*	GOFS16	$Wx0.1$ $\lambda_j = 0.2$
BFM17-BS03.03	*CMEMS Reanalysis*	*ECMWF Analysis at G.P.*	GOFS16	$Wx0.1$ $\lambda_j = 0.2$ $\Lambda_{N^{(3)}} = 0.001$
BFM17-BS03.04	*CMEMS Reanalysis*	*ECMWF Analysis at G.P.*	GOFS16	$Wx0.1$ $\lambda_j = 0.2$ $\Lambda_{N^{(3)}} = 0.001$ $\alpha_{R_C^{(2)}}^{(sinkC)}$, $\xi_{N^{(1)}}$, $\xi_{N^{(3)}} = 0.01$

Considering that T, S and τ_W profiles have been already shown (Fig. 4.2), here we want to present the general circulation verical velocity profiles (W) that have been chaneged in these experimens.

Let's start showing the monthly mean vertical profiles of W used in the validation experiment, which is the same of the one used for all the simulations in Table 4.1, and the ones obtained from GOFS16 data (Fig. 4.6).

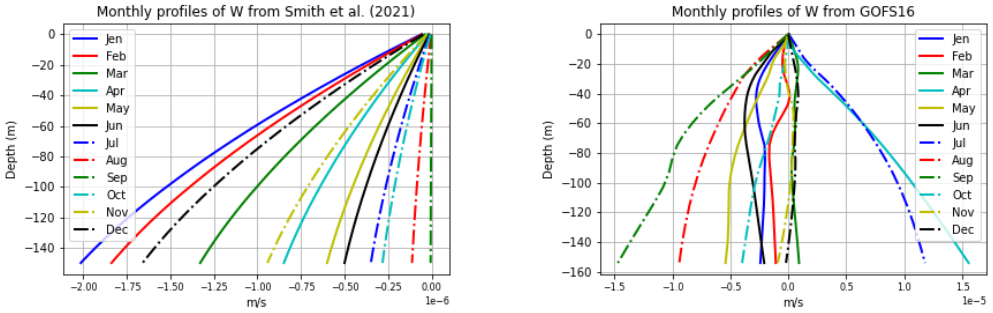

(a) (b)

Figure 4.6: Comparision between the monthly mean vertical profiles obtained from: (a) 20 years BATS/BTM observations [62] and (b) 3 years GOFS16 data

Here can be seen that W is quite different between BFM17-BATS and G.P. First, there is an order of magnitude of difference between the idialized W chosen for BATS/BTM [6] and the GOFS16 data; moreover, while the profile used for the first class of experiments is obtained starting from monthly averages of a 20-year climatology of the wind stress curl and then adapted according to Bianchi et al. [6], with values of zero at the surface, maximum at the bottom and all negative, the monthly profiles of GOFS16, instead, are the result of a reanalysis of only three years (2017-2019) and also show positive values.
So, after the experiment BFM17-BS03, where we use the pure GOFS16 values, we changed W in order to have, at least, the same order of magnitude of the previous experiments. The results of the simulation are presented in figures 4.7 - 4.16 where first are shown the 5 year simulation results, and then there are only the last year monthly mean profiles. Note that the red vertica lines are indicating the end of each simulation year.

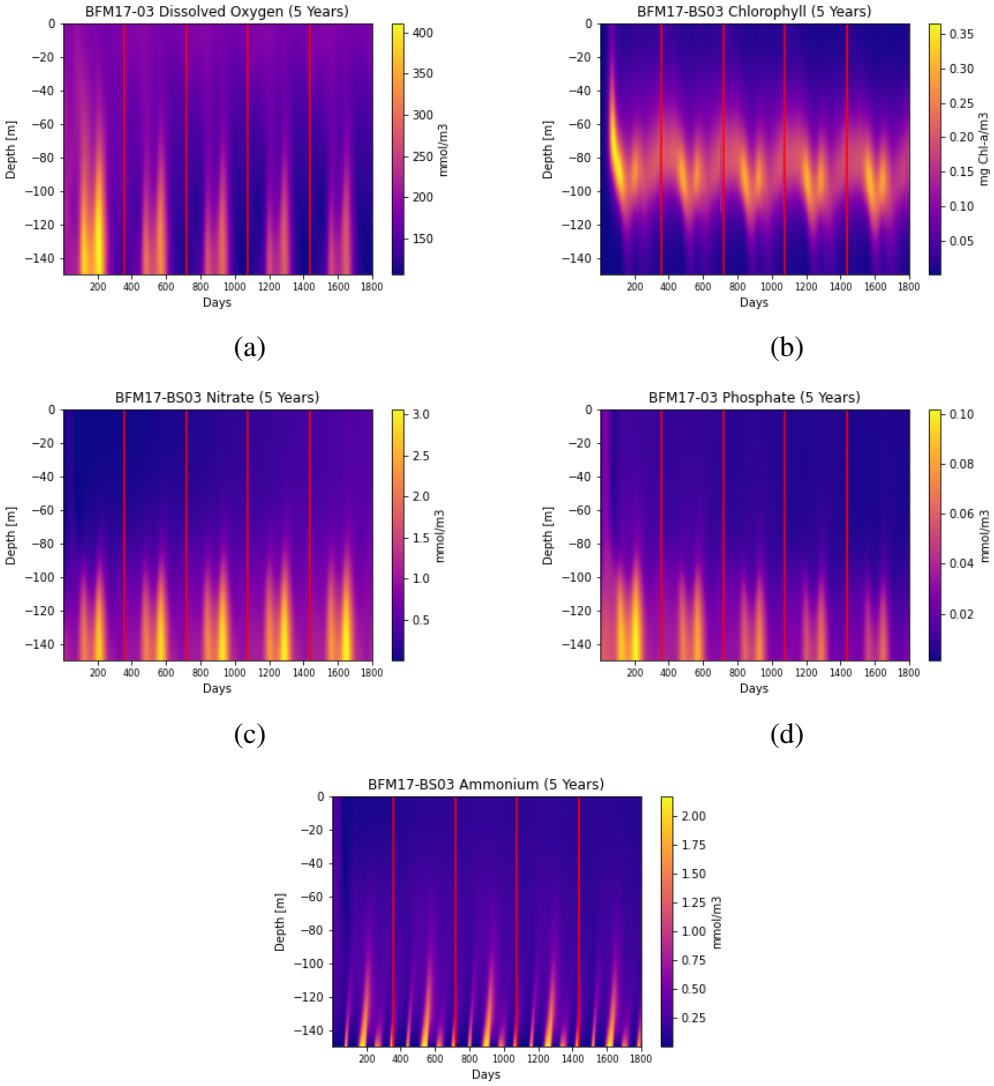

Figure 4.7: BFM17-POM1D 5 years concentration results for the simulation BFM17-BS03: (a) Dissolved Oxygen, (b) Chlorophyll, (c) Nitrate, (d) Phosphate and (e) Ammonium

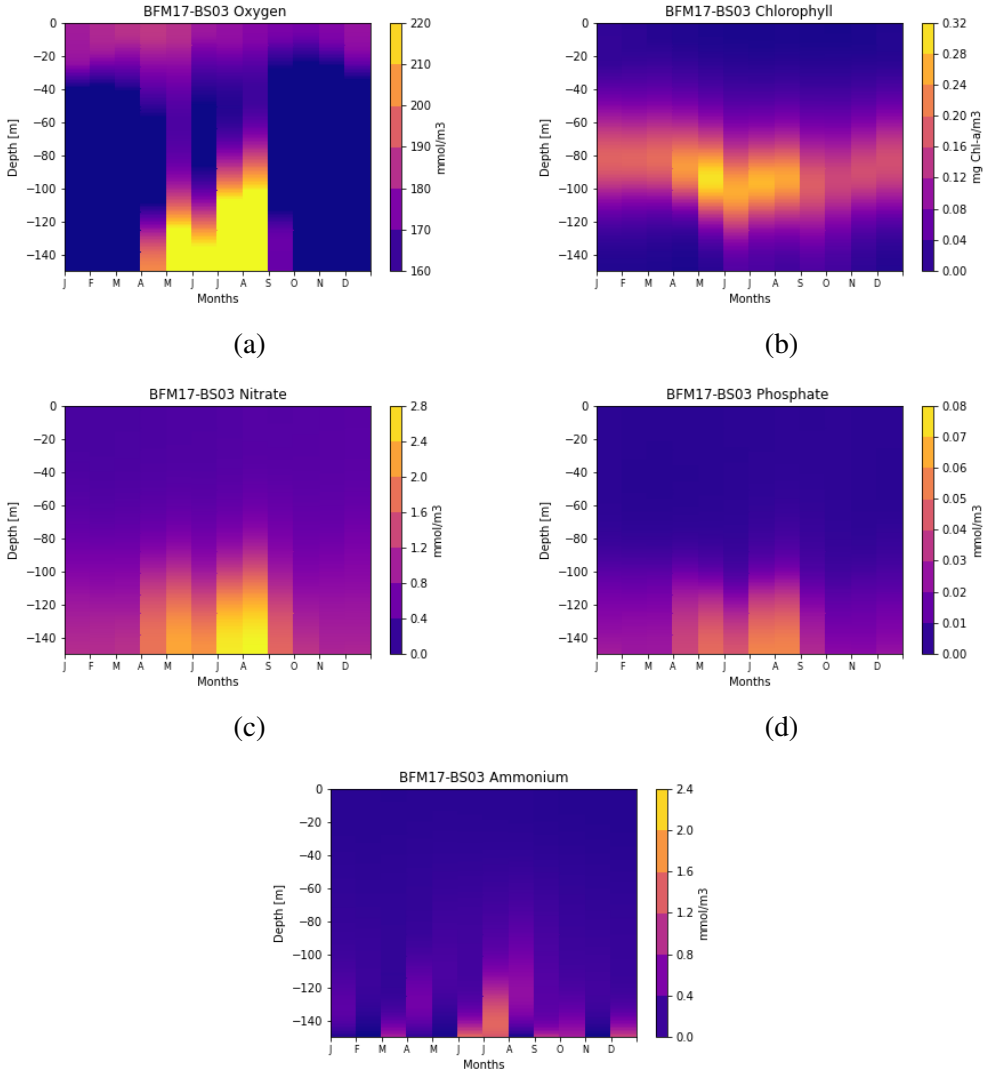

(a) (b)

(c) (d)

(e)

Figure 4.8: BFM17-POM1D last year concentration results for the simulation BFM17-BS03: (a) Dissolved Oxygen, (b) Chlorophyll, (c) Nitrate, (d) Phosphate and (e) Ammonium

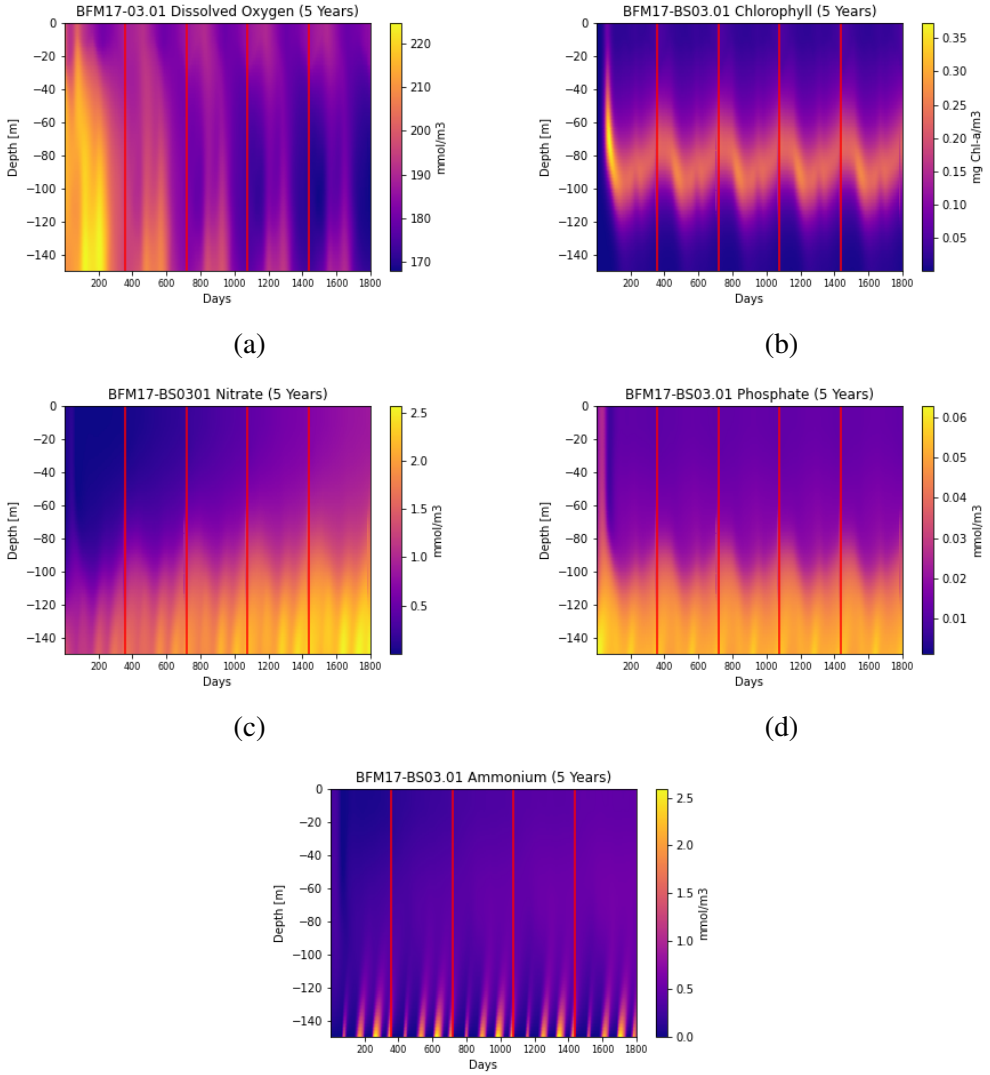

Figure 4.9: BFM17-POM1D 5 years concentration results for the simulation BFM17-BS03.01: (a) Dissolved Oxygen, (b) Chlorophyll, (c) Nitrate, (d) Phosphate and (e) Ammonium

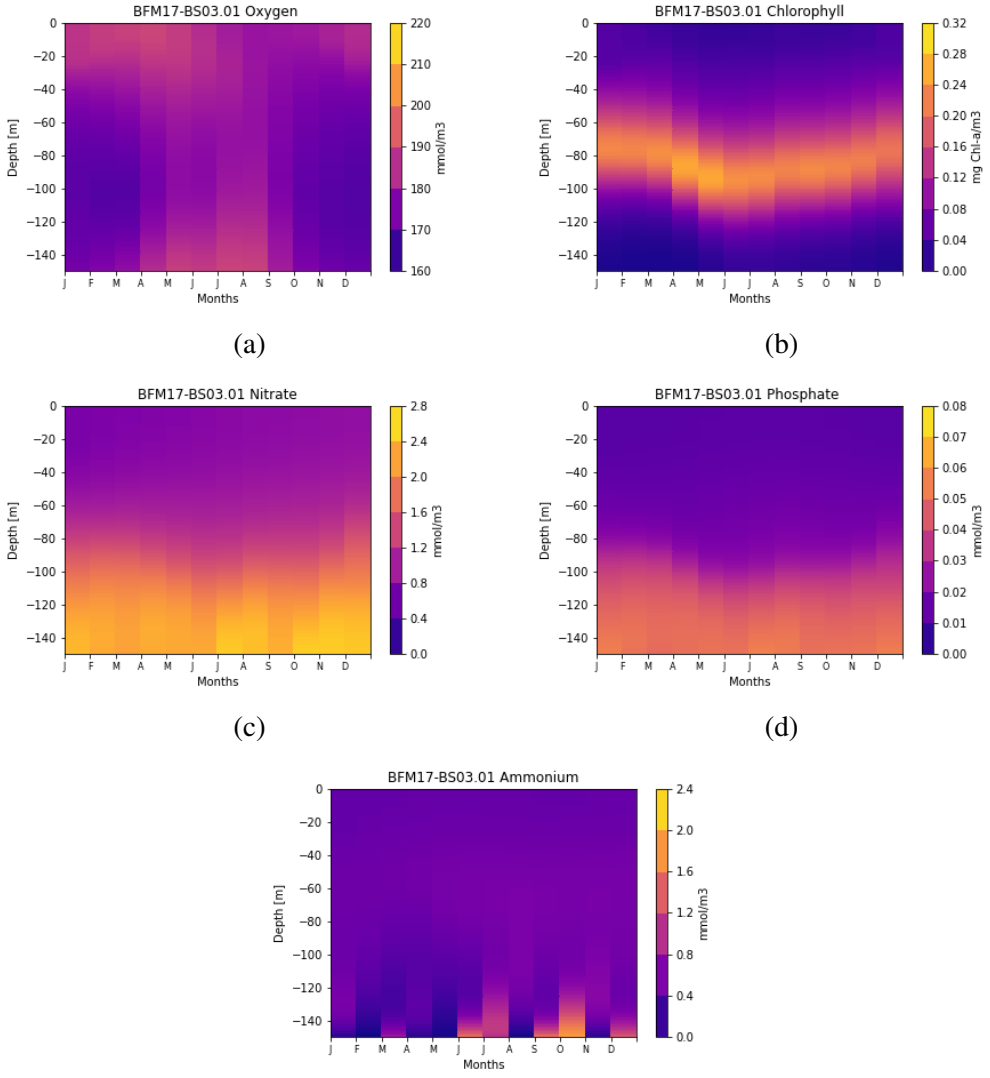

(a) (b) (c) (d) (e)

Figure 4.10: BFM17-POM1D last year concentration results for the simulation BFM17-BS03.01: (a) Dissolved Oxygen, (b) Chlorophyll, (c) Nitrate, (d) Phosphate and (e) Ammonium

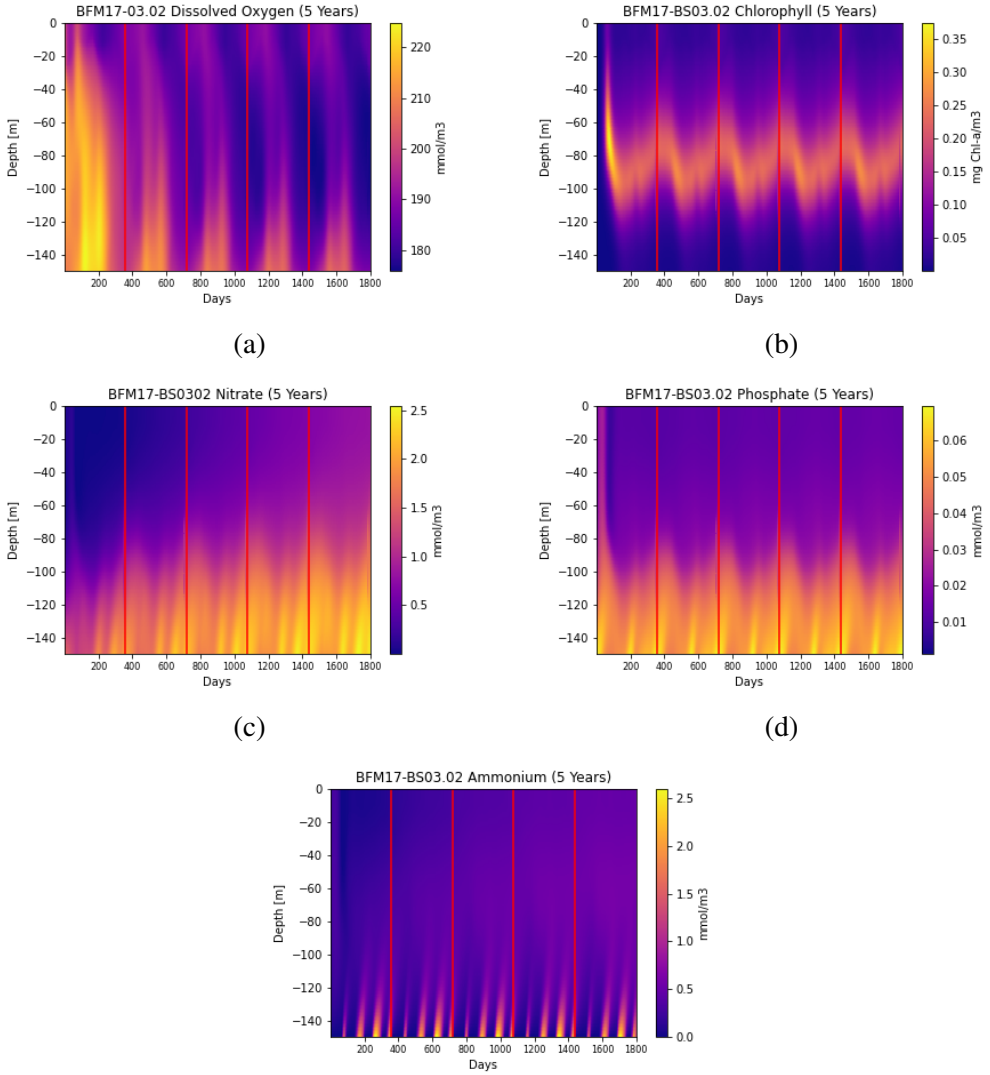

Figure 4.11: BFM17-POM1D 5 years concentration results for the simulation BFM17-BS03.02: (a) Dissolved Oxygen, (b) Chlorophyll, (c) Nitrate, (d) Phosphate and (e) Ammonium

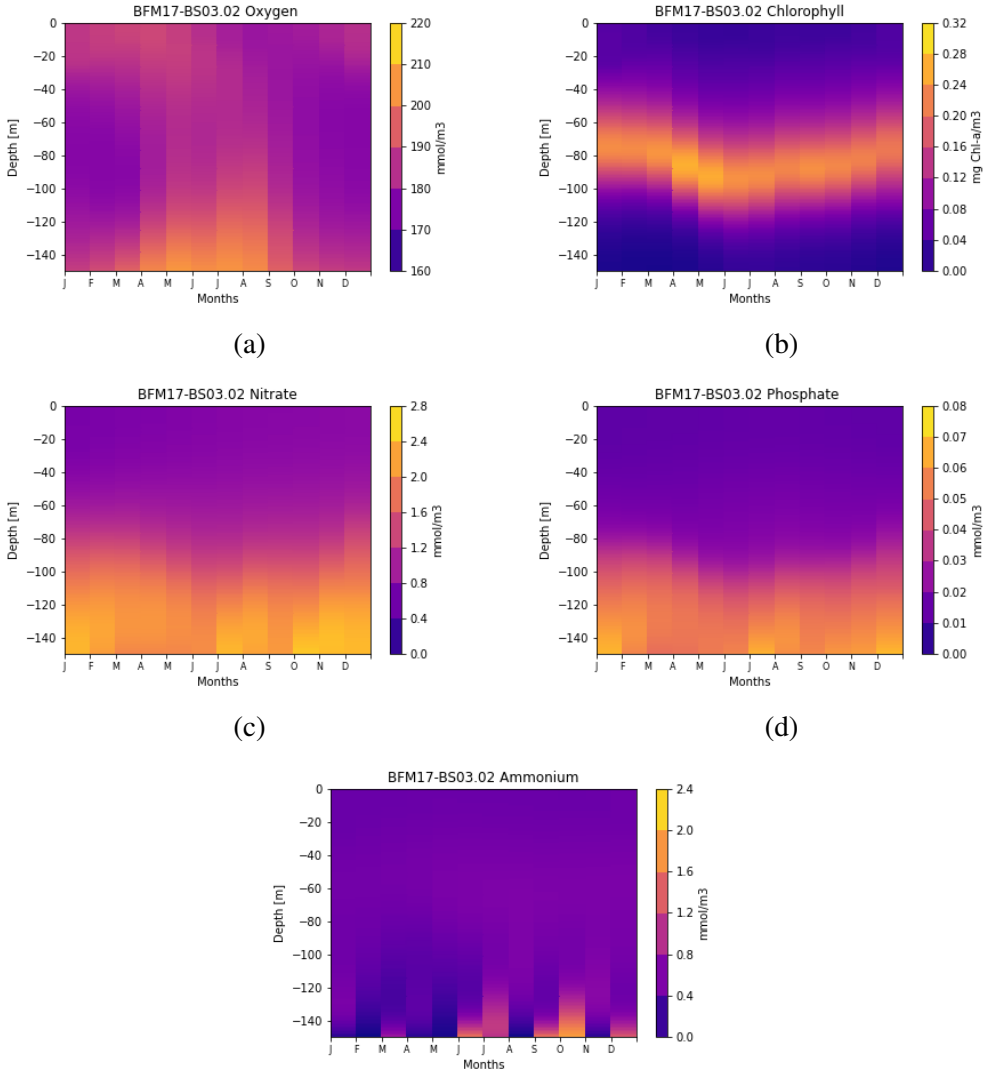

(a) (b) (c) (d) (e)

Figure 4.12: BFM17-POM1D last year concentration results for the simulation BFM17-BS03.02: (a) Dissolved Oxygen, (b) Chlorophyll, (c) Nitrate, (d) Phosphate and (e) Ammonium

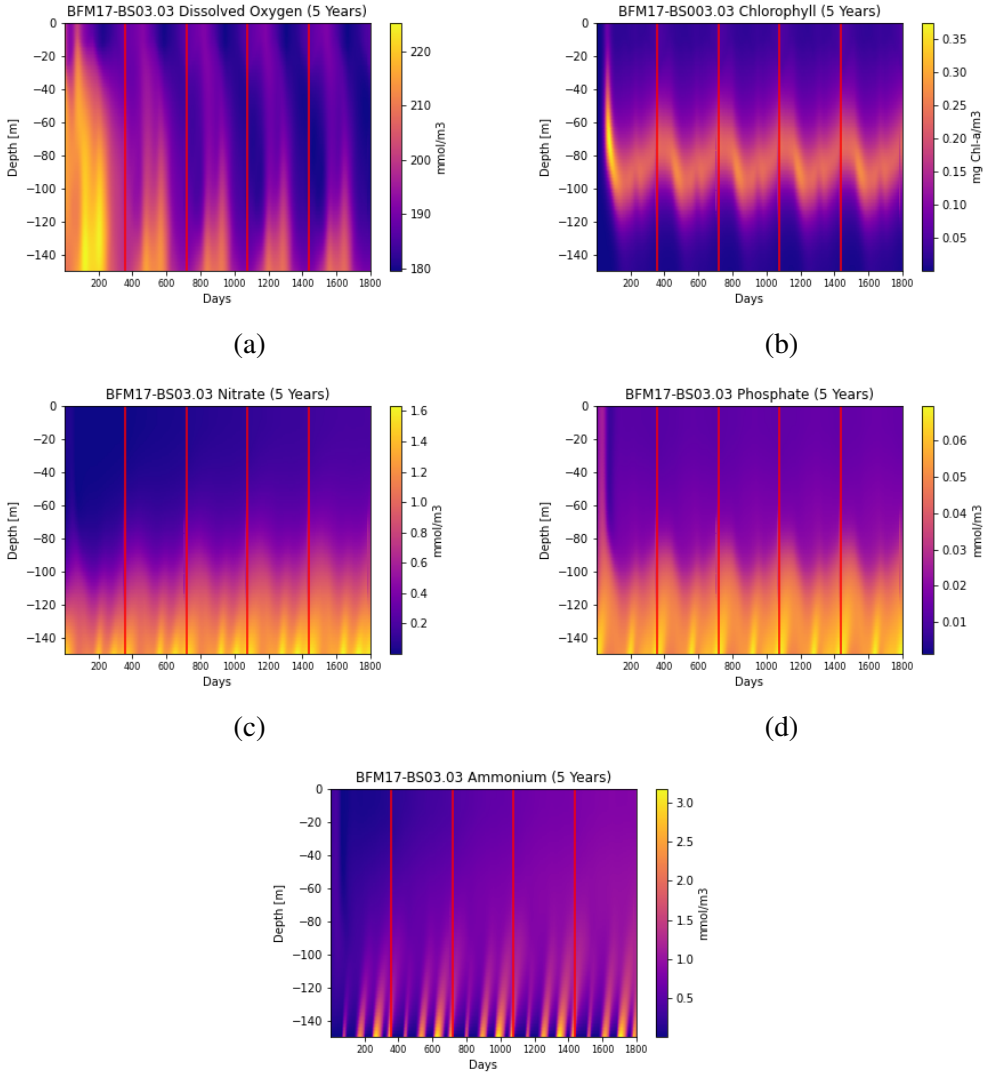

Figure 4.13: BFM17-POM1D 5 years concentration results for the simulation BFM17-BS03.03: (a) Dissolved Oxygen, (b) Chlorophyll, (c) Nitrate, (d) Phosphate and (e) Ammonium

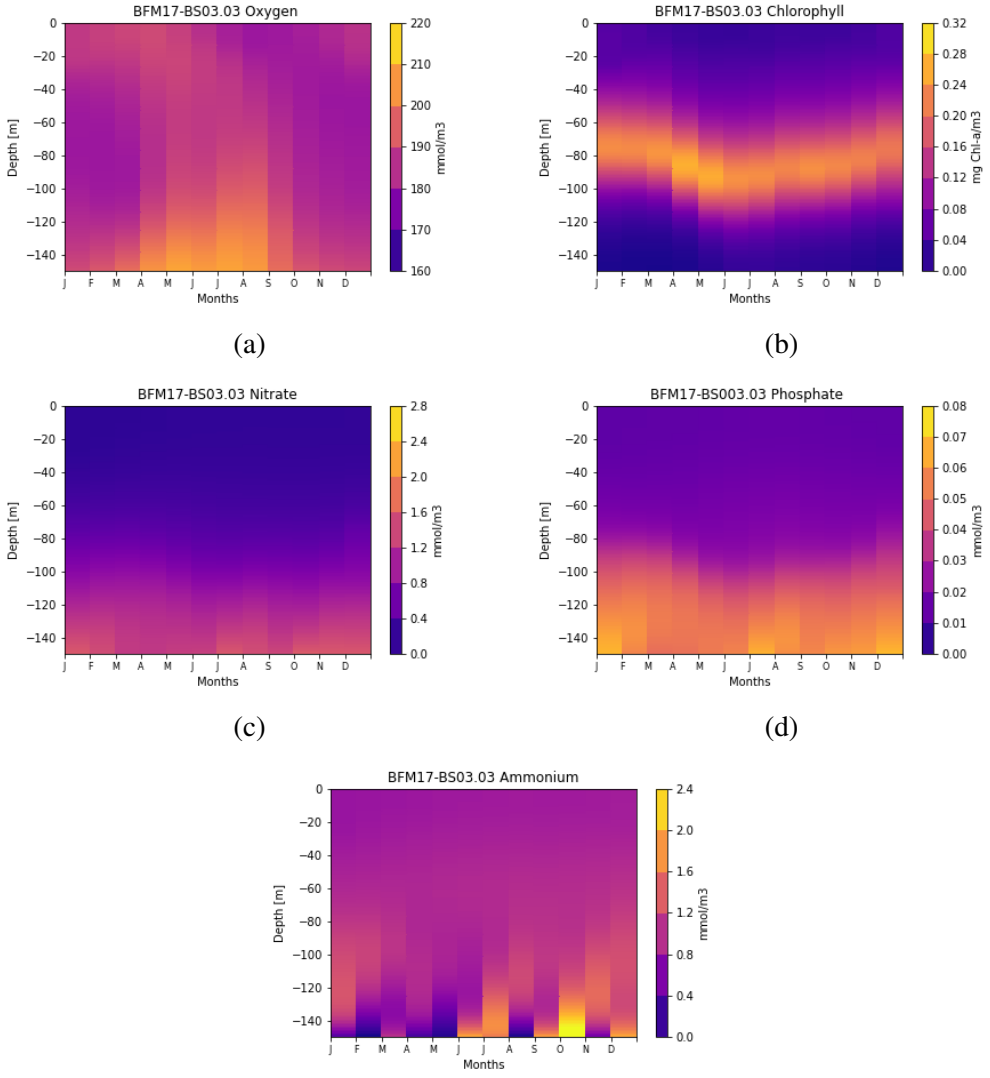

Figure 4.14: BFM17-POM1D last year concentration results for the simulation BFM17-BS03.03: (a) Dissolved Oxygen, (b) Chlorophyll, (c) Nitrate, (d) Phosphate and (e) Ammonium

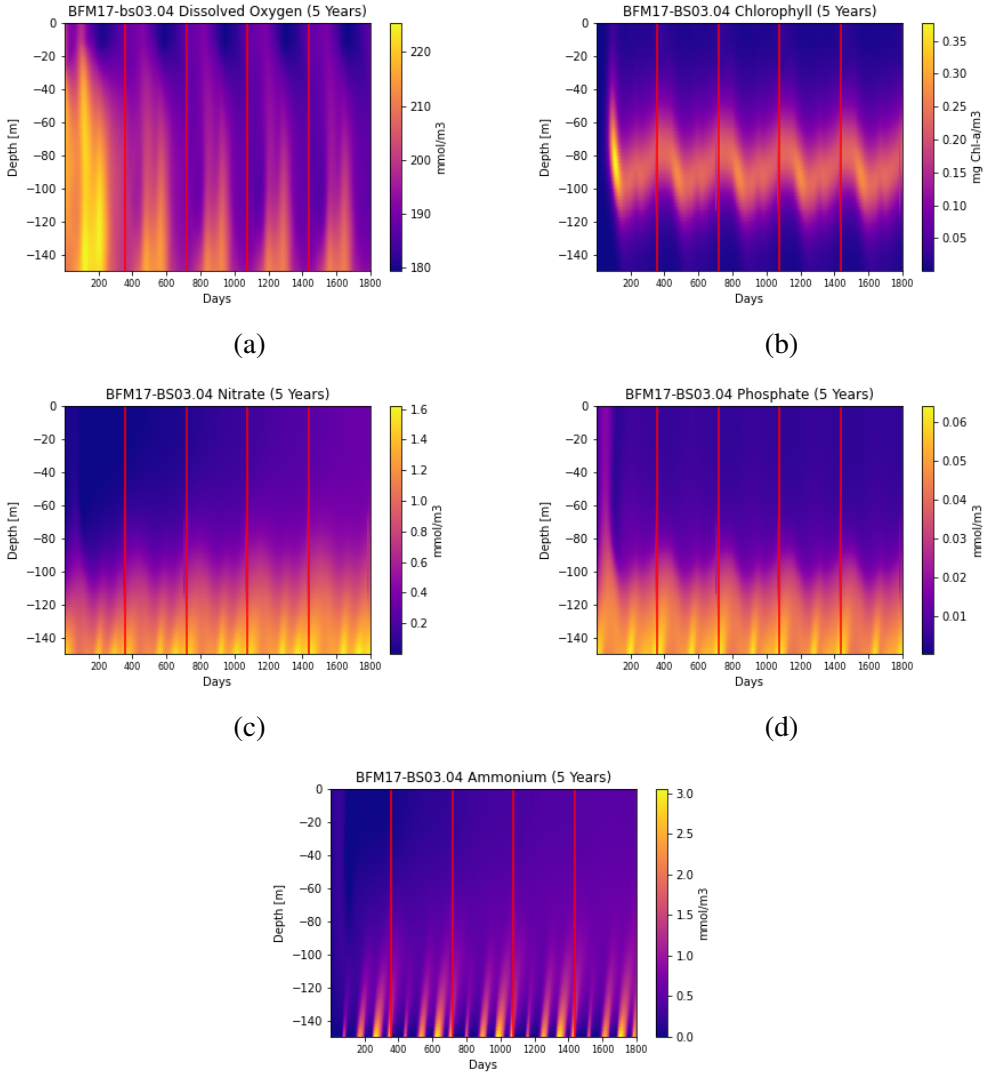

Figure 4.15: BFM17-POM1D 5 years concentration results for the simulation BFM17-BS03.04: (a) Dissolved Oxygen, (b) Chlorophyll, (c) Nitrate, (d) Phosphate and (e) Ammonium

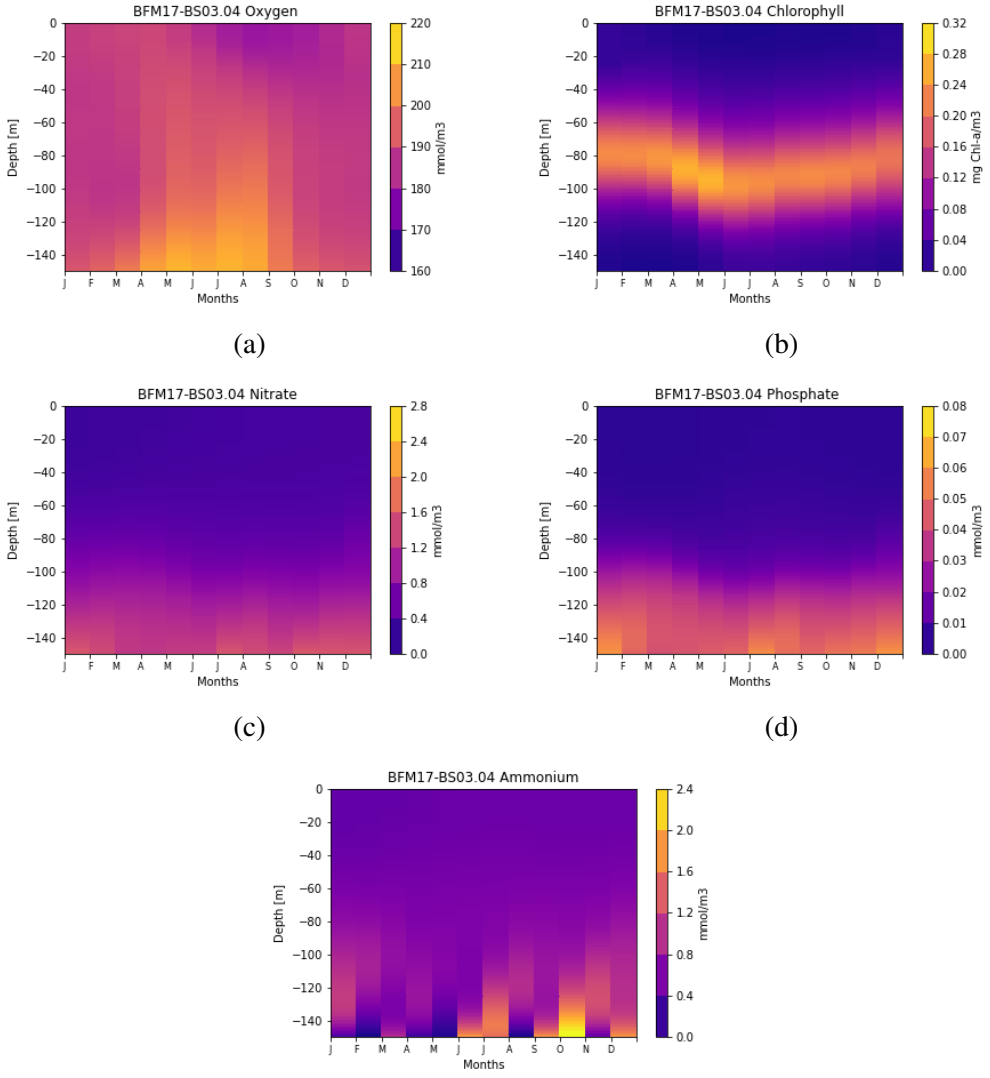

Figure 4.16: BFM17-POM1D last year concentration results for the simulation BFM17-BS03.04: (a) Dissolved Oxygen, (b) Chlorophyll, (c) Nitrate, (d) Phosphate and (e) Ammonium

The results show that comparing BS03 with BS03.01 we can see the role of an order of magnitude of difference in the vertical velocity: the lower values of vertical velocity bring back the values of oxygen to values similar to the BFM17-BATS control run that seems to be consistent.
From figure 4.8 it can be seen that, in BS03.03, there is a real blob of nutrients in the period from May to August which are the months immediately following April and July which, as can be seen in figure 4.6, have been showing the most intense velocity profiles. In BS03.01, on the other hand, the result is once again more comparable, at least in the range of values, with respect to the previous experiments. Furthermore, by observing only the BS03, it is clear that there is an accumulation for the nutrients in the solution and this may be attributable to the boundary conditions that enter or do not allow matter to exit. So in the BS03.02 experiment it was decided to decrease the relaxation time of the nutrients, changing the relaxation constant and passing from 0.06 to 0.2 m/d. This leads to relaxation times ranging from 15 days to 5 days. By comparing, for example, the oxygen of the experiment BS03.02 and that one obtained from the BS03.01, it is possible to appreciate a homogeneous rising of oxygen, in the first, which is no longer retained as in the second one. However, observing the nitrates and the phosphates of BS03.02 it is possible to see, especially for the former, a considerable drift that leads to a marked increase in nitrate concentrations over the 5 years of simulation. Therefore, in the BS03.03 experiment the nitrification parameter was modified, reducing it by an order of magnitude and making it go from 0.01 to 0.001 d^{-1}. Looking at ocean biochemistry for nitrification, it acts as a source for nitrates and is driven by an oxidation of ammonium. So while for nitrates, nitrification is a source, for ammonium it represents a sink. Decreasing the nitrification rate, what is oserved is a consequential reduction in the concentration of nitrates and an increase in oxygen and ammonium that are not consumed by the process. In any case, the phosphate values do not vary and it is noted that the drift has moved to the ammonium. The dynamics of ammonium is parameterized in a more complex way than nitrates, as bacteria also act on them through remineralization processes. This is why in the BS03.04 experiment the remineralization rates of particulate matter were reduced by an order of magnitude (from 0.1 to 0.01 d^{-1}). Here we can appreciate a reduction in phosphate concentrations as it happens for ammones. This is due to the fact that the bacterial activity of remineralization of the particulate organic matter represents a source of both ammonium and phosphates; therefore by reducing the value of the respective reminiralization rates it makes sense to find lower concentrations for these two nutrients. Also comparing the oxygen in the last month of the simulation BS03.03 and BS03.04

we can see, in the latter, an increase in concentration. This may be due to the fact that, as it's shown in eq. 2.41 the carbon remineralization rate appears as a sink so, descreasing this quantity it's reasonable to expect an increase in O concentration.

4.3 Hurricane effects

In this last section we are going to present the hurricane effects detected by the coupled model on the ocean ecosystem.

Table 4.3: Hurricane effects at G.P.

Name	**T and S profiles**	**Wind stress components**	**W profile**	**Notes**
BFM17-BS04	*CMEMS Reanalysis*	*ECMWF Analysis at G.P.*	$GOFS16+$ 2017 W *in October*	-
BFM17-BS04.01	*CMEMS Reanalysis*	*ECMWF Analysis at G.P.*	$GOFS16+$ 2017 W *in October*	$\lambda_j = 0.2$ $\Lambda_{N^{(3)}} = 0.001$ $\alpha^{(sinkC)}_{R^{(2)}_C}$,$\xi_{N^{(1)}}$, $\xi_{N^{(3)}} = 0.01$
BFM17-BS04.02	*CMEMS Reanalysis*	*ECMWF Analysis at G.P.*	$GOFS16+$ 2017 W *in October*	$Wx0.1$ $\lambda_j = 0.2$ $\Lambda_{N^{(3)}} = 0.001$ $\alpha^{(sinkC)}_{R^{(2)}_C}$,$\xi_{N^{(1)}}$, $\xi_{N^{(3)}} = 0.01$

Due to the hurricane indiced vertical velocities is shown in figure 4.17. The hurricane, in fact, produces strong upwelling velocities during its passage over the G.P. and we made the approximation that such vertical velocities are mantained for the whole month of October.

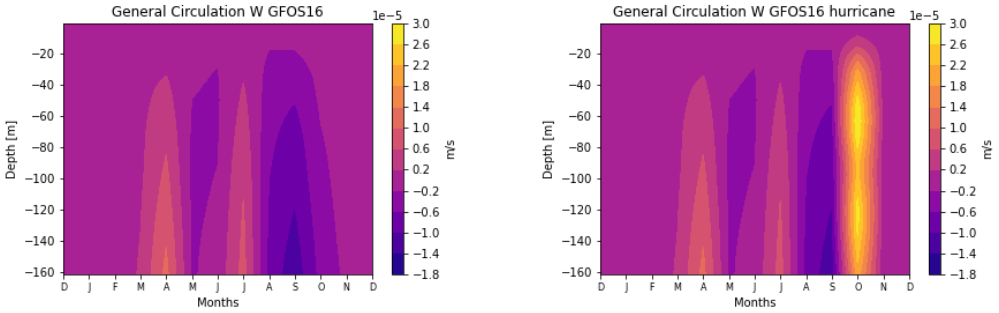

(a) (b)

Figure 4.17: GOFS16 vertical velocity profile: (a) 3 years monthly mean (b) 3 years monthly mean + hurricane

The passage of a hurricane is parametrized by the value of monthly mean vertical velocity for September 2017 regarding Hurricane Josè, a Category 4 hurricane which had more or less the same path and lifetime of Gonzalo. It crossed G.P. region from the 10th to the 20th September and so we insert the monthly mean values as our hurricane scenario in Gonzalo's month, that is Octobern (Fig. 4.17). The simulation results are shown in the figures 4.18 - 4.23.

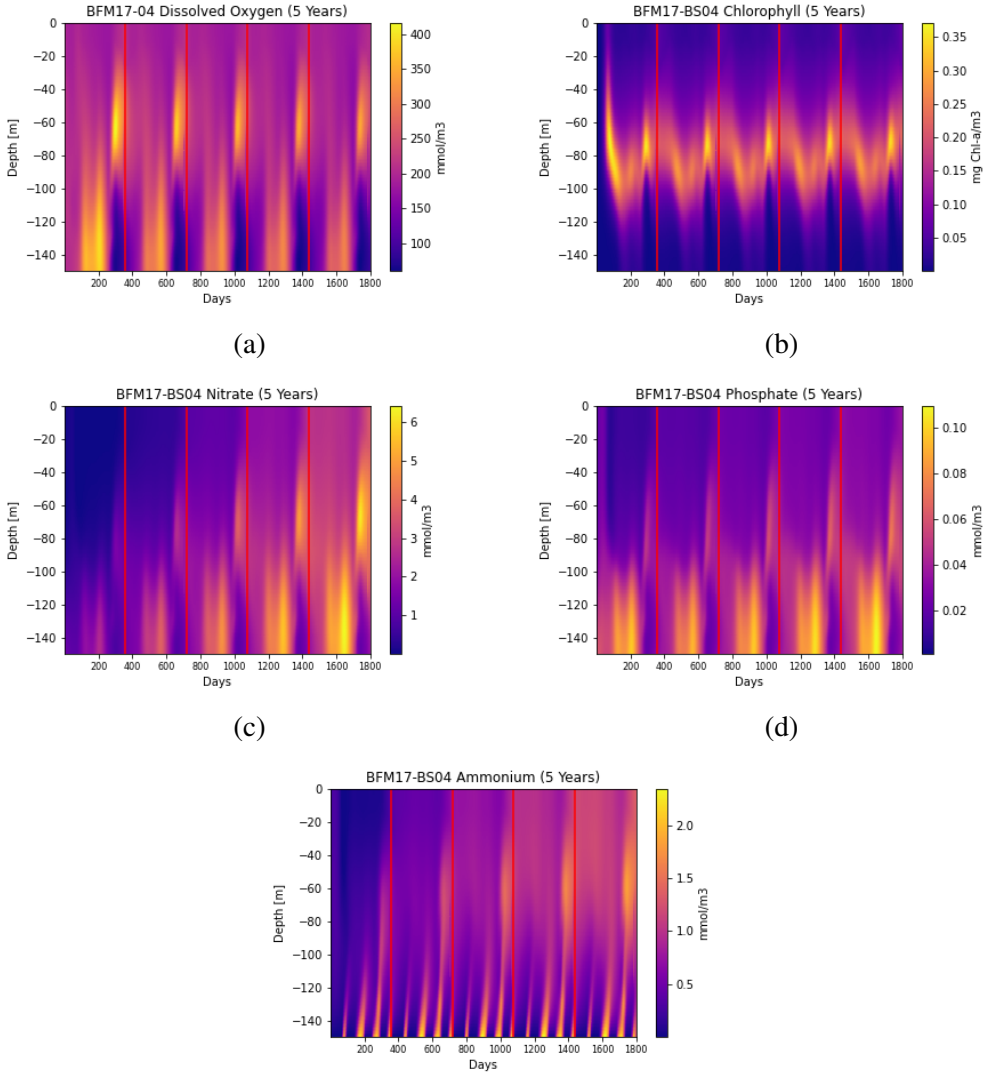

Figure 4.18: BFM17-POM1D 5 years concentration results for the simulation BFM17-BS04: (a) Dissolved Oxygen, (b) Chlorophyll, (c) Nitrate, (d) Phosphate and (e) Ammonium

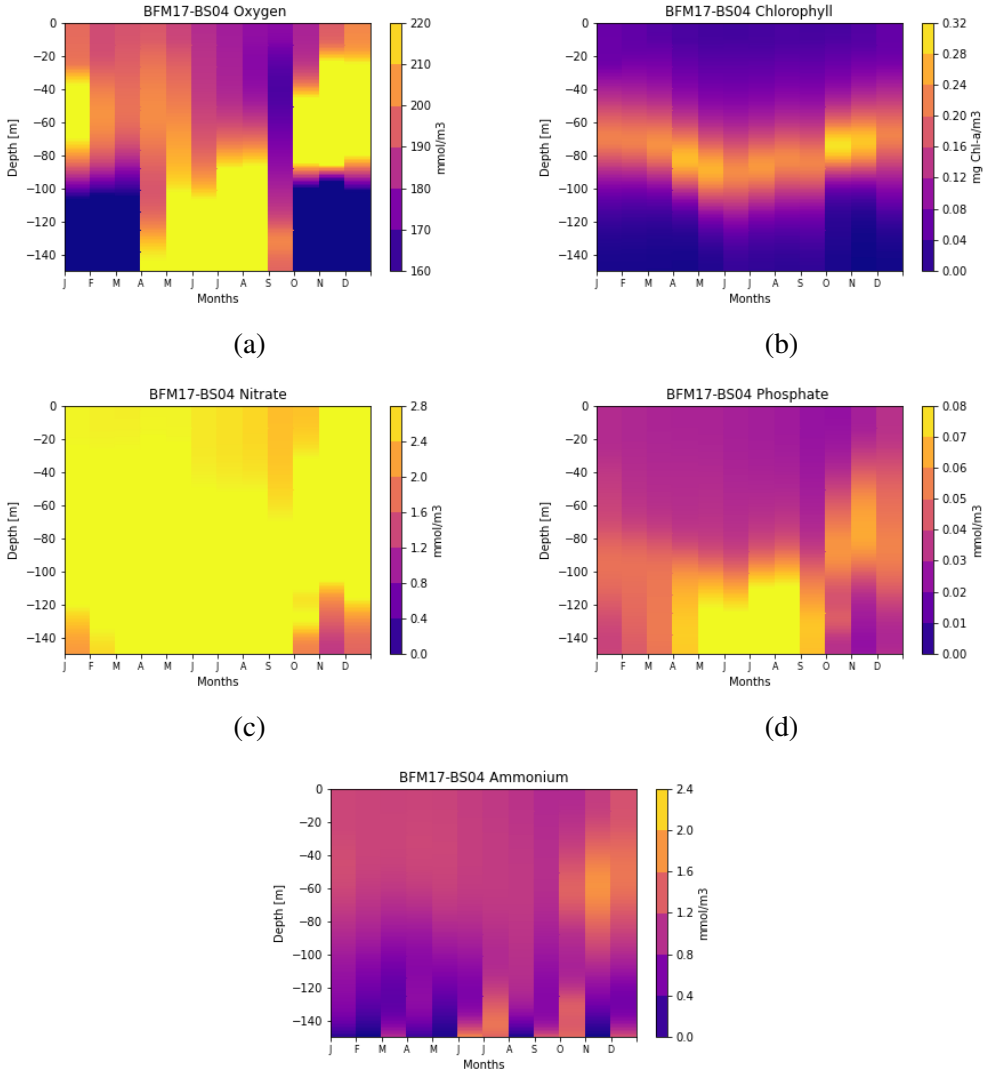

Figure 4.19: BFM17-POM1D last year concentration results for the simulation BFM17-BS04: (a) Dissolved Oxygen, (b) Chlorophyll, (c) Nitrate, (d) Phosphate and (e) Ammonium

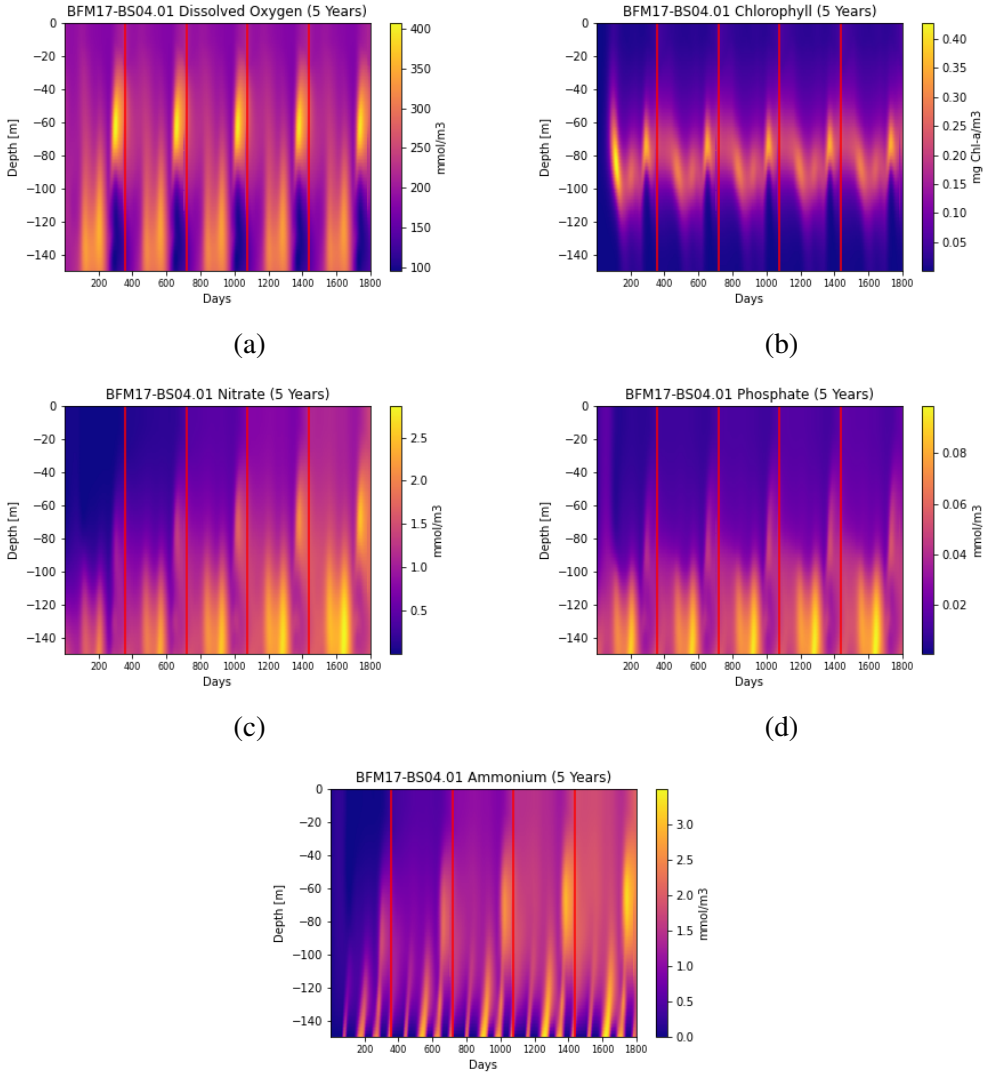

Figure 4.20: BFM17-POM1D 5 years concentration results for the simulation BFM17-BS04.01: (a) Dissolved Oxygen, (b) Chlorophyll, (c) Nitrate, (d) Phosphate and (e) Ammonium

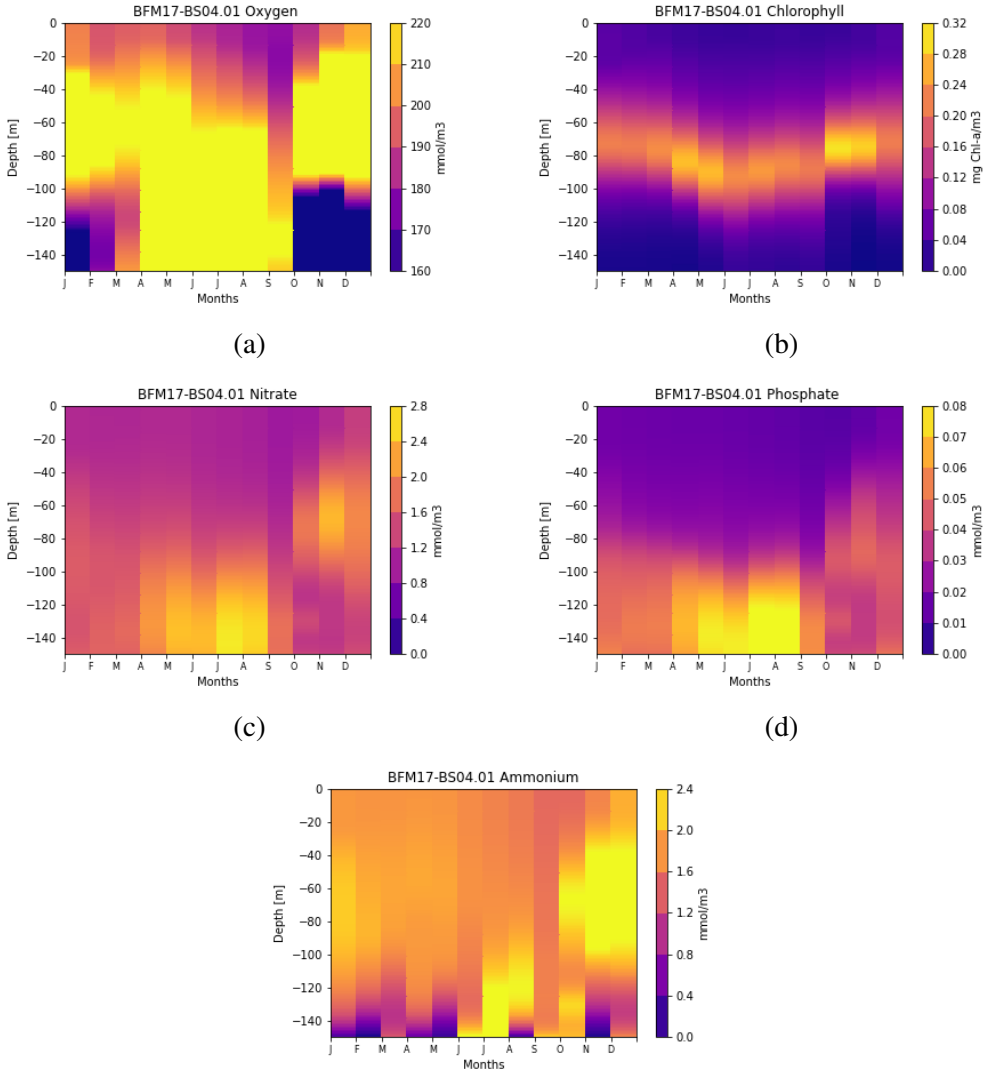

(a) (b) (c) (d) (e)

Figure 4.21: BFM17-POM1D last year concentration results for the simulation BFM17-BS04.01: (a) Dissolved Oxygen, (b) Chlorophyll, (c) Nitrate, (d) Phosphate and (e) Ammonium

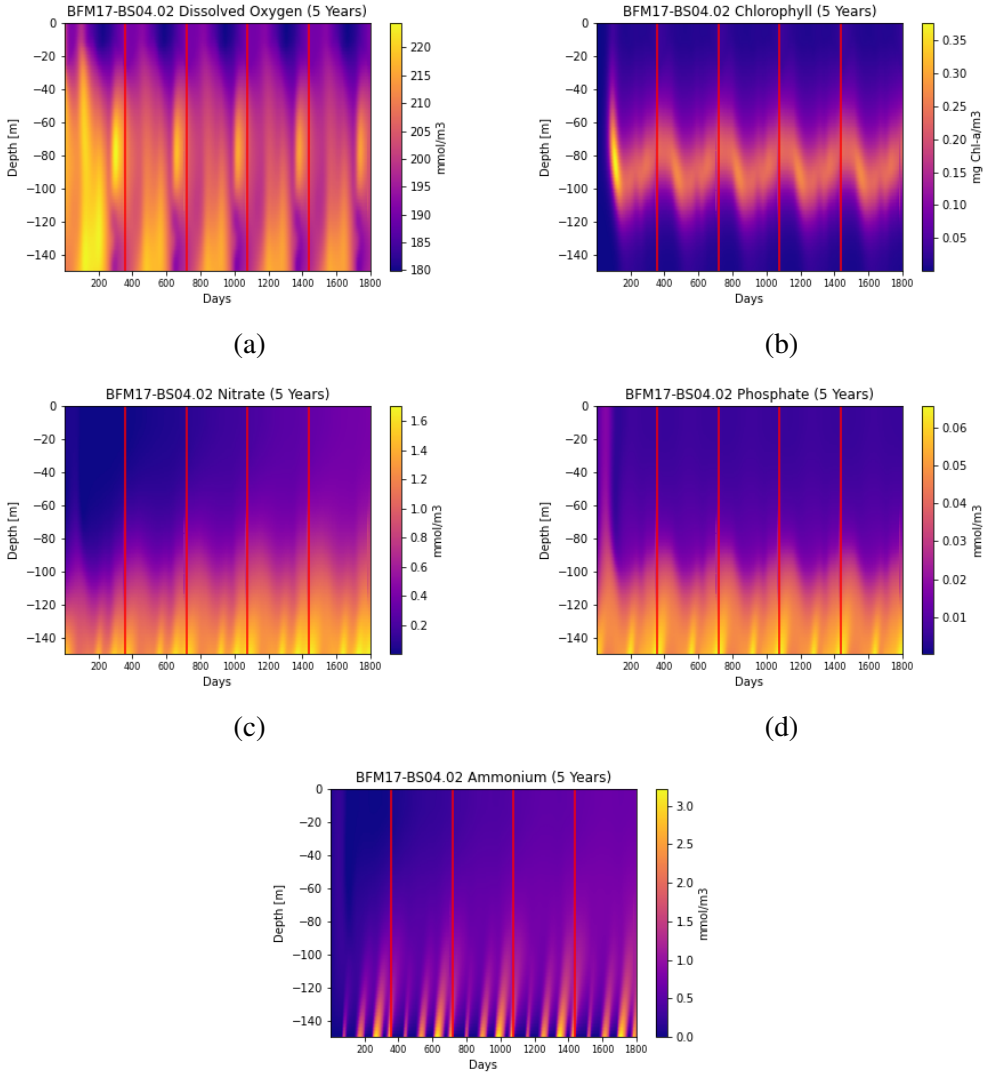

Figure 4.22: BFM17-POM1D 5 years concentration results for the simulation BFM17-BS04.02: (a) Dissolved Oxygen, (b) Chlorophyll, (c) Nitrate, (d) Phosphate and (e) Ammonium

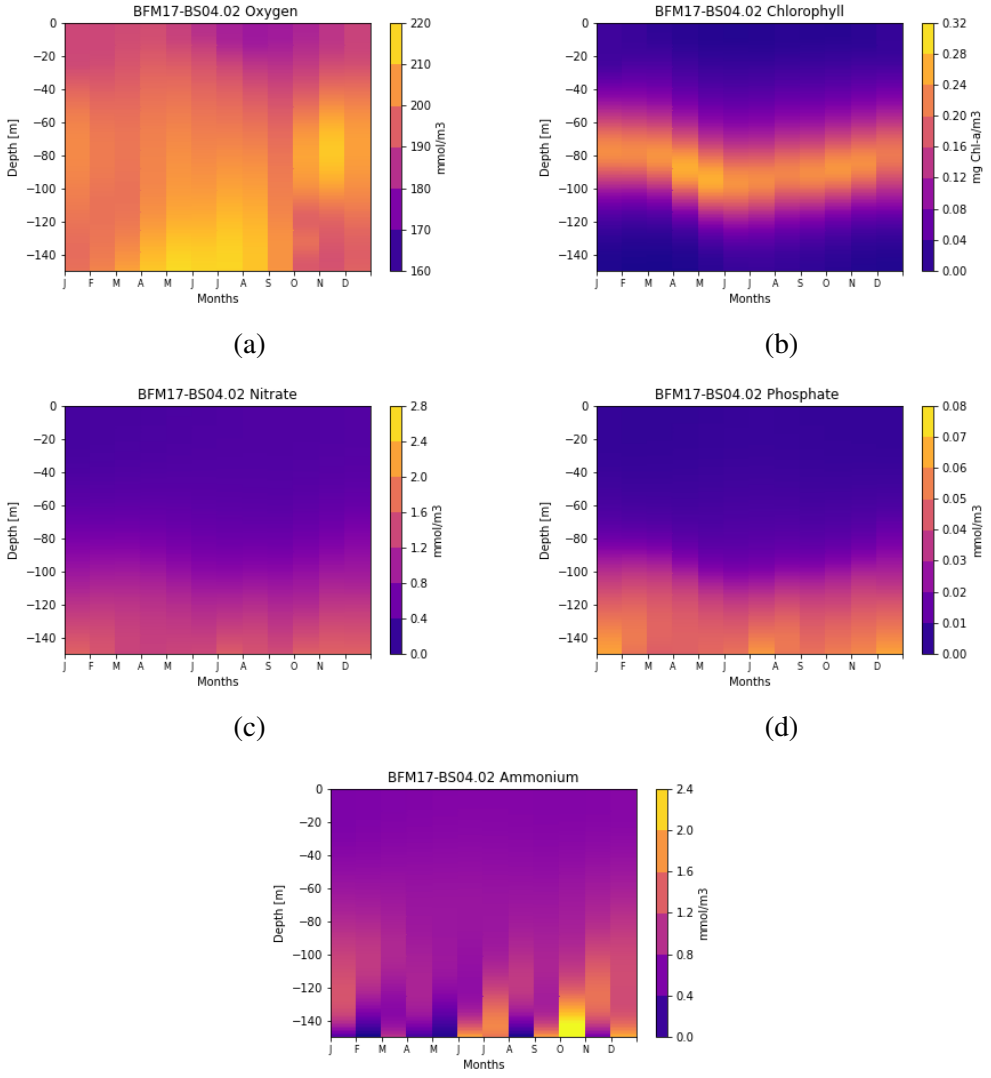

Figure 4.23: BFM17-POM1D last year concentration results for the simulation BFM17-BS04.02: (a) Dissolved Oxygen, (b) Chlorophyll, (c) Nitrate, (d) Phosphate and (e) Ammonium

The hurricane impact, in the BS04 experiment, corresponds to an increase of all nutrients compared to all the other experiments shown so far. On the other hand, the reappearance of the drift already discussed in the previous experiments can be seen, and therefore for this purpose the parameters of the biochemical processes were first changed, bringing them back to the same values as the BS03.04 experiment. In the BS04.01 it's possible to note an increase in the SCM which reach highets values and it's found at higher level in the water column. However, a particular thing happens if we look at the last two months of BS04.01 for phosphate and ammonium. In this case, compared to the respective nutrient in th BS04, the phosphate decreases while the ammonium increases. In this experimen we have again changed the nitrification and the remineralization rates. As can be seen in the equations 2.42 and 2.44, for both of them appear the remineralization as a source term, while nitrification in present only in ammonium equation as a sink term. So, while for the phosphate the shown result is reasonable, for the ammonium we can understand that with the effect of the hurricane the impact of nitrification dominates over the remineralization and so a descrease in both rates brings an increase of the ammonium concentartion. The experiment BS04.02 has exactly the same configuration of BS03.04 where both of them have the same new values for the parameters and the W descreased of a factor 10, but, in BS04.02 it has also the hurricane. So, finally, here are presented the differences between this two experiments, in order to have a conclusive and more complete understanding on the hurricane impact 4.24.

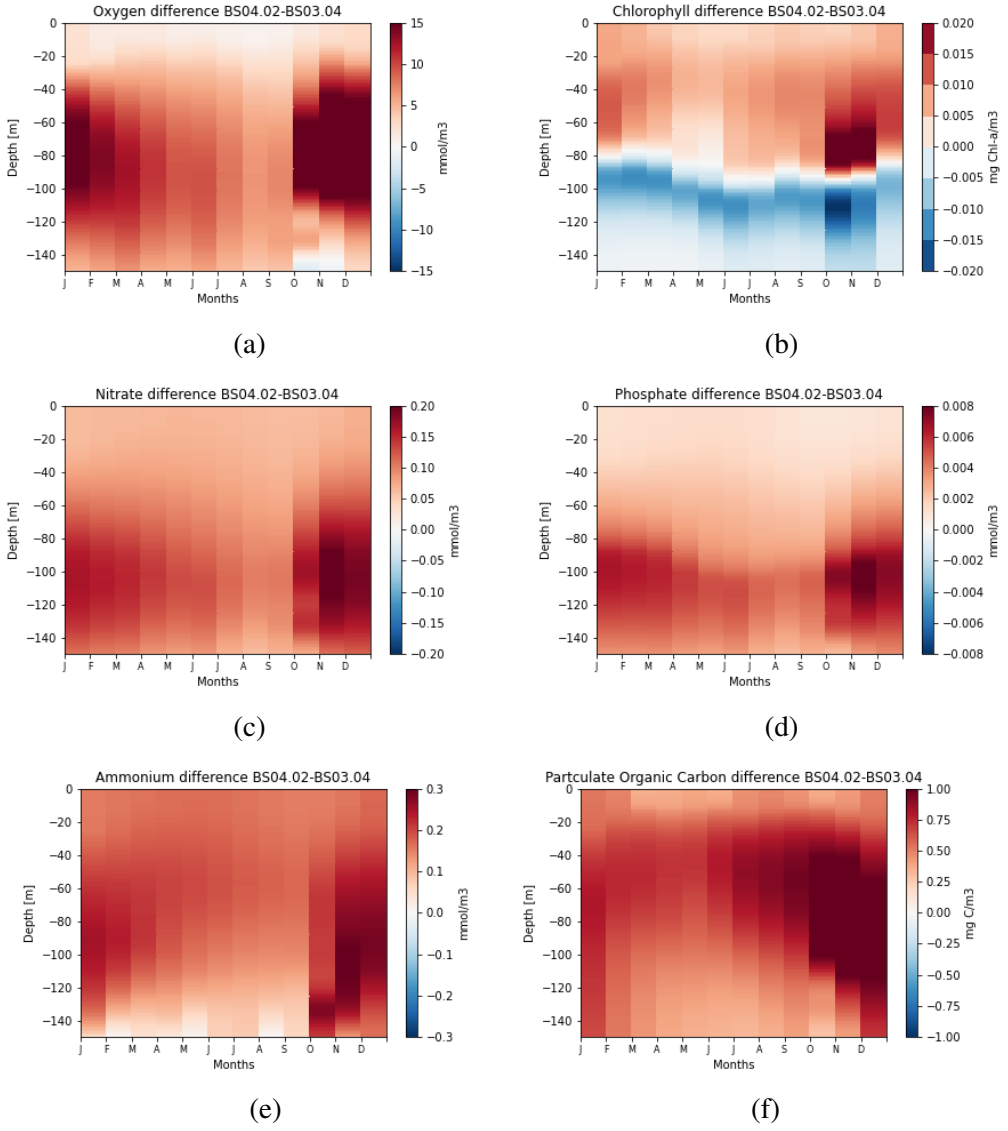

Figure 4.24: BFM17-POM1D last year concentration differences between the experiments BFM17-BS04.02 and BFM17-BS03.04 for the simulation BFM17-BS04.02: (a) Dissolved Oxygen, (b) Chlorophyll, (c) Nitrate, (d) Phosphate, (e) Ammonium and (f) Particulate Organic Carbon

Conclusions

This thesis has allowed a vision of how complex ocean biogeochemistry is: there are numerous processes affecting the biogeochemical component of the marine ecosystem and the perturbations induced by a hurricane amplify the sensitivity of the model.
Despite all the simplifications introduced for the purposes of this work, the results are nevertheless comforting in terms of the expected and observed results. In fact, it was possible to appreciate a change in nutrients as the location changes, passing precisely from the BATS area to that of Gonzalo.
The major variations are the result of changes in temperature and salinity forcing which, with respect to the wind, have a strong impact on the biological activity of the ocean. Furthermore, it was also possible to observe the role of certain biochemical processes, also managing to deduce how the various constituents influence each other. Obviously the same process can turn out to be both a source and a sink: it always depends on which nutrient we are considering and which biological functional groups influence it.
As expected, a reduction in the nitrification rate leads to an increase in oxygen and ammonium as it reduces the oxidation of the latter which would lead to the production of nitrates, which in fact decrease.
The remineralization of particulate organic matter has also been taken into consideration: it acts as a source for ammonium and phosphate while it is a sink for oxygen as the remineralization rate describes the bacterial activity that consumes oxygen to release the other nutrients. That's why it's consistent to find, with a reduction of the remineralization rates, an increase in oxygen and a descrease in ammonium anf phosphate concentrations.
Finally we were also able to appreciate the impact of a hurricane: it was in fact possible to observe a net increase in nutrient concentrations with a strong upwelling induced by the same and an increase in the SCM that reaches lower depths, approaching the surface clearly as it's possible to see from the figure 4.24. Here,

we also added the particulate organic carbon differences, which show an increase with the hurricane which is coherent with SCM depth.
In the future, a sensitivity study is needed to evaluate the most sensitive model parameters, both in BFM17 as in the 1-D physical model. Also a study on the rates modified in this thesiscould be undertaken constraining their values further improving the model representation of actual observations. It should be cheked how some other process changes act on the ocean ecosystem and how they are influenced by a hurricane.
Finally a hurricane case changing more forcings, such as PAR, could be tested.

Acknowledgements

First of all, I would like to extend my sincere and heartfelt thanks to my supervisors, Professor Nadia Pinardi and Doctor Momme Butenschön. They taught me a lot both from a scientific and non-scientific point of view. I could learn to have a critical and objective point of view and always question myself about what I see. In a period that we will all remember due to the pandemic, they, through a camera, were able to convey to me all the passion and dedication necessary for this work. I really wish anyone who decides to undertake an academic path, to be followed by people like that. Thank you.

Thanks to my family because you were always there also when I used to stay in Bologna. You were a huge support and my biggest fans. I'll never forget all your sacrifices... withouth you, all this would have been only a dream.

Thanks to the best classmates and friends I could meet. You made me feel home, always. Love you all.

Thanks to my brother, Federico, wherever you are I hope you can be proud of me. This is dedicated to you.

Lastly I really want to thank every single person I had the opportunity to meet during this large journey: all the BFM/CMCC community, in particular Dr. Rita Lecci and Dr. Vladyslav Lyubartsev, thanks for your support and huge availability.

I really hope that this will be only the beginning!

Bibliography

[1] G.C. ANDERSON. Subsurface chlorophyll maximum in the northeast pacific ocean 1. In *Subsurface Chlorophyll Maximum in the Northeast Pacific Ocean1*, pages 386–391. 1969.

[2] J.W. BARETTA et al. The european regional seas ecosystem model, a complex marine ecosystem model. In *Netherlands Journal of Sea Research*, pages 233–246. 1995.

[3] J. G. BARETTA-BEKKER et al. Microbial dynamics in the marine ecosystem model ersem ii with decoupled carbon assimilation and nutrient uptake. In *Journal of Sea Research*, pages 195–211. 1997.

[4] C.R. BENITEZ-NELSON. The biogeochemical cycling of phosphorus in marine systems. In *Earth-Science Reviews*, pages 109–135. 2000.

[5] S.A.H.W. BEUSEN et al. Beusen, a. h. w., et al. estimation of global river transport of sediments and associated particulate c, n, and p. In *Global Biogeochemical Cycles*. 2005.

[6] D. BIANCHI et al. Simulations of ecosystem response during the sapropel s1 deposition event. In *Palaeogeography, Palaeoclimatology, Palaeoecology*, pages 265–287. 2006.

[7] R.E. BLANKENSHIP et al. Anoxygenic photosynthetic bacteria. 2006.

[8] A.F. BLUMBERG and G.L. MELLOR. A description of a three-dimensional coastal ocean circulation model. In *Three-dimensional coastal ocean models*. 1987.

[9] D.P. BROWN. NATIONAL HURRICANE CENTER, TROPICAL CYCLONE REPORT: Hurricane Gonzalo. `https://www.nhc.noaa.gov/data/tcr/AL082014_Gonzalo.pdf`, 2015.

[10] E. CALLAWAY. A new kind of chlorophyll. http://blogs.nature.com/news/2010/08/a_new_kind_of_chlorophyll_and.html, 2010.

[11] D.G. CAPONE. Trichodesmium, a globally significant marine cyanobacterium. In *Science*, pages 1221–1229. 1997.

[12] N. CHACKO. Chlorophyll bloom in response to tropical cyclone hudhud in the bay of bengal: Bio-argo subsurface observations. In *Deep Sea Research Part I: Oceanographic Research Papers*, pages 66–72. 2017.

[13] L.L. CLARK and others. Marine organic phosphorus cycling; novel insights from nuclear magnetic resonance. In *American Journal of Science*, pages 724–737. 1999.

[14] L.H.N. COOPER. Redefinition of the anomaly of the nitrate-phosphate ratio. In *Journal of the Marine Biological Association of the United Kingdom*. 1938.

[15] COPERNICUS. https://www.copernicus.eu/.

[16] MARINE COPERNICUS. https://marine.copernicus.eu/.

[17] J.J. CULLEN. The deep chlorophyll maximum: Comparing vertical profiles of chlorophyll a. In *Canadian Journal of Fisheries and Aquatic Sciences*, pages 791–803. 1982.

[18] J.J. CULLEN. Subsurface chlorophyll maximum layers: Enduring enigma or mystery solved? In *Annual Review of Marine Science*, pages 207–239. 2015.

[19] N. DIERSING. In *Phytoplankton blooms: The basics*. 2009.

[20] ECMWF. https://www.ecmwf.int/.

[21] M. ESTRADA and otehrs. Variability of deep chlorophyll maximum characteristics in the northwestern mediterranean. In *Marine Ecology Progress Series*, pages 289–300. 1993.

[22] K. FITCH and C. KEMKER. Algae, phytoplankton and chlorophyll. fundamentals of environmental measurements. 2014.

[23] R.H. FLEMING and R. REVELLE. Physical processes in the ocean. In *Recent marine sediments: Tulsa, Am. Assoc. Petroleum Geologists*. 1939.

[24] K.B. FOLLMI. 160 my record of marine sedimentary phosphorus burial: Coupling of climate and continental weathering under greenhouse and ice-house conditions. In *Geology*, pages 503–506. 1995.

[25] F.O. GLöCKNER et al. In *Marine Microbial Diversity and its role in Ecosystem Functioning and Environmental Change*. 2012.

[26] N. GRUBER. Gruber, nicolas. the dynamics of the marine nitrogen cycle and its influence on atmospheric co2 variations. In *The ocean carbon cycle and climate*, pages 97–148. 2004.

[27] G.E. HASLE et al. Identifying marine diatoms and dinoflagellates. 1996.

[28] R. HATZENPICHLER. Diversity, physiology, and niche differentiation of ammonia-oxidizing archaea. In *Applied and environmental microbiology*. 2012.

[29] R.D. HEITZER and OTTAOW J.C.G. New denitrifying bacteria isolated from red sea sediments. In *Marine Biology*. 1976.

[30] G.J. HERNDL and T. REINTHALER. Microbial control of the dark end of the biological pump. In *Nature geoscience*, pages 718–724. 2013.

[31] R.W. HOWARTH. Nutrient limitation of net primary production in marine ecosystems. In *Annual review of ecology and systematics*, pages 89–110. 1988.

[32] B.L. HUA et al. An objective analysis of the polymode local dynamics experiment. part ii: Streamfunction and potential vorticity fields during the intensive period. In *Journal of Physical Oceanography*, pages 136–143. 1986.

[33] W HUNDSDORFER and J.G. VERWER. In *Numerical solution of time-dependent advection-diffusion-reaction equations*. 2013.

[34] D. IOVINO et al. A 1/16° eddying simulation of the global nemo sea-ice–ocean system. In *Geoscientific Model Development,*, pages 2665–2684. 2016.

[35] D. IOVINO et al. GOFS16: a global ocean forecast system at eddying resolution. In *EGU General Assembly Conference Abstracts*. 2018.

[36] A. JAKHELLN. Oceanographic investigation in east greenland waters in the summers of 1930-1932. 1936.

[37] I. KATARA et al. Atmospheric forcing on chlorophyll concentration in the mediterranean. In *Essential Fish Habitat Mapping in the Mediterranean*, pages 33–48. 2008.

[38] P.D. KILLWORTH. Time interpolation of forcing fields. In *Journal of Physical Oceanography*, pages 136–143. 1996.

[39] E.J. KLEKOWSKI. The ecology and evolution of clonal plants. 1997.

[40] C. LABRY and others. Phytoplankton and bacterial alkaline phosphatase activities in relation to phosphate and dop availability within the gironde plume waters (bay of biscay). In *Journal of Experimental Marine Biology and Ecology*, pages 213–225. 2005.

[41] C. LALLI and R. TIMOTHY. In *Biological oceanography: an introduction*. 1997.

[42] D.F. LEIPPER. Observed ocean conditions and hurricane hilda. In *Journal of the Atmospheric Sciences*, pages 182–186. 1967.

[43] W.M. MANNING and H.H. STRAIN. Chlorophyll d, a green pigment of red algae. In *Journal of Biological Chemistry*, pages 1–19. 1943.

[44] P. MAY and S. COTTON. Molecules that amaze us. 2015.

[45] C.R. McCLAIN and J. FIRESTONE. An investigation of ekman upwelling in the north atlantic. In *Journal of Geophysical Research: Oceans*, pages 12327–12339. 1993.

[46] G.L. MELLOR. One-dimensional, ocean surface layer modeling: a problem and a solution. In *Journal of Physical Oceanography*, pages 790–809. 2001.

[47] G.L. MELLOR and T. YAMADA. Development of a turbulence closure model for geophysical fluid problems. In *Reviews of Geophysics*, pages 851–875. 1982.

[48] A.M. MERRITT-TAKEUCHI et al. Case studies of tropical cyclones and phytoplankton blooms over atlantic and pacific regions. In *Earth Interactions*, pages 1–19. 2013.

[49] F.M. MONALDO et al. Satellite imagery of sea surface temperature cooling in the wake of hurricane edouard (1996). In *Monthly Weather Review*, pages 2716–2721. 1997.

[50] M. MUSSAP et al. A management oriented 1-d ecosystem model: Implementation in the gulf of trieste (adriatic sea). In *Regional Studies in Marine Science*, pages 109–123. 2016.

[51] A. PAYTAN and K. McLAUGHLIN. The oceanic phosphorus cycle. In *Chemical reviews*, pages 563–576. 2007.

[52] S. T. PETSCH. The global oxygen cycle. In *Treatise on geochemistry*, pages 515–555. 2003.

[53] L. POLIMENE et al. A numerical simulation study of dissolved organic carbon accumulation in the northern adriatic sea. In *Journal of Geophysical Research: Oceans*. 2007.

[54] J.F. PRICE. Upper ocean response to a hurricane. In *Journal of Physical Oceanography*, pages 153–175. 1981.

[55] A.C. REDFIELD. Oganic derivatives in sea:water and their relation to: the composition of phytoplankton. 1934.

[56] WORLD OCEAN REVIEW. WOR-1 Living with the oceans. A report on the state of the world's oceans. `https://worldoceanreview.com/en/wor-1/ocean-chemistry/`, 2010.

[57] F. RICHARDS. Oxygen in the ocean. In *Treatise on Marine Ecology and Paleoecology*, chapter 9, pages 185–238. 1957.

[58] D.B. RISIEN, C.M. adn CHELTON. The scatterometer climatology of ocean winds (scow). 2011.

[59] K.C. RUTTENBERG. The global phosphorus cycle. In *Treatise on Geochemistry*, pages 499–558. 2014.

[60] S.P. SEITZINGER et al. Sources and delivery of carbon, nitrogen, and phosphorus to the coastal zone: An overview of global nutrient export from watersheds (news) models and their application. In *Global Biogeochemical Cycles*. 2005.

[61] D.A. SIEGEL and W.G. DEUSER. Trajectories of sinking particles in the sargasso sea: modeling of statistical funnels above deep-ocean sediment traps. In *Deep Sea Research Part I: Oceanographic Research Papers*, pages 1519–1541. 1997.

[62] K.M. SMITH et al. Bfm17 v1. 0: a reduced biogeochemical flux model for upper-ocean biophysical simulations. In *Geoscientific Model Development*, pages 2419–2442. 2021.

[63] S.V. SMITH. Phosphorus versus nitrogen limitation in the marine environment 1. In *Limnology and oceanography*, pages 1149–1160. 1984.

[64] D.K. STEINBERG and otehrs. Overview of the us jgofs bermuda atlantic time-series study (bats): a decade-scale look at ocean biology and biogeochemistry. In *Deep Sea Research Part II: Topical Studies in Oceanography*, pages 1405–1447. 2001.

[65] L. SUN et al. Ocean responses to typhoon namtheun explored with argo floats and multiplatform satellites. In *Atmosphere-Ocean*, pages 15–26. 2012.

[66] H. SVERDRUP et al. In *The Oceans, Their Physics, Chemistry, and General Biology*, chapter 7. 1942.

[67] K. TODAR. Diversity of metabolism in procaryotes. In *Today's Online Textbook of Bacteriology*. 2011.

[68] J. R. TOGGWEILER. Variation of atmospheric CO2 by ventilation of the ocean's deepest water. In *Paleoceanography*, pages 571–588. 1999.

[69] T. TYRRELL. The relative influences of nitrogen and phosphorus on oceanic primary production. In *Nature*, pages 525–531. 1999.

[70] M. VICHI et al. Calibration and validation of a one-dimensional complex marine biogeochemical flux model in different areas of the northern adriatic shelf. In *Annales Geophysicae*, pages 413–436. 2003.

[71] M. VICHI et al. A generalized model of pelagic biogeochemistry for the global ocean ecosystem. part i: Theory. pages 89–109. 2007.

[72] N.D. WALKER et al. Hurricane-forced upwelling and chlorophyll a enhancement within cold-core cyclones in the gulf of mexico. In *Geophysical Research Letters*. 2005.

[73] R. WANNINKHOF. Relationship between wind speed and gas exchange over the ocean. In *Journal of Geophysical Research: Oceans*, pages 7373–7382. 1992.

[74] R. WANNINKHOF. Relationship between wind speed and gas exchange over the ocean revisited. In *Limnology and Oceanography: Methods*, pages 351–362. 1992.

[75] B. WARD. Nitrification and denitrification: probing the nitrogen cycle in aquatic environments. In *Microbial Ecology*, pages 247–261. 1996.

[76] K. WESTON and otehrs. Primary production in the deep chlorophyll maximum of the central north sea. In *Journal of Plankton Research.*, pages 909–922. 2005.

[77] R.G. WETZER. In *Limnology: Lake and River Ecosystems*. 2001.

[78] J.D. WOODS and W. BARKMANN. The response of the upper ocean to solar heating. i: The mixed layer. In *Quarterly Journal of the Royal Meteorological Society*, pages 1–27. 1986.

[79] L.V. WORTHINGTON. On the north atlantic circulation. 1976.

[80] K. YOSHIYAMA et al. Catastrophic shifts in vertical distributions of phytoplankton the existence of a bifurcation set. In *Journal of mathematical biology*, pages 235–276. 2006.

[81] M. ZAVATARELLI et al. Coupling BFM with ocean models: the 1D Princeton Ocean Model. `https://bfm-community.github.io/www.bfm-community.eu/`, 2020.

[82] J.P. ZEHR. Nitrogen fixation by marine cyanobacteria. In *Trends in microbiology*, pages 162–173. 2011.